

NPS ARCHIVE  
1966  
EDWARDS, R.

LT. RODERICK YERKES EDWARDS , JR., USCG

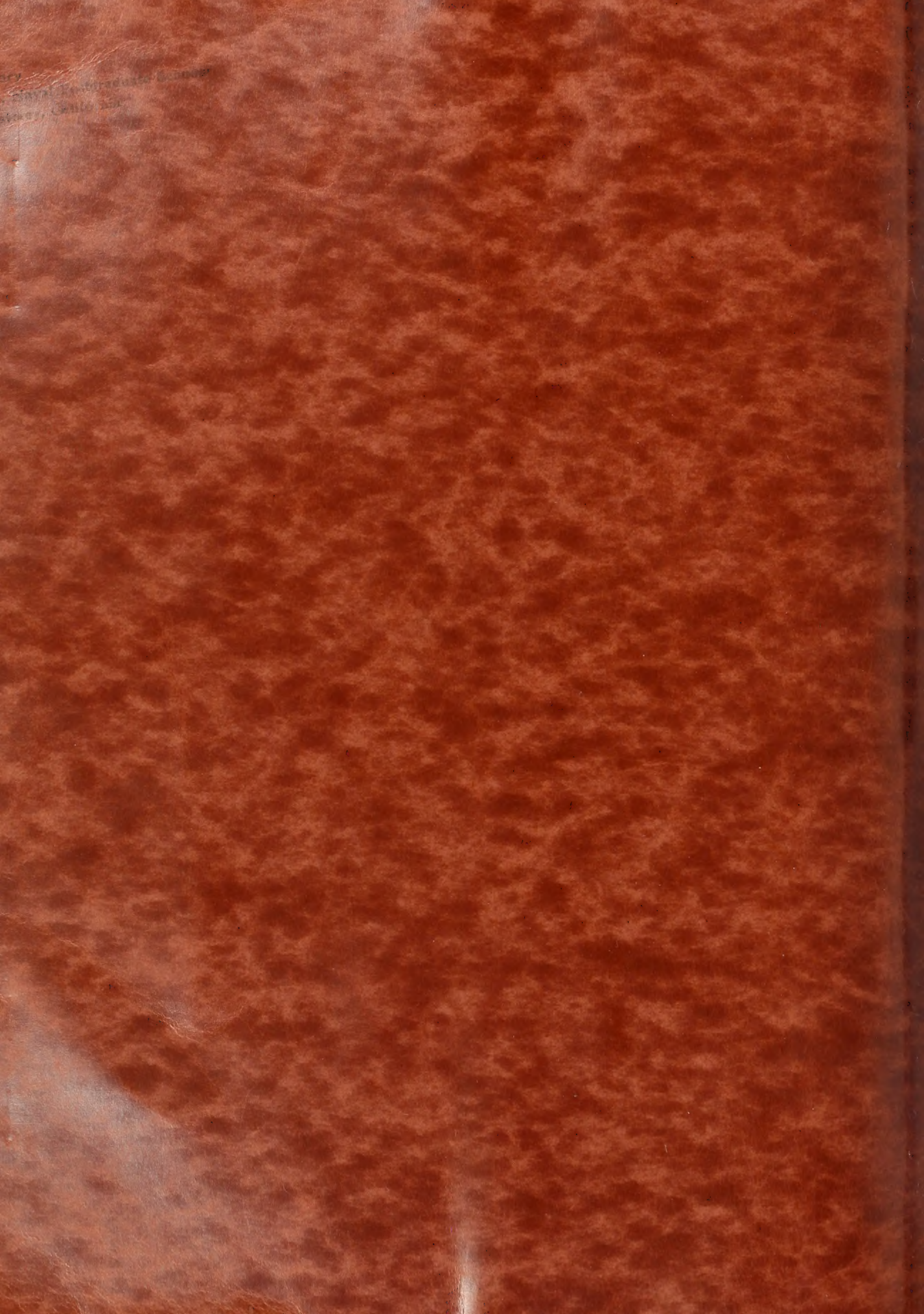
XIII A

PREDICTION OF BOUNDARY LAYER EFFECTS

ON MARINE PROPELLER SECTIONS

Thesis  
E254





Library  
of the University of California  
Berkeley, Calif. 94720



-1-

PREDICTION OF BOUNDARY LAYER EFFECTS ON  
MARINE PROPELLER SECTIONS

by

LT. ROBERT TRENKES EDWARDS, Jr., USCG

SUBMITTED TO THE DEPARTMENT OF NAVAL ARCHITECTURE AND MARINE  
ENGINEERING IN PARTIAL FULFILLMENT OF THE REQUIREMENTS FOR  
THE MASTER OF SCIENCE DEGREE IN MECHANICAL ENGINEERING  
AND THE PROFESSIONAL ENGINEER, NAVAL ENGINEER

at the

MASSACHUSETTS INSTITUTE OF  
TECHNOLOGY

May, 1966

Signature of Author .....  
Department of Naval Architecture and  
Marine Engineering, May 20, 1966

Certified by .....  
Thesis Supervisor

Certified by .....  
Thesis Supervisor

Accepted by .....  
Chairman, Departmental Committee  
on Graduate Students







ABSTRACT

PREDICTION OF BOUNDARY LAYER EFFECTS ON  
MARINE PROPELLER SECTIONS

by

Lt. Roderick Veritas Edwards, Jr., USCG

Submitted to the Department of Naval Architecture and Marine Engineering on May 20, 1966 in partial fulfillment of the requirements for the Master of Science Degree in Mechanical Engineering and the Professional Degree, Naval Engineer.

Heretofore viscous corrections used in the design of thin marine propeller and hydrofoil sections have been based upon data obtained from experiments with relatively thick sections. In an attempt to improve this process, the viscous effects on the lift of an extremely thin, low camber airfoil section were studied experimentally.

An airfoil of small thickness and low camber was constructed and instrumented for the measurement of pressure distribution along the chord. Measurements were made of the velocity distribution normal to the surface of the foil at points along the chord for several angles of attack and two Reynolds Numbers, using "Lake" type sensors. The displacement thickness of the boundary layer along the chord was then determined. Increasing the dimensions of the actual foil by the displacement thickness and treating the resulting form as a solid body in potential flow was the method used for determining the viscous correction in this work. The result of the



ABSTRACT

INVESTIGATION OF STREAM LINE FLOW IN

WATER TUNNELS

BY

DR. J. H. P. VAN DER KAM, D. Sc., D. Eng.

Submitted to the Department of Mechanical Engineering and Marine Engineering

on May 10, 1934 in partial fulfillment of the requirements for

the Master of Science degree in Mechanical Engineering and the Professional

Engineer, Naval Engineers.

Investigations of stream line flow in the design of this tunnel

propeller and hydrofoil sections have been based upon data obtained from

experiments with relatively thick sections. In an attempt to improve this

process, the various effects on the lift of an extremely thin, low section

hydrofoil section were studied experimentally.

An analysis of small thickness and low section was conducted and

instrumented for the measurement of pressure distribution along the chord.

Measurements were made of the velocity distribution normal to the surface

of the foil at points along the chord for several angles of attack and

two Reynolds numbers, using "hot" wire anemometer. The displacement thick-

ness of the boundary layer along the chord was also determined. Following

the dimensions of the actual foil by the displacement thickness and treating

the resulting form as a solid body in potential flow over the model used

for determining the viscous correction in this work. The results of the



solution to potential flow about this altered body was then compared with the experimentally determined pressure distribution. Comparison of the limited amount of data with theoretical predictions is not conclusive, but suggests that with improved instrumentation, this relatively straightforward procedure will be successful.



relation to potential flow about this altered body was then compared with the experimentally determined pressure distribution. Comparison of the listed amount of data with theoretical predictions is not conclusive, but suggests that with improved instrumentation, this relatively straightforward procedure will be successful.

The purpose of this investigation was to determine the effect of the shape of the body on the pressure distribution. The results of the investigation are presented in the following sections. The first section is a description of the experimental apparatus. The second section is a description of the results of the investigation. The third section is a discussion of the results. The fourth section is a conclusion. The fifth section is a list of references.

The experimental apparatus consisted of a water tunnel, a body of revolution, and a pressure measuring system. The water tunnel was of the closed-circuit type, and was operated at a flow rate of 100 gpm. The body of revolution was of the type known as a "bullet" shape, and was made of brass. The pressure measuring system consisted of a series of pressure taps, connected to a series of manometers. The pressure taps were located at various points along the length of the body, and the manometers were connected to these taps by means of small diameter tubes. The results of the investigation are presented in the following sections.

The first section is a description of the experimental apparatus. The second section is a description of the results of the investigation. The third section is a discussion of the results. The fourth section is a conclusion. The fifth section is a list of references.



### ACKNOWLEDGMENTS

The author expresses his appreciation for the contributions of Professor J. E. Kerwin, Thesis Supervisor, who first aroused my interest in viscous effects on Marine Propeller and foil design, and to Professor Hal L. Moses, for his help on the subject of boundary layers.

I am particularly grateful to Professor J. Micknell for his guidance in the wind tunnel work and to Messers, Massamouth, Christensen, and Herbert Johnson of the various gas turbine laboratory shops, for their help in building the model.

I wish to thank Lieutenant Peter Bergen, RCN, Lieutenant Millard Fitchamph, USN, Lieutenant Robert Cheney, USN, and Lieutenant Paul Amos, USN, all of whom assisted me in the wind tunnel, and without whose help I would have been unable to operate the tunnel.

Finally, I would like to thank Mrs. Joyce Edwards, Jr., who spent several weeks in the wind tunnel taking data with me at night and who has patiently deciphered my "rough drafts" in typing this thesis.



APPENDIX

The author expresses his appreciation for the contribution of  
Professor J. E. Davis, Thesis Supervisor, who first proposed the  
and in various efforts on thesis preparation and final design, and to  
Professor J. E. Davis, for his help in the subject of boundary layers.  
I am particularly grateful to Professor J. E. Davis for his guid-  
ance in the wind tunnel work and in the design, construction,  
and testing phases of the various gas turbine laboratory shops, for  
their help in building the model.

I wish to thank Lieutenant Peter Bergan, MS, Lieutenant William  
Pierobon, MS, Lieutenant Robert Gentry, MS, and Lieutenant Paul Rogers,  
MS, all of whom assisted me in the wind tunnel, and without whose help  
I would have been unable to operate the tunnel.  
Finally, I would like to thank Mrs. Joyce Edwards, Jr., who spent  
several weeks in the wind tunnel taking data with me at night and who  
has patiently deciphered my "rough drafts" in typing this thesis.



## TABLE OF CONTENTS

	<u>PAGE</u>
ABSTRACT .....	2
ACKNOWLEDGMENTS .....	4
TABLE OF CONTENTS .....	5
LIST OF FIGURES .....	7
 I. INTRODUCTION	
A. BACKGROUND .....	9
B. STATEMENT OF THE PROBLEM .....	11
C. OBJECTIVES .....	12
 II. PROCEDURE	
A. EXPERIMENTAL APPARATUS .....	14
1. PAUL BURNIN .....	14
2. DESIGN OF THE TEST SECTION .....	16
3. MEASURING APPARATUS .....	16
4. SET UP PROCEDURE .....	19
B. EXPERIMENTAL METHOD .....	20
C. ANALYSIS OF THE DATA .....	25
1. BOUNDARY LAYER DETERMINATION .....	25
2. CALCULATION OF THE WRENNING COEFFICIENTS .....	30
 III. RESULTS	
A. RESULTS OF THE BOUNDARY LAYER MEASUREMENTS .....	32
B. RESULTS OF THE WRENNING COEFFICIENT MEASUREMENTS ..	34
C. RESULTS OF STREAMLINE PLOTS .....	36
D. CARBON BLACK TRACKS .....	37





IV.	DESCRIPTION OF MODEL	
A.	GENERAL .....	39
B.	BOUNDARY LAYER PROFILES .....	41
C.	EXAMINATION OF POTENTIAL FLOW CALCULATIONS WITH CORRECTED FORMS .....	46
V.	CONCLUSIONS .....	49
VI.	RECOMMENDATIONS FOR FURTHER STUDY .....	51
VII.	BIBLIOGRAPHY .....	53
VIII.	APPENDIX .....	55
A.	TABLE OF DATA	
B.	GRAPHS OF DATA	
C.	COMPUTER OUTPUTS	





LIST OF FIGURES

	<u>PAGE</u>
FIGURE 1. DETAIL OF PRESSURE TAPS .....	15A
FIGURE 2. DETAIL OF END WALLS .....	15B
FIGURE 3. BOUNDARY LAYER RAKE .....	17A
FIGURE 4. INCLINED MANOMETER BANK .....	17A
FIGURE 5. AUXILIARY BOUNDARY LAYER RAKE .....	17A
FIGURE 5A. AUXILIARY STATIC PROBES .....	17A
FIGURE 6. BOUNDARY LAYER RAKE AND MANOMETER .....	17A
FIGURE 7. INCLINED MANOMETER IN POSITION .....	20A
FIGURE 8. INDIRECT READING MANOMETER .....	20A
FIGURE 9A. RAKE IN POSITION SHOWING "STRIPATUBE" .....	20A
FIGURE 9B. RAKE POSITIONED ADJACENT TO STATIC TAPS .....	20A
FIGURE 10A. FOIL IN TEST SECTION SHOWING STANCHION .....	25A
FIGURE 10B. FOIL IN TEST SECTION SHOWING ADDITIONAL TUBES FROM AUXILIARY RAKE .....	25A
FIGURE 11. CARBON BLACK TRANSITION TESTS .....	25A
FIGURE 12. CHORD WISE DISPLACEMENT THICKNESS DEVELOPMENT .. $\alpha = 0.0^\circ$	B1
FIGURE 13. CHORD WISE DISPLACEMENT THICKNESS DEVELOPMENT .. $\alpha = 2.0^\circ$	B2
FIGURE 14. VELOCITY PROFILES FOR $\alpha = 0^\circ$ , $Re = 3.67 \times 10^6$ .. Top Surface	B3
FIGURE 15. VELOCITY PROFILES FOR $\alpha = 0^\circ$ , $Re = 3.67 \times 10^6$ .. Bottom Surface	B4
FIGURE 16. VELOCITY PROFILES FOR $\alpha = 2^\circ$ , $Re = 3.67 \times 10^6$ .. Top Surface	B5
FIGURE 16A. VELOCITY PROFILES FOR $\alpha = 2^\circ$ , $Re = 3.67 \times 10^6$ .. Bottom Surface	B6



APPENDIX

101	.....	101	.....
102	.....	102	.....
103	.....	103	.....
104	.....	104	.....
105	.....	105	.....
106	.....	106	.....
107	.....	107	.....
108	.....	108	.....
109	.....	109	.....
110	.....	110	.....
111	.....	111	.....
112	.....	112	.....
113	.....	113	.....
114	.....	114	.....
115	.....	115	.....
116	.....	116	.....
117	.....	117	.....
118	.....	118	.....
119	.....	119	.....
120	.....	120	.....
121	.....	121	.....
122	.....	122	.....
123	.....	123	.....
124	.....	124	.....
125	.....	125	.....
126	.....	126	.....
127	.....	127	.....
128	.....	128	.....
129	.....	129	.....
130	.....	130	.....
131	.....	131	.....
132	.....	132	.....
133	.....	133	.....
134	.....	134	.....
135	.....	135	.....
136	.....	136	.....
137	.....	137	.....
138	.....	138	.....
139	.....	139	.....
140	.....	140	.....
141	.....	141	.....
142	.....	142	.....
143	.....	143	.....
144	.....	144	.....
145	.....	145	.....
146	.....	146	.....
147	.....	147	.....
148	.....	148	.....
149	.....	149	.....
150	.....	150	.....

	<u>PAGE</u>
FIGURE 17. VELOCITY PROFILES FOR $\alpha = 0^\circ$ , $Re = 5.45 \times 10^6$ .. Top Surface	B7
FIGURE 17A. VELOCITY PROFILES FOR $\alpha = 0^\circ$ , $Re = 5.45 \times 10^6$ .. Bottom Surface	B8
FIGURE 18. WAKE SURVEYS AT $0.0^\circ$ .....	B9
FIGURE 19. WAKE SURVEYS AT $2.0^\circ$ .....	B10
FIGURE 20. EXPERIMENTAL PRESSURE DISTRIBUTION ALONG CHORD OF NACA 66 AIRFOIL .....	B11
$\alpha = 0.0^\circ$ , $Re = 3.67 \times 10^6$	
FIGURE 21. TOP SURFACE PRESSURE DISTRIBUTION WITH RAKE ON THE SURFACE .....	B12
FIGURE 22. POTENTIAL THEORY PREDICTION FOR PRESSURE DISTRIBUTION AROUND NACA 66 AIRFOIL .....	B13
$\alpha = 0.0^\circ$ , $Re = 3.67 \times 10^6$	
FIGURE 23. EXPERIMENTAL PRESSURE DISTRIBUTION ALONG THE CHORD OF A NACA 66 AIRFOIL .....	B14
$\alpha = 0.0^\circ$ , $Re = 5.45 \times 10^6$	
FIGURE 24. EXPERIMENTAL PRESSURE DISTRIBUTION ALONG THE CHORD OF A NACA 66 AIRFOIL .....	B15
$\alpha = 2.0^\circ$ , $Re = 3.67 \times 10^6$	
FIGURE 25. POTENTIAL THEORY PREDICTION FOR PRESSURE DISTRIBUTION AROUND NACA 66 AIRFOIL .....	B16
$\alpha = 2.0^\circ$ , $Re = 3.67 \times 10^6$	
FIGURE 26. MOMENTUM THICKNESS VERSUS CHORD FOR THE TOP SURFACE .....	B17
$\alpha = 0.0^\circ$ , $Re = 3.67 \times 10^6$	





## I. INTRODUCTION

### A. Background

As the design of high performance marine propellers and hydrofoils has become more exact, the desire to investigate all of the mechanisms of efficiency loss has naturally increased. One of the most evasive of these loss mechanisms is that of viscosity. It is obvious that viscosity, both molecular viscosity and the virtual or eddy viscosity arising in turbulent flow, contribute to the drag of the foil by providing for transfer of energy from the foil to the medium in which it operates, thereby increasing the power required to move the foil through this medium. A little less obvious is the fact that due to the way we have chosen to treat the motion of the foil mathematically, viscosity causes a discrepancy between the pressure distribution as we calculate it and what is actually measured in experiment.

In order to make the solution of the flow about a lifting form tractable, we choose not to solve the Navier Stokes Equations in all their glory, but rather by applying the unrealistic boundary condition of 100% slip at the boundary, we use Laplace's Equation for solving the so-called potential flow and apply the Kutta Condition at the trailing edge of the form to prevent the solution from giving results which we have observed do not occur, i.e. flow across the trailing edge. However, at the Reynolds Numbers around which these lifting surfaces operate, experiments indicate that there is a region around the foil where viscous effects are noticeable and in fact are of the same order of magnitude as the inertia forces. Thus, the existence of the boundary or shear layer around





the foil must be acknowledged if the artifice of potential theory is used to estimate flow behavior near the foil. The boundary layer is defined as the region quite near the surface of the foil where the velocity varies from zero at the surface to some high fraction of the velocity predicted by potential theory; in this thesis 0.992 has been chosen for this fraction. The flow then does not actually encounter the boundaries of the solid body as predicted by potential theory but it is assumed that it encounters boundaries which include the virtual thickness of the boundary layer, which allows no flow, i.e. displacement thickness. This change in the effective shape of the body then must change the lift since potential flow theory predicts a lift coefficient which is a function of geometry only. The boundary layer generally grows unsymmetrically about the nose-tail line of the foil and therefore moves the center of the trailing edge in the direction of the thickest surface boundary layer. This effectively changes the angle of attack of the section which the flow encounters causing an additional change in lift.

Limited experiments pursuing the determination of viscous effects on the lift of airfoil sections have been carried out by Pinkerton (1), Preston (2), Schneider (3), and Spence (4). In fact as far back as 1933, investigations were made into boundary layer development along two dimensional airfoils by Stuper (5). These experiments have been limited to foils of large thickness. However, for lack of better information, the results of these investigations have been used in the prediction of viscous effects in the design of thin marine propeller and hydrofoil sections, if viscous effects on the lift of these devices is considered





at all. Leopold (6), suggests that the above procedure is fallacious and proposes that since the boundary layer development on the surface of a foil is strongly dependent on the pressure distribution ( $\frac{dp}{dx}$ ) and chord-wise Reynolds Number, the effects of thickness and Reynolds Number must indeed be incorporated in any consideration of lift alteration due to viscosity. Leopold recommends that the boundary layer on the surface of the foil be calculated using an approach developed by Moses (7), which has been programmed to accept the surface velocities predicted by potential theory, then the displacement thickness,  $\delta^* = \int_0^{\delta} (1 - \frac{v}{V}) dy$  around the section is incorporated in the linear theory to predict the lift of the section in viscous flow. The concluding sections of Leopold's work recommend experimental work oriented toward establishing the validity of this approach.

#### B. STATEMENT OF THE PROBLEM

A proposed theory then exists for the determination of viscous lift correction which would be useful in the design of all foil sections but which is particularly applicable to foils used in Marine designs. However, no experimental work is available to uphold the theory. Errors may exist due to the difficulty in exactly stipulating the behavior of turbulent boundary layers in pressure gradients, and it is by no means clear that the pressure distribution around a body in viscous flow can be exactly modeled by the pressure distribution resulting from calculating the potential flow around the body "corrected" by  $\delta^*$ . This method is, at best, an iterative approximation to the complicated Navier-Stokes Equations. The problem then, is first, to determine whether the measured





boundary layer thickness or more correctly, displacement thickness, when added to the dimensions of a foil, produces a shape whose potential flow solution for pressure distribution conforms to the measured pressure distribution. Second, since most algorithms for solving the turbulent boundary layer problem are accurate only for particular types of flow, i.e. (some breakdown in strong adverse pressure gradients, others in favorable gradients), the applicability of the boundary layer calculation chosen by Leopold must be checked in this particular physical situation. Perhaps the most elusive factor is the effect of the location of laminar-turbulent transition on both surfaces. The position of transition is extremely difficult to predict and is dependent on such parameters as surface roughness, turbulence level of the oncoming flow, and perturbations caused by vibration, in addition to the parameters which we feel we have reasonable ability to predict ( $dp/dx$  and  $Re_x$ ). The thickness of the boundary layer toward the trailing edge and its effect on the angle of attack of the adjusted form is highly dependent on the transition point on each surface as well as on the relative transition points on the top and bottom surfaces.

### C. OBJECTIVES

The objective of this thesis was to build and instrument a model of an extremely thin, low camber two dimensional section of a marine propeller or hydrofoil, measure the pressure distribution at reasonably high Reynolds Numbers and simultaneously measure the velocity distribution normal to the surface at points along the chord on both the pressure and suction sides. The dimensions of the foil were then to be





increased by the value of  $\zeta^*$  gotten from the experimental results. Now, with the offsets of this altered form, the pressure distribution around it was to be calculated, using the most convenient and accurate potential theory type calculation. The computer program organized by T. Brockett (8) was used for this purpose, rather than linear theory as recommended by Leopold (6). The pressure distribution obtained from this calculation was then to be compared with that which was experimentally determined. The boundary layer measurements were to be compared with results of the calculations due to Moses (7), as modified by Leopold (6).





## II. PROCEDURE

### A. EXPERIMENTAL APPARATUS

The primary requirement of this experiment was to be able to measure accurately, (1) the chord-wise pressure distribution and (2) the velocity distribution in the boundary layer. These items were to be obtained at as high a Reynolds Number as is experienced by the 0.7 radius section of a marine propeller. This Reynolds Number is approximately  $10^7$ . The requirement for the test piece was that it be a reasonable model of a standard two dimensional foil section used in the design of propellers and hydrofoils.

#### 1. FOIL DESIGN

The foil chosen was a NACA 66 modified nose and tail airfoil. The thickness ratio was to be 0.0333. A 1.0 mean line with 2% camber with a chord length of 60 inches was planned. Strength calculations were made, based on uniform lift along a 7 foot span with simple supports, and the results appeared marginal. The span was originally chosen to fit the vertical dimension of the test section of the Wright Brother's Wind Tunnel. Since it appeared that conventional foil construction methods would result in danger of structural failure at high Reynolds Numbers and high angles of attack as well as excess flexibility which might permit fluttering vibrations, it was decided to construct the foil of solid Honduras Mahogany reinforced in the span-wise direction by steel tubes. For reasons of economy, the span was reduced to four feet. Even with this modest span, robust construction was still necessary. Static pressure taps were installed in the upper and lower





surfaces by drilling down to the span-wise tubes and filling the holes with Epoxy. After the surface of the Epoxy was finished flush with the surface of the foil, 0.035 inch holes were drilled into the Epoxy normal to the surface and down into the tubes. The leading and trailing edges were milled out of solid aluminum, and fitted into the wooden part of the foil with steel keys.

The method of getting the pressure readings out of the wing as originally planned, appeared simple but, did not work out satisfactorily (Fig. 1). The center of each span-wise tube was plugged; effectively dividing each one into two tubes. The pressure taps were drilled down offset from the center of the span so that the upper and lower taps entered the tubes on either side of the plugs. This arrangement would allow the suction side pressures to be taken from one side of the foil and the pressure side from the other, thereby obtaining twenty-six pressure readings with only thirteen tubes. Unfortunately rendering the center plugs in the tubes air tight turned out to be impossible, and an alternate plan was used.

Galvanized steel sheet end plates were bolted to the ends of the foil. The ends of the pressure take-off tubes were threaded and used as fastenings for the end plates. The plates were used to cover the openings in the end walls of the test section which were required to allow the pressure tubes to swing in a  $10^\circ$  arc. They also served the purpose of housing bolts to hold the foil in position at various angles of attack (Fig. 2).



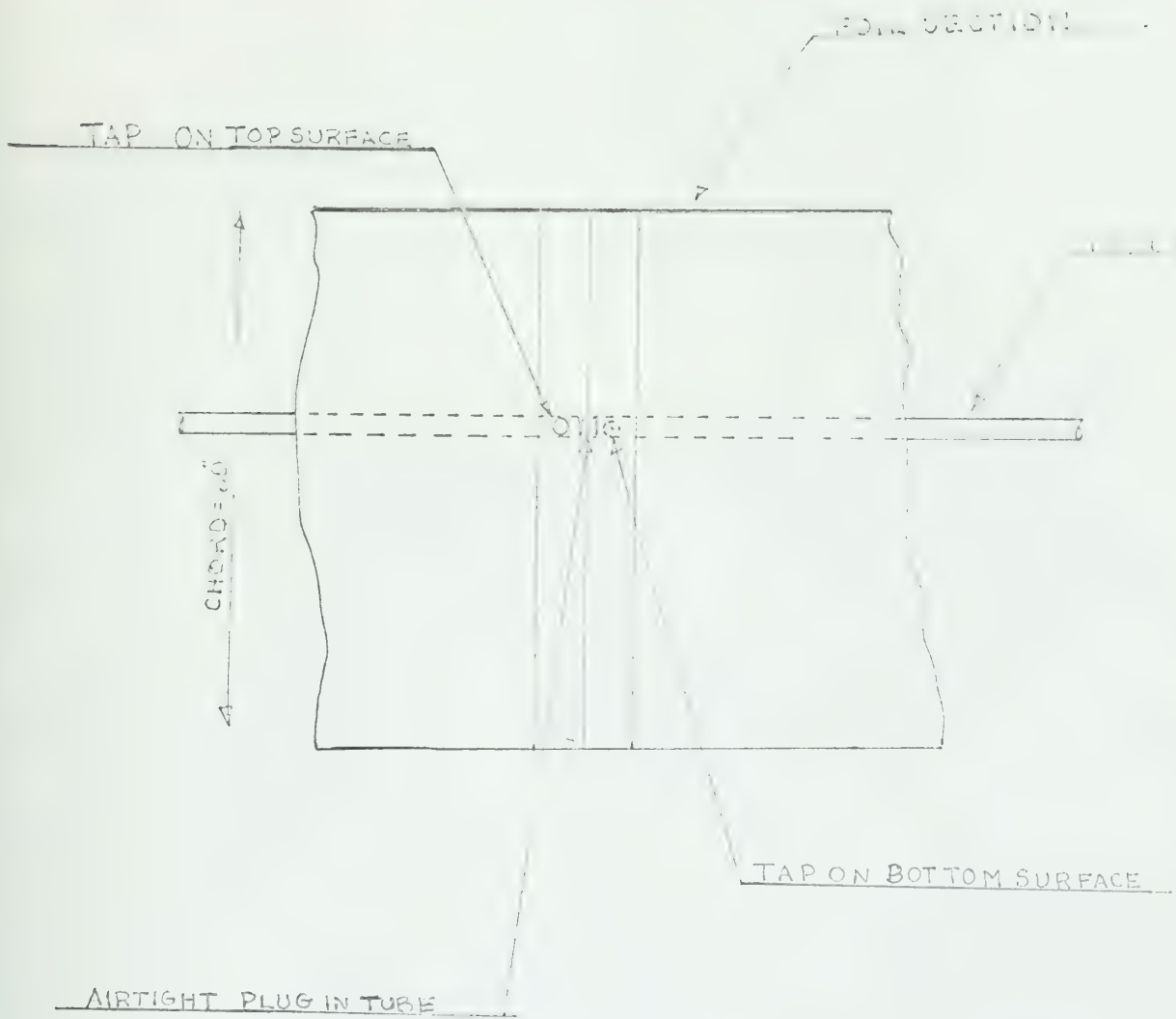


FIG. 1  
DETAIL OF PRESSURE TAPS





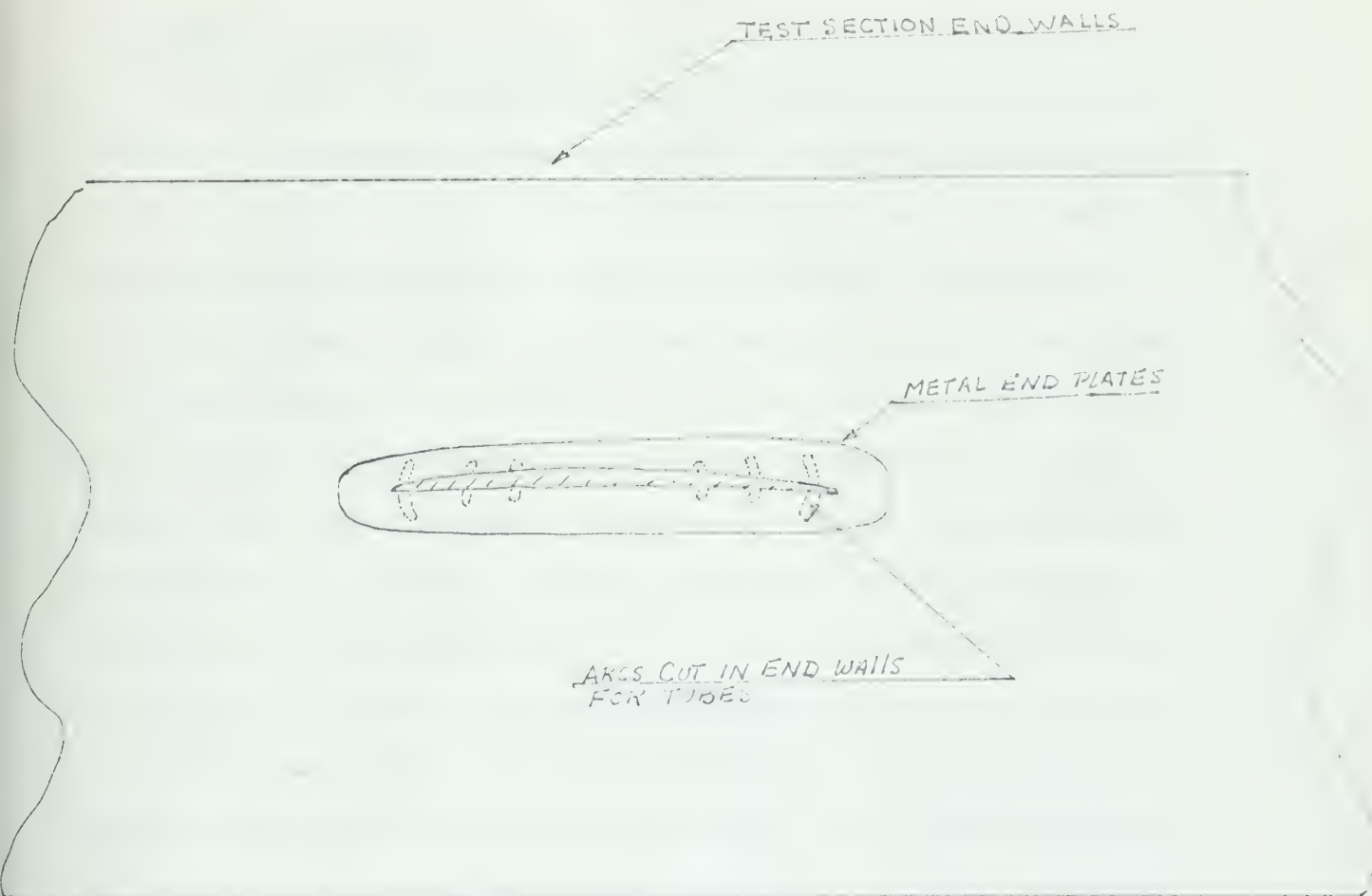


FIGURE 2.  
END PLATES AND END WALLS





## 2. DESIGN OF THE TEST SECTION

The originally planned seven foot span would have enabled the test section of the Wright Brothers Wind Tunnel to be used without significant alteration. However, when the four foot span section was built instead, an elaborate test section was necessitated. The foil was to be placed horizontally in the tunnel between end walls which would span the entire length and height of the tunnel test section. These walls were fabricated from sections of fibre board fastened to foundations bolted to the tunnel overhead. The center of the fabricated test section had circular arcs cut into it which would allow all of the protruding pressure tubes to swing freely when the angle of attack of the section was changed. The part of the end walls into which the foil was fitted was given additional bracing, and metal bearing plates were bolted to them to accept the pivotal tube of the airfoil. The overall dimensions of the test section were  $7\frac{1}{2}$ ft. high by 16ft. long with 4ft. between the end walls. The walls were toed out at the trailing edge by  $\frac{3}{8}$ in. on each side to compensate for the nozzle effect caused by the development of a boundary layer along the test section. The amount of toe-out was determined by a simple flat plate turbulent boundary layer calculation for  $\delta^*$ .

## 3. MEASURING APPARATUS

As mentioned in section 1, airtight plugging of the centers of the pressure tubes was not successful, therefore, the neoprene tubing from both sides of these tubes was connected to "T" joints and single tubes from the "T"s were connected to thirteen of the openings of a twenty-four



tube inclined manometer bank. Top and bottom pressures were measured on separate runs. When not in use, the holes of either suction or pressure sides were covered with a single long strip of very fine transparent tape.

The total pressure readings in the boundary layer on the surface of the foil were taken using a ten tube rake, built by the Aerodynamics Projects Laboratory (Fig. 3). The top tube of this rake was a static tube; the remaining nine tubes were total pressure tubes ranging in distance from the surface from 0.02in. to 1.0in. The tubes had elliptical openings to aid resolution. The dimensions of the tube openings were: major axis 0.03in., minor axis 0.01in. The major axis was parallel to the surface. The tubes connecting the rake to the manometer are called by the brand name "Stripatube" and the ten tubes come in a single strip with overall dimensions  $1/8$ " by  $2\frac{1}{2}$ " wide. The strip was led aft over the trailing edge down to a stanchion mounted on the tunnel floor, down the stanchion, along the tunnel floor and thence out of the test section to ten of the tubes on the inclined manometer bank (Fig. 4). The purpose of the stanchion was to reduce the angle at which the Stripatube fell away from the foil surface, thereby reducing drag on the tubing and hence eliminating the possibility of having the rake removed from the surface in the middle of a run. An additional total pressure rake was used in regions where the boundary layer thickness exceeded 0.8 inches. It consisted of two total pressure tubes approximately 1.25 inches and 1.50 inches above the surface. These tubes also had elliptical openings with the major axis parallel to the surface of the foil (Fig. 5).







FIG. 3  
WAKE SURVEY RAKE



FIG. 4  
AUXILIARY BOUNDARY LAYER RAKE



FIG. 5  
AUXILIARY STATIC PROBE

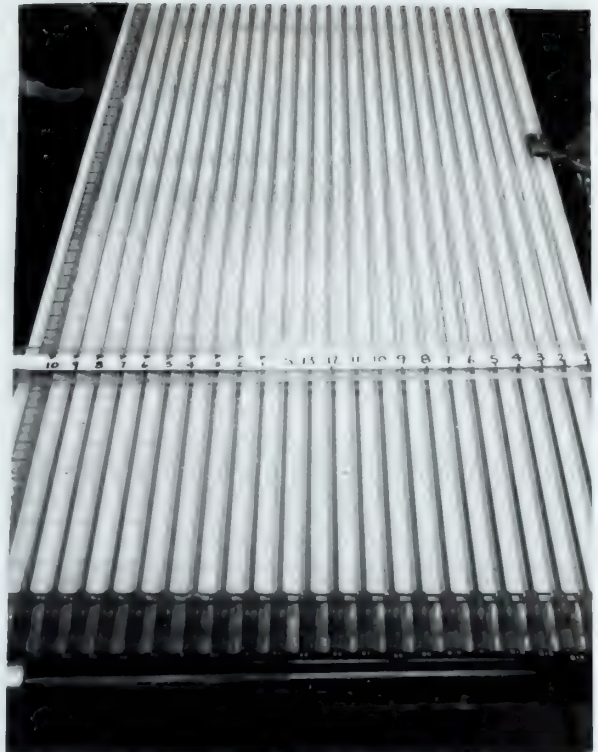


FIG. 6  
INCLINED MANOMETER



WAKE SURVEY RAKE AND VERTICAL  
MANOMETER

FIG. 7



A pitot-static tube was mounted in the test section about five feet ahead of the foil. The tubes were led to an indirect reading manometer at the control board of the wind tunnel. A tee joint was placed in the static pressure tubing from the probe and a tube was led from it to the inclined manometer table so that the tunnel static pressure ( $P_{stat \infty}$ ) could be readily compared with the static pressures along the surface of the foil, which are also displayed on the inclined manometer bank.

Surveying the boundary layer just aft of the trailing edge required the use of an additional rake. This one consisted of alternating groups of three total pressure tubes and one static tube (Fig. 6). Only twenty of the tubes were read. The entire rake was moved up and down, traversing the wake in intervals of 0.1 to 0.2 inches. The tubes from this rake were led to a vertical manometer in the tunnel control room. This rake was simply bolted to the floor of the tunnel just behind the foil and adjusted by hand between runs.

An inclined manometer obtained from the Gas Turbine Laboratory was set up at an angle with the floor of  $14.5^\circ$ , giving an amplification factor of 4.0 to the readings (Fig. 7). The fluid used was Meriam Oil with a specific gravity of 0.827 at  $60^\circ\text{F}$ . The columns on the inclined manometer are numbered 1 thru 13 for the the thirteen static taps. "S" is the tunnel static lead and numbers 1 thru 10 are the leads from the rake. The indirect reading manometer was of the inclined type with a vernier scale for adjusting the height of the inclined section (Fig. 8). It was filled with alcohol whose specific gravity was 0.806. The vertical manometer used for the wake survey also used alcohol of the same specific gravity (Fig. 6).





#### 4. SET UP PROBLEMS

The main difficulty rested in the design of the foil section. The experiment would not be particularly meaningful if the section tested were not a "thin" section. Also, large span was considered necessary to remove the possibility of end effects disturbing the boundary layer at the center section. The combination of large span and small cross sectional moment of inertia introduced a considerable strength problem. In addition, the small thickness introduced obvious construction difficulties. After conversing with several sheet metal fabricators, the idea of building the foil in a manner similar to a conventional wing, using ribs and frames with sheet metal covering, was abandoned by the author. This was unfortunate, since excellent instrumentation of this type of model could have been obtained. The method of building the foil of chord-wise strips of mahogany fitted over steel tubes was adopted. The installation of the pressure tubes seemed simple and foolproof. However, the finished surfaces of the Epoxy plugs were unsatisfactory in many instances due to the inclusion of small bubbles, and no amount of wet sanding seemed to help. Drilling the 0.035 holes through the plugs, regardless of how carefully done, heated some of the plugs enough to cause them to bulge slightly above the surface of the foil. Any small discontinuity in the surface can obviously make static pressure measurements inaccurate.

The foil itself, when returned by the model maker had several discrepancies. The foil did not conform to the template supplied by the author. It was in fact, drastically thinner and had greater camber.



The exact dimensions of the foil were obtained by the author, using a clay impression. It had been planned to leave the center section of the three sections of the leading and trailing edges unattached to the foil except by the key. This was to enable the author to further instrument the leading and trailing edges. Unfortunately the model maker misunderstood and returned the foil solidly together in all aspects. As a result, a rather crude job was done in getting pressure readings from the leading and trailing edges.

## B. EXPERIMENTAL METHOD

With the model set up in the tunnel at the desired angle of attack, the rake was attached to the surface of the foil using pieces of tape. The leading edges of the tape were blended to the foil surface using fine Scotch Tape. The rake was always positioned with the openings of its static tube on the same chord-wise line as a surface static tap (Fig. 9). This facilitated comparison between the surface static pressure and the static pressure at the edge of the boundary layer. In regions of separated flow or where large streamline curvature existed, no significant correlation was expected. The total pressures and static pressures from the rake, the static pressures on the foil surface and the tunnel static pressure upstream of the wing were read on the inclined manometer. The tunnel velocity head was measured on the indirect reading manometer.

Twelve runs were made on each foil surface, coinciding with twelve of the thirteen surface taps. The rake could not be placed far enough back on the trailing edge to get a run for a position corresponding to number thirteen surface tap.







FIG. 7  
INSTANTANEOUS MAN METER IN POSITION

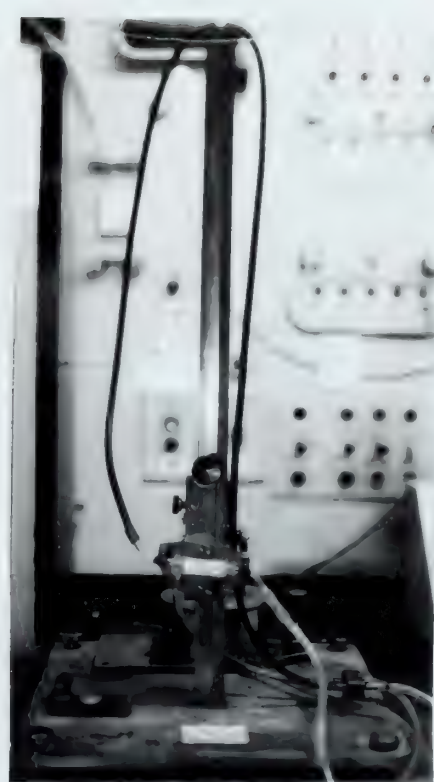


FIG. 8  
DIRECT READING MAN METER  
FOR MEASURING TUNNEL VELOCITY



FIG. 9  
PUMP IN POSITION FOR THE  
DYNAMIC INVESTIGATION



FIG. 10  
RATE OF CHANGE RELATIONSHIP  
STATIC CASE



Each of the runs actually were made at slightly different Reynolds Numbers, since the tunnel velocity would not return to the same value after the tunnel was shut down for repositioning the rake for the next run.

However, the difference in the velocity head for the various runs amounted to, at most, 0.06 inches of fluid of specific gravity 0.806, which is equivalent to 1.1 feet per second. This, obviously has little effect on Reynolds Number and therefore no loss in accuracy of the measurements of viscous phenomena is expected.

The runs were to be made on both surfaces of the foil. And the original plan was to take measurements at five different angles of attack and at two Reynolds Numbers. This amounts to 240 runs. Since, the total pressure tubes on the boundary layer took close to thirty-five minutes to steady down, and since it was necessary to measure the heights of the rake tubes above the foil surface and carefully reposition the rake after each run, bringing the total "run time" to about forty-five minutes, it was not possible to make nearly the number of measurements originally planned. When it was necessary to leave the wind tunnel, the following information had been obtained:

a.) At zero angle of attack:

1. Total head profiles at 23 stations  
(11 on the suction side and 12 on the pressure side,  
at a Reynolds Number of  $3.67 \times 10^6$ )
2. Total head profiles at 12 stations  
(6 on the suction side and 6 on pressure side,  
at a Reynolds Number of  $5.45 \times 10^6$ )





3. Wake surveys of total and static pressures at both Reynolds Numbers
4. Static pressures at the surface of the foil for both Reynolds Numbers.
5. Rough ideas of the location of transition from laminar to turbulent flow using lampblack traces.

b.) At  $+2^\circ$  angle of attack

1. Same as number (1.) above
2. Wake survey at a Reynolds Number of  $3.67 \times 10^6$
3. Static pressure at the surface for Reynolds Number of  $3.67 \times 10^6$ .

c.) At  $+5^\circ$  and  $-4^\circ$  angle of attack

1. Only total head profiles on the top surface of the foil at Reynolds Number of  $3.67 \times 10^6$  at 12 stations

At zero angle of attack, surface pressures on the foil were recorded every time a total pressure profile was measured. This was necessary only to determine how positioning of the rake along the chord affected the chord-wise pressure distribution. It was found that, with the rake in position on the foil, the pressure distribution was slightly greater in magnitude and shifted along the chord toward the trailing edge. But the differences between the distributions were small and the slopes were essentially the same, so no noticeable effects on the boundary layer development were expected. This practice was then discontinued since it was time consuming and did not produce any additional meaningful data. It should be noted that the effect of moving the rake along the foil was



extremely small and differences were noticed only between the conditions of the rake on or the rake off, regardless of position.

The surface static pressure readings on the leading and trailing edge sections were measured using a variety of small probes since only the top surface tap on the trailing edge was airtight. A small 0.03% O.D. tube, with an 81 gage hole drilled into its surface was designed in such a way that it would have the same curvature as the leading edge, and its orifice would be in the same position as the proposed surface tap. It was placed on the leading edge and fastened to the surface with tape. Before using it, the probe was placed on the same chord-wise line as several other of the static taps and the readings were compared. Agreement of the readings obtained using the two different sources was good. The measured differences were of the order of 0.02% inches of Meriam Oil, with a total reading of 4.00 inches.

A similar tube was used to obtain the static pressures around the trailing edge. The only difference was, that the probe used on the trailing edge had a 90° angle bend close to the end so that readings could be taken within 1.0 inches of the trailing edge without having a plastic tube projecting beyond the foil. These readings did not seem to be steady and reliable and as a result, were not exploited. This was unfortunate, since after plotting the resulting pressure coefficients, the ones obtained with this probe seemed to fair in nicely with other data. More information about the trailing edge static pressures would have helped make a more intelligent explanation of the observed boundary layer development in this region.



...and the ... of the ...

...the ... of the ...

...the ... of the ...

...the ... of the ...

...the ... of the ...

...the ... of the ...

...the ... of the ...

...the ... of the ...

...the ... of the ...

...the ... of the ...

...the ... of the ...

...the ... of the ...

...the ... of the ...

...the ... of the ...

...the ... of the ...

...the ... of the ...

...the ... of the ...

...the ... of the ...

...the ... of the ...

...the ... of the ...

...the ... of the ...

...the ... of the ...

...the ... of the ...

...the ... of the ...

...the ... of the ...

...the ... of the ...

A brief review of the overall procedure is as follows:

1. Test the system for leaks.
2. Position the rake adjacent to a static tap.
3. Light-off the wind tunnel and obtain the desired speed.
4. Read the inclined manometer when steady.
5. Read indirect reading manometer for tunnel velocity upstream.
6. Shut down tunnel.
7. Measure and record the rake tube heights.
8. Reposition the rake.
9. Repeat this until top and bottom surfaces have been traversed at the required angle of attack.
10. Change the angle of attack and repeat items 1. through 9. Checks were made for leaks on the static tubes after changing the angle of attack because the static pressure leads were often disturbed by the tubes swinging through the arc cut in the end walls.
11. After obtaining all the desired total pressure surveys on the surface, remove the rake and Stripatube support stanchion. Install wake survey apparatus.
12. Read total and static pressure in the wake on vertical manometer.
13. Reposition rake vertically. Repeat readings until reasonable coverage of a region 2.0 inches above and below the foil is obtained.
14. Obtain surface static pressure readings for both surfaces at required angles of attack using the surface tap and probes and

... ..

[illegible]

6.6. The following table shows the number of people who have been convicted of a crime in the past 10 years, by age group and gender.

0.15 m/s. The mean velocity of the flow was 0.15 m/s.



reading the results on the inclined manometer. These readings were taken without any tubes or other apparatus on the foil surface.

## C. ANALYSIS OF THE DATA

### 1. BOUNDARY LAYER COMPUTATION

The previous section outlines the general data which was obtained by the end of the experiment. The information on the foil at  $0.0^\circ$  angle of attack was most important. At each of the stations on both surfaces (the stations coincide with the surface taps) there is a series of ten or twelve total head measurements at various distances from the surface of the foil. There were two static pressures available for obtaining the dynamic head in these profiles. One of these was read on the top tube on the rake and the other measured at the adjacent surface static tap. After plotting the pressure coefficients along the chord obtained from both the rake and the static taps, and noting that the difference between the coefficients was small, it was decided to use the reading on the rake static tube for boundary layer calculations. The foil has such low curvature that it is doubtful that any appreciable pressure drop across the boundary layer  $dp/dr = \rho v^2/2$  is to be expected except right on the leading edge, and no attempt was made to obtain total head measurements very close to the nose of the foil. In computing the dynamic heads in the boundary layer then, a constant local  $h$  static was subtracted from the measured total pressure:  $h(\text{dynamic}) = h(\text{total}) - h(\text{static local})$ .

To insure that the top probes of the boundary layer rake were indeed out of the layer, the total head measured at the topmost total head



...the ... ..

...the ... ..

...the ... ..

...the ... ..

...the ... ..

...the ... ..

...the ... ..

...the ... ..

...the ... ..

...the ... ..

...the ... ..

...the ... ..

...the ... ..

...the ... ..

...the ... ..

...the ... ..

...the ... ..

...the ... ..

...the ... ..

...the ... ..

...the ... ..

...the ... ..

...the ... ..

...the ... ..

...the ... ..



FIG. 10a  
FOIL IN TEST SECTION SHOWING STANCHION

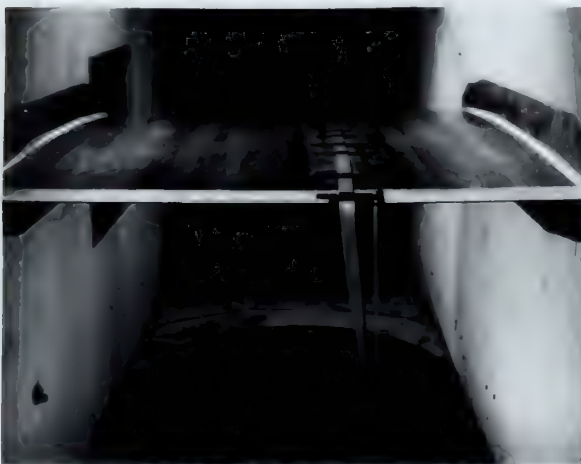
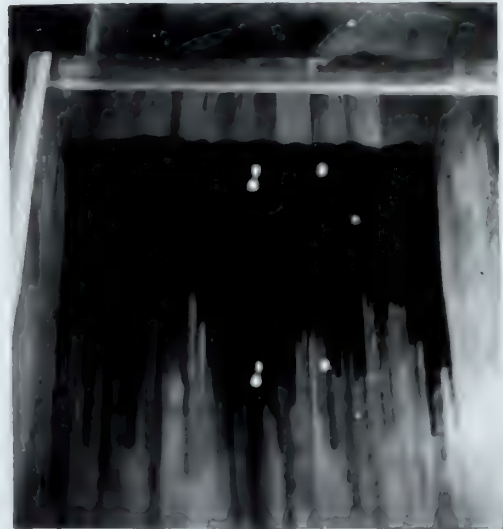


FIG. 10b  
FOIL IN TEST SECTION SHOWING ADDITIONAL  
STRUCTURE FROM SCREWDRIVE BLADE

FIG. 11  
CARBON BLACK TRANSITION TESTS



$\alpha = 2.0^\circ$   $Re = 3.67 \times 10^6$



$\alpha' = 0.0^\circ$   $Re = 7.15 \times 10^6$



tube on the rake was compared with the total head of the stream upstream of the foil section. This was accomplished by converting the dynamic head upstream of the foil (measured on the vertical indirect reading manometer) to the same scale as the inclined manometer. First the inclination must be considered and then of course the difference in specific gravities as follows:

$$h(\text{ind}) \times \frac{\text{spg. of fluid in ind. read. man.}}{\text{spg. of fluid in incl. man.}} \times \frac{1}{\sin(\theta \text{ line})} = h(\text{inclined}) \quad (1)$$

Now with both upstream dynamic head and local total head in the same measurement system, the upstream static head read on the inclined manometer was subtracted from upstream dynamic head. If the total pressure tubes in the top section of the wake are out of the shear layer and in a region of essentially potential flow, then from Bernoulli,  $H_{\text{total}} = C$  thus the two readings must be the same. In this experiment the agreement between the total pressures was usually quite good. Differences of a few hundredths of an inch as read on the inclined manometer were most frequently encountered. The maximum disagreement was 0.15 inches on the inclined manometer. And this amounts to an error of about one percent in the ratio of  $h_{\text{dynamic}}(\text{boundary layer})$  to  $h_{\text{dynamic}}(\text{potential})$ .

After all of the total pressure readings had been corrected for manometer zero, etc., they were compared with the potential flow dynamic head as follows:

$$\frac{h_{\text{dynamic}}(\text{B.L.})}{h_{\text{dynamic}}(\text{Potential})} = \frac{h_{y \text{ total}} - P_{\text{stat}}(\text{local})}{H - P_{\text{stat}}(\text{local})} \quad (2)$$

$v/V$  was then computed by taking the square root of this ratio.

$$v/V = \left[ \frac{h_{y \text{ total}} - P_{\text{stat}}(\text{local})}{H - P_{\text{stat}}(\text{local})} \right]^{1/2} \quad (3)$$





After this calculation is carried out for each total pressure tube reading across the boundary layer, it is possible to plot the non-dimensional boundary layer velocities against distance  $y$ . This was accomplished for all of the stations on the top and bottom surface of the foil at  $0.0^\circ$  and  $\pm 2.0^\circ$  angle of attack.

In order to proceed further into the numerical analysis of the boundary layer, a limit for  $v/V$  must be defined which will be, for the purpose of calculation, the outer edge of the boundary layer. 0.992 has been chosen. This figure is usually applied to the laminar boundary layer where a clear boundary between the viscous and inviscid flow does not exist. Depending on roughness, however, the turbulent layer may have a reasonably distinct boundary. Nonetheless, the figure 0.992 for  $v/V$  was used as an outer limit for both turbulent and laminar layers for no other reason than to standardize the limits of the graphical integration of the velocity profiles.

Since the primary purpose of the experiment was to determine the effect of the boundary layer on the pressure loading of the foil, a quantity must be obtained from the velocity distribution in the shear layer which represents the distance the potential flow streamlines are displaced in "moving around" the low velocity region of the boundary layer. It has been stated earlier that this quantity is called  $\delta^*$  and is defined as

$$\delta^* = (1 - v/V) dy. \quad (b)$$

We call the boundary layer thickness, the region in which  $v/V$  is less than 0.992. We then define  $\delta^*$  as equal to the height which when

The first part of the paper is devoted to the study of the properties of the function  $f(x)$  defined by the equation  $f(x) = \int_0^x f(t) dt$ . It is shown that  $f(x)$  is a constant function, and the value of this constant is determined by the initial condition  $f(0) = 1$ . The second part of the paper is devoted to the study of the properties of the function  $g(x)$  defined by the equation  $g(x) = \int_0^x g(t) dt$ . It is shown that  $g(x)$  is a constant function, and the value of this constant is determined by the initial condition  $g(0) = 1$ .

The third part of the paper is devoted to the study of the properties of the function  $h(x)$  defined by the equation  $h(x) = \int_0^x h(t) dt$ . It is shown that  $h(x)$  is a constant function, and the value of this constant is determined by the initial condition  $h(0) = 1$ . The fourth part of the paper is devoted to the study of the properties of the function  $k(x)$  defined by the equation  $k(x) = \int_0^x k(t) dt$ . It is shown that  $k(x)$  is a constant function, and the value of this constant is determined by the initial condition  $k(0) = 1$ .

The fifth part of the paper is devoted to the study of the properties of the function  $l(x)$  defined by the equation  $l(x) = \int_0^x l(t) dt$ . It is shown that  $l(x)$  is a constant function, and the value of this constant is determined by the initial condition  $l(0) = 1$ . The sixth part of the paper is devoted to the study of the properties of the function  $m(x)$  defined by the equation  $m(x) = \int_0^x m(t) dt$ . It is shown that  $m(x)$  is a constant function, and the value of this constant is determined by the initial condition  $m(0) = 1$ .

The seventh part of the paper is devoted to the study of the properties of the function  $n(x)$  defined by the equation  $n(x) = \int_0^x n(t) dt$ . It is shown that  $n(x)$  is a constant function, and the value of this constant is determined by the initial condition  $n(0) = 1$ . The eighth part of the paper is devoted to the study of the properties of the function  $o(x)$  defined by the equation  $o(x) = \int_0^x o(t) dt$ . It is shown that  $o(x)$  is a constant function, and the value of this constant is determined by the initial condition  $o(0) = 1$ .

The ninth part of the paper is devoted to the study of the properties of the function  $p(x)$  defined by the equation  $p(x) = \int_0^x p(t) dt$ . It is shown that  $p(x)$  is a constant function, and the value of this constant is determined by the initial condition  $p(0) = 1$ . The tenth part of the paper is devoted to the study of the properties of the function  $q(x)$  defined by the equation  $q(x) = \int_0^x q(t) dt$ . It is shown that  $q(x)$  is a constant function, and the value of this constant is determined by the initial condition  $q(0) = 1$ .



subtracted from the actual height of the layer, results in a height which if multiplied by the free stream velocity gives the same flow per unit width as the boundary layer permits.

$$V(\delta - \delta^*) = \int_0^{\delta} v \, dy \quad (5)$$

$$-V\delta^* = -V\delta + \int_0^{\delta} v \, dy \quad (6)$$

$$V\delta^* = \int_0^{\delta} (V - v) \, dy \quad (7)$$

Giving:

$$\delta^* = \int_0^{\delta} (1 - v/V) \, dy \quad (8)$$

To obtain  $\delta^*$ , the velocity profiles were plotted to a large scale on sheets of millimeter cross section paper. The height scale was twenty times the actual height of the boundary layer and the scale for  $v/V$  was spread out over a twenty inch abscissa. The resulting profiles were then mechanically integrated using a planimeter to obtain  $\delta^*$ .

The series of total pressure heads and static readings obtained in the wake survey were treated in a similar manner, and a value for  $\delta^*$  was obtained for the regions of the wake either side of a center line extending back from the center of the trailing edge parallel to the tunnel floor. The values of  $\delta^*$  along the chord of the foil and at the point in the wake,  $x/c = 1.023$ , were plotted versus cord-wise distance/cord length.

The behavior of the boundary layer at the trailing edge was not determined experimentally due to limitations in the measuring devices and is not entirely known but judging from the pressure gradient measured in that region, it must continue to grow rapidly to the trailing edge



Let  $f: X \rightarrow Y$  be a continuous map between topological spaces. Then the image of a closed set under  $f$  is not necessarily closed.

Example: Let  $X = \mathbb{R}$  and  $Y = \mathbb{R}$ . Define  $f: \mathbb{R} \rightarrow \mathbb{R}$  by  $f(x) = \sin(x)$ .

Consider the closed interval  $[0, 2\pi]$  in  $\mathbb{R}$ . Its image under  $f$  is the closed interval  $[-1, 1]$ .

However, the image of the open interval  $(0, 2\pi)$  under  $f$  is the open interval  $(-1, 1)$ .

Thus, the image of a closed set is not necessarily closed.

Another example: Let  $X = \mathbb{R}$  and  $Y = \mathbb{R}$ . Define  $f: \mathbb{R} \rightarrow \mathbb{R}$  by  $f(x) = x^2$ .

Consider the closed interval  $[-1, 1]$  in  $\mathbb{R}$ . Its image under  $f$  is the closed interval  $[0, 1]$ .

However, the image of the open interval  $(-1, 1)$  under  $f$  is the open interval  $(0, 1)$ .

Thus, the image of a closed set is not necessarily closed.

More generally, if  $f: X \rightarrow Y$  is a continuous map, then the image of a closed set is closed if and only if  $f$  is a closed map.

Definition: A continuous map  $f: X \rightarrow Y$  is called a closed map if the image of every closed set in  $X$  is closed in  $Y$ .

Example: Let  $X = \mathbb{R}$  and  $Y = \mathbb{R}$ . Define  $f: \mathbb{R} \rightarrow \mathbb{R}$  by  $f(x) = x^2$ .

Consider the closed interval  $[-1, 1]$  in  $\mathbb{R}$ . Its image under  $f$  is the closed interval  $[0, 1]$ .

However, the image of the open interval  $(-1, 1)$  under  $f$  is the open interval  $(0, 1)$ .

Thus,  $f$  is not a closed map.

Definition: A continuous map  $f: X \rightarrow Y$  is called an open map if the image of every open set in  $X$  is open in  $Y$ .

Example: Let  $X = \mathbb{R}$  and  $Y = \mathbb{R}$ . Define  $f: \mathbb{R} \rightarrow \mathbb{R}$  by  $f(x) = x^2$ .

Consider the open interval  $(-1, 1)$  in  $\mathbb{R}$ . Its image under  $f$  is the open interval  $(0, 1)$ .

Thus,  $f$  is an open map.

Definition: A continuous map  $f: X \rightarrow Y$  is called a homeomorphism if it is a bijection and both  $f$  and  $f^{-1}$  are continuous.

Example: Let  $X = \mathbb{R}$  and  $Y = \mathbb{R}$ . Define  $f: \mathbb{R} \rightarrow \mathbb{R}$  by  $f(x) = x$ .

Then  $f$  is a homeomorphism.

Definition: A topological space  $X$  is called a Hausdorff space if for any two distinct points  $x, y \in X$ , there exist disjoint open sets  $U, V \subset X$  such that  $x \in U$  and  $y \in V$ .

and then fall as the flow around the trailing edge causes the pressure to drop. The wake point indicates that some discontinuity exists in the slope of the  $\psi$  versus  $x/\text{chord}$  curve at the trailing edge. With this in mind the  $\psi$  curve was extrapolated back to the trailing edge, and values for  $\psi$  were obtained from the plots at points on the abscissa corresponding to the required ordinates of the computer program for the potential flow calculation. Ref. (8).

The actual shape of the foil was obtained using a clay impression and the dimensions were listed at the "required ordinate". The displacement thickness values were then added to the dimensions of the foil and an intermediate form determined. The foil dimensions by definition, are symmetrical about the nose tail line at the trailing edge. The boundary layer however, is not, and after adjusting the shape of the foil by  $\psi$  we have a foil which is unsymmetrical about the original nose tail line. The new center of the trailing edge was then determined and the new nose-tail line defined. The end of the nose-tail line now passes through a point whose relative distance to the original center of the leading edge is given by

$$e = \frac{\psi_{\text{top}} - \psi_{\text{bottom}}}{2} \quad (8)$$

The angle of attack used to enter the numerical conformal mapping program must be adjusted accordingly. One additional correction is necessary. The nose-tail line, once shifted due to the unsymmetrical trailing edge thickness, changes the value of the ordinates once again, so all of the dimensions must be corrected by

$$y = x \tan \alpha \quad (9)$$





$$\begin{aligned} y &= x \quad a/c = x/c + c \cdot a/c \\ y &= a \quad x/c \end{aligned} \quad (10)$$

Whether  $y$  is to be added or subtracted from the ordinates depends, of course, on which ordinates we are altering and the sign of the angular change. The ordinates of this thrice corrected foil and corrected angle of attack are then entered as inputs to a numerical conformal mapping program, (Ref. 8), for the solution of flow around arbitrary profiles. The output of this program is primarily the chord-wise pressure distribution of the foil in question. The results of this program were to be compared with the pressure distribution obtained in the experiment.

## 2. CALCULATION OF THE PRESSURE COEFFICIENTS

Both the static pressure at the head of the test section and the static pressures sensed by the tap tube on the boundary layer rake and the surface taps were measured on the inclined manometer. The computation of the pressure coefficients  $c_p = \frac{p - p_\infty}{\frac{1}{2} \rho V^2}$  was then a matter of applying the corrections to compensate for the tilt of the manometer table not in the plane of inclination and subtract  $h_{static}$  at the head of the tunnel from the local static head measured with the rake or the taps. The dynamic head observed on the indirect reading manometer was again converted to the same scale as the inclined manometer and the resulting quantity

$$h(\text{inclined}) = \frac{0.806}{0.827} \times \frac{1}{\sin 14.5^\circ} h(\text{indirect}) \quad (1)$$

$$h(\text{inclined}) = 3.93 h(\text{indirect})$$

is divided into the static head difference.



1000

1000

1000

1000

1000

1000

1000

1000

1000

1000

1000

1000

1000

1000

1000

1000

1000

1000

1000

1000

1000

1000

1000

1000

1000

1000

$$\frac{h_{\text{stat local}} - h_{\text{stat upstream}}}{3.9) h(\text{indirect})} = c_p \quad (11)$$

The only slight difficulty which arises, is when the pressure coefficients are calculated from the measurements taken on the rake static probe. Each measurement is made at slightly different tunnel speed and so each calculation involves different dynamic and static pressures. The pressure coefficients fall into five categories:

- (a.) Those determined from surface static tap readings with no apparatus on the foil.
- (b.) Those determined from the tap probe on the boundary layer rake with the rake on the foil, of course.
- (c.) Those determined from surface static tap readings with the rake on the foil.
- (d.) Those determined by the potential flow calculation around the real body.
- (e.) Those determined by the potential flow calculation around the corrected foil.

All five were plotted as a function of chord-wise distance/ chord length, to obtain an idea of the error caused by the presence of the rake, and to determine the agreement of the theory with experiment.



### III. RESULTS

#### A. RESULTS OF THE BOUNDARY LAYER MEASUREMENTS

The results of the total pressure surveys made along the chord are shown in figures 10 and 11. The displacement thickness is plotted as a function of distance/chord length. The figures show the effects of the pressure gradients along the chord on the development of the boundary layer. The actual computed values of boundary layer thickness and displacement thickness are tabulated in Tables III and IV. In addition the velocity profiles at each chord-wise station are listed in Table VI. The plots of velocity distribution versus  $y/$  are shown in figures 12 through 17. The original plots of  $v/V$  versus  $y$  were done on huge sheets of paper and have not been included in this report.

The displacement thickness in the wake 1.35 inches in back of the trailing edge was determined by a survey of wake total pressures. The wake surveys are tabulated in Table V and shown graphically in figures 18 and 19.

The boundary layer surveys indicate an extremely rapid thickening of the boundary layer in the presence of adverse pressure gradients toward the trailing edge. This may be seen quite clearly by observing both the measured pressure distribution in figure 20 and the curve of  $\delta^*$  versus  $x/c$ , figure 10. Although this is for a nominal angle of attack of  $0.0^\circ$  the location of the stagnation point is indicated in figure 20 as being on the upper surface which belies an effective negative angle of attack. In figures 11 and 24, the correlation between pressure distribution and boundary layer development may also be noted.



THE HISTORY OF THE UNITED STATES

The history of the United States is a story of growth and change. It begins with the first settlers who came to the continent, and it ends with the present day. The story is full of challenges and triumphs, and it is a story that we can all learn from. The early years of the United States were marked by a struggle for independence from Britain. The American Revolution was a turning point in the nation's history, and it led to the creation of a new government. The years following the Revolution were a time of rapid growth and expansion. The United States became a major power in the world, and it played a leading role in the development of the modern world. The history of the United States is a story of a nation that has overcome many challenges and has achieved many great things. It is a story that we can all be proud of, and it is a story that we can all learn from.

The history of the United States is a story of a nation that has overcome many challenges and has achieved many great things. It is a story that we can all be proud of, and it is a story that we can all learn from. The early years of the United States were marked by a struggle for independence from Britain. The American Revolution was a turning point in the nation's history, and it led to the creation of a new government. The years following the Revolution were a time of rapid growth and expansion. The United States became a major power in the world, and it played a leading role in the development of the modern world. The history of the United States is a story of a nation that has overcome many challenges and has achieved many great things. It is a story that we can all be proud of, and it is a story that we can all learn from.

Again referring to figure 13, what appears to be transition occurs somewhere between  $x/c = 0.5$  and  $0.6$ . Figure 17 displaying the velocity distribution at various chord-wise points shows also a noticeable change in the shape of the velocity profile between these chord-wise points. A distinct rise in surface pressure may also be observed in figure 20, at this point. Actually this behavior does not really firmly indicate transition and other possibilities for what may be occurring here will be discussed later. The main point to observe in the boundary layer growth at nominal zero angle of attack is the fact that the behavior of the boundary layer along with the pressure distribution curve show the foil to be at some negative angle of attack. Notice that rapid boundary layer growth commences immediately on the forward portion of the bottom surface and how retarded laminar flow exists on the top surface up until the aforementioned point of suspected transition. Obviously the stagnation point is on the upper surface of the wing and the low pressure region caused by the corner flow around the nose causes the boundary layer on the bottom to separate immediately and reattach in turbulent region. On the top surface the large negative pressure gradient at the leading edge, as may be seen in figure 20, laminarizes the flow in the region; thus retarding its growth.

At an angle of attack of  $2.0^\circ$  the top surface growth is quite rapid and observing the velocity profiles in figures 16 and 17, we see that no distinct changes in shape occur. The pressure gradient on the top surface at  $2^\circ$  angle of attack is adverse all the way from  $x/c = 0.10$  hence, the boundary layer and corresponding displacement thickness are quite large at the trailing edge.





The wake surveys shown in figures 10 and 19 show nothing of particular note. They were taken only to obtain a figure for displacement thickness as close to the trailing edge as possible. The points plotted on figures 10 and 11, are not a particular aid in predicting trailing edge behavior since it has been experimentally established by Tani and Sweeting (Ref. 12), that  $\delta^*$  and  $\delta^*/\theta$  suffer a slope discontinuity at the trailing edge. This can be observed (with imagination) in this experiment if we observe the pressure gradients and the trend of the boundary layer growth and extrapolate to the trailing edge, then proceed from this point to the wake point directly. This has been done with dotted lines in the figures.

## 9. RESULTS OF THE PRESSURE COEFFICIENT MEASUREMENTS

The pressure distribution curves have been mentioned in the previous section as an aid in visualizing what was happening to the boundary layer. In this respect they appear reasonable. The measured gradients seem to agree with other measured characteristics of the experiment. However, as may be seen upon comparing the measured pressure distribution (Figs. 20, 23, and 24), with the potential flow distributions obtained from T. Brackett's computer program (Ref. 8), (Figs. 22 and 25), agreement here is poor.

The pressure distribution on the unaltered foil section as predicted by potential flow shows, for the nominal  $2^\circ$  angle of attack, a lift coefficient of 0.127683.

The foil corrected for displacement thickness and with the resulting angle of attack change (effective angle of attack =  $1.7569^\circ$ ) predicts a





lift coefficient of 0.1116. The measured pressure distribution when mechanically integrated results in a lift coefficient of 0.1X. This would correspond to an angle of attack of about 1.15 degrees. At this angle of attack the pressure distribution was plotted on Figure 7K. The prints were also displayed in Figure 7L for comparison. Reasonable agreement can be seen right up to within  $x/s = 0.975$  for the top surface. At this point the influence of the corner on the square trailing edge causes the potential calculation to predict very low pressures. Since no data was obtained for this region, no adequate comparison can be made. The bottom surface data however, agrees with the predicted pressure distribution only in general trend up to within a few percent to the trailing edge. The magnitude is greater by 1XK.

The results of the potential flow calculations around the body corrected by displacement thickness and with angle of attack adjusted by the arctan of the ratio of displacement thickness difference to chord length at the trailing edge, agrees with the potential theory for the mid chord area but, at the leading edge the small angle of attack change shows up and at the trailing edge the thickness effects become apparent and the corrected foil pressures in the region of  $x/s = 0.75$  to  $x/s = 1.0$  flatten out and then fall rapidly at the trailing edge due to the accelerating flow.

It appears then that there are three sources of disagreement. First, the pressure distribution as predicted by potential theory does not agree well with the experimental data. Second, the pressure distribution around the corrected form does not agree with the experimental data.





Third, the pressure distribution around the corrected form not only does not agree with the potential theory but it predicts a correction which although is the logical result of the input is just the opposite of the result which is sought.

Figure 23 displays the pressure distribution around the foil at a Reynolds Number of  $5.15 \times 10^5$ . Considering the scale of the plot, it agrees well with the measurements obtained at  $Re = 3.67 \times 10^5$ . There was some slight change in the boundary layer behavior (Fig. 10) at the two Reynolds Numbers but nothing which would "cause" significant difference in the pressure distribution except perhaps due to movement of the transition points.

#### 6. RESULTS OF CORRECTED FOIL

Table II lists the original dimensions of the foil which was tested. It is not a NACA 66 with a 1.0 mean line nor does it have the originally desired thickness ratio of 0.033. It is thinner and has more camber. Table II also lists the displacement thickness at the required ordinates of Ref. 8 and, the correction in the effects for adjusted angle of attack and finally the completely corrected foil dimensions for 0.00 and 2.00 angle of attack. These forms were used as inputs to the computer program and the results of these computations have been outlined in the previous section. The potential flow results for both the corrected and uncorrected foils have been plotted in Figures 22 and 24. Seeing the large disagreement, an attempt was made to find the angle of attack for which the experimental foil was tested. The computer results were obtained for a range of angles from  $-2.50^\circ$  to  $+2.50^\circ$  at small intervals. At angles



The first of these is the fact that the system is not a simple one. It is a complex one, and it is one that is not easily understood. It is a system that is not easily understood, and it is one that is not easily understood.

It is a system that is not easily understood, and it is one that is not easily understood.

The second of these is the fact that the system is not a simple one. It is a complex one, and it is one that is not easily understood. It is a system that is not easily understood, and it is one that is not easily understood.

It is a system that is not easily understood, and it is one that is not easily understood.

It is a system that is not easily understood, and it is one that is not easily understood.

The third of these is the fact that the system is not a simple one. It is a complex one, and it is one that is not easily understood. It is a system that is not easily understood, and it is one that is not easily understood.

The fourth of these is the fact that the system is not a simple one. It is a complex one, and it is one that is not easily understood. It is a system that is not easily understood, and it is one that is not easily understood.

The fifth of these is the fact that the system is not a simple one. It is a complex one, and it is one that is not easily understood. It is a system that is not easily understood, and it is one that is not easily understood.

for which the lift coefficient due to theory agreed with that of experiment, the resulting pressure distribution was plotted. At  $7^\circ$  nominal angle of attack, reasonable agreement was gotten between measured and calculated pressure distribution for the top surface at  $1.25^\circ$  but the bottom surface was considerably off. At  $0.0^\circ$  nominal angle of attack, the program output agreed somewhat with the top surface data at an angle of attack of  $-0.10^\circ$ , and here the bottom surface data disagreed in magnitude. In fact the experiment gave small negative pressure coefficients where theory predicted small positive ones as may be seen on comparing figure 20 and 22.

The results of the measurements of the pressure distribution with the rake on the surface is shown in figure 21. Comparison of this graph with figure 20 indicates little difference in the distribution obtained with the rake on and off the surface.

#### D. CARBON BLACK TRACER

Two photographs depicting the use of carbon black on the foil surface are shown in figure 9. Usually carbon black and oil is used to predict separation. However, since the structure of turbulent flow is quite different from that of laminar, the author felt that some insight might be gained into the location of transition as well as separation, if any, by using carbon black. At zero angle of attack and Reynolds Number  $= 3.67 \times 10^6$  the flow of the carbon black flow pattern changed completely between stations 7 and 8 which correspond roughly to  $x/c = 0.5$  and  $0.6$ . On the bottom surface the same behavior was observed



between stations 3 and 4. Figure 9 shows the behavior of the carbon black at an incidence of  $2.0^\circ$  and indicates transition near station four. There is no reinforcement of this behavior in the plot of  $\epsilon''$  for  $2^\circ$  as shown in figure 11.





THE UNIVERSITY OF CHICAGO  
DEPARTMENT OF CHEMISTRY  
1100 SOUTH EAST ASIAN AVENUE  
CHICAGO, ILLINOIS 60607-7070  
TEL: (773) 936-7000 FAX: (773) 936-7001

RECEIVED  
JAN 10 1997  
11 00 AM  
FROM: [illegible]  
TO: [illegible]

SUBJECT: [illegible]  
[illegible]  
[illegible]

[illegible]  
[illegible]  
[illegible]

[illegible]  
[illegible]  
[illegible]

[illegible]

#### IV. DISCUSSION OF RESULTS

##### A. GENERAL

A brief review of the experimental results is in order at this point.

First, the foil is obviously not at the angle of attack measured in the wind tunnel. Some rough comparison with the data for even fifty odd angles of attack gotten from potential theory, indicate that the foil may be below the measured angles of attack anywhere from 0.1 to 0.8 degrees. The measured pressure distributions for actual zero and  $2.0^\circ$  angles of attack produce lift coefficients of 0.115 and 0.335 respectively. Both of these figures are well below those predicted by the potential theory calculations; 0.242 and 0.111 for  $0.0^\circ$  and  $2.0^\circ$  respectively. The values from theory were obtained by mechanically integrating the pressure distributions obtained from the program output. The  $C_l$  listed by the program depends upon a given ideal angle of attack and lift slope. Since these values were not available exactly for the foil used in the experiment, it was necessary to check the program results in this manner.

Secondly, even when pressure distributions obtained from the program at angles of attack, which gave the same lift as experimental data predicted were compared with the data, the pressure distributions did not agree particularly well. In addition, attempts were made to find angles of attack for which pressure distributions on one of the surfaces agreed with theory, and then compare the pressure distribution on the other surface as well as the lift coefficient. For an angle of attack



of 1.2° the top surface data agree reasonably with the computed pressure distribution whereas the computed bottom surface pressures are much higher than those for the experiment. The trend of the computed pressures is however, essentially the same but the lift coefficient is slightly higher.

After unsuccessfully attempting to come up with an angle of attack at which the potential flow calculations resembled the experimental results, it was decided to figure what experimental error was responsible for the mismatching. The first thought was that, perhaps the sign of the static head on the inclined manometer may have been read wrong but, since for example, on the readings at zero angle of attack for the bottom, the static pressure was so close to zero on the manometer board that a difference in sign would not make any difference (at most 0.1%). However, if the pitot-static tube at the head of the tunnel were in error, say, ten percent, then the readings obtained with it as a reference would be seriously in error. This is true since both  $P_{static}$  and  $q_{\infty}$  are obtained from this instrument. This can be illustrated by the assuming that total pressure is known accurately and that the static taps are perfect. If a pressure coefficient of 0.1 were being measured and

$$\frac{h_{static} - h_{static \infty}}{q_{\infty}} = 0.1$$

if  $q_{\infty}$  is around 12, as in this experiment, then  $h_{static} - h_{static \infty} = 1.2"$ . Then suppose the pitot static tube was in error by 1% or 1.2". If  $h_{total}$  is known, and it usually is known quite accurately, then  $P_{static \infty}$





changes by  $1.2^\circ$ , therefore for readings this close to the zero a change of  $1.2^\circ$  if in the right direction could double the pressure coefficient and change its sign. In general, the effect of not knowing dynamic pressure exactly can change the scale of the pressure distribution scale as well as shifting the axis because it is  $q_{\infty}$  and  $h_{static}$  that we are uncertain of in this equation

$$C_p = \frac{h - h_{static}}{q_{\infty}} \quad .$$

The static pressure readings were not taken at the same time on both surfaces which adds to the difficulty of putting a finger on the problem. The bottom surface readings were taken toward the end of the experiment and the pitot-static tube and its associated lines and manometers may well have developed an error between the measurements of the two distributions. However, the data for the top surface at  $2^\circ$  nominal angle of attack was obtained in between bottom surface readings for zero and  $2.0^\circ$  angles of attack and both top surface measurements appear to be reasonable.

If we rule out the possibility that the static tube and equipment were in error there remain only a few more reasons for the difficulty and these have to do with the effects of the walls and ceiling and the possibility of a vertical dynamic head variation. The pitot tube was mounted in the upper section of the tunnel about two feet from the overhead. The height of the tunnel is approximately  $7\frac{1}{2}$  feet and the foil was mounted about  $3\frac{1}{2}$  feet from the floor.

Glauert (Ref. 9), has obtained corrections to the effective angle of attack of a two dimensional foil in a closed jet. This was



accomplished by replacing the floor and overhead by air foil images and continuing until an infinite cascade was produced. The results are as follows:

$$\alpha = + \frac{1}{2} \frac{c^2}{h^3} \frac{c^2}{h} (C_1' + 4C_m' h) \quad (573) \quad (12)$$

and

$$C_1 = C_1' \left( 1 - \frac{c^2}{h^3} \frac{c^2}{h} \right) \quad (13)$$

where  $C_m' (1)$  is the moment about the quarter chord where  $C/h$  is the ratio of chord length to tunnel height. In this experiment it was equal to 0.667.

$C_1'$  is the measured lift in the tunnel.

$$C_1 = 0.9066 C_1'.$$

At nominal values of angle of attack of  $0.0^\circ$  and  $2.0^\circ$  the true lift coefficient was then 0.1312 and 0.306 respectively.

$C_m' (1)$  was estimated from the measured pressure distributions as 0.0361 at zero degrees and 0.08 for  $2.0^\circ$ . With these values, the correction to angle of attack becomes:

$$\alpha = 0.11^\circ \quad (0.0^\circ)$$

$$\alpha = 0.31^\circ \quad (2.0^\circ)$$

Clearly, these corrections are not sufficient to account for the poor data.

If there existed a vertical dynamic head variation in the tunnel, due to poor design of the contraction nozzle, then having the pitot-static



The first part of the paper is devoted to the study of the properties of the function  $f(x)$  defined by the equation

$$f(x) = \frac{1}{2} \left( \frac{1}{x} + \frac{1}{x+1} \right) \quad (1)$$

It is easy to see that the function  $f(x)$  is defined for all  $x \neq 0, -1$  and that it is symmetric with respect to the line  $x = -\frac{1}{2}$ .

Let us now consider the function  $f(x)$  for  $x > 0$ . It is easy to see that  $f(x) > 0$  for all  $x > 0$  and that  $f(x)$  is strictly decreasing for  $x > 0$ . Moreover,  $f(x) \rightarrow \frac{1}{2}$  as  $x \rightarrow \infty$  and  $f(x) \rightarrow \infty$  as  $x \rightarrow 0^+$ . Therefore, the function  $f(x)$  is a strictly decreasing function on the interval  $(0, \infty)$  which approaches the horizontal asymptote  $y = \frac{1}{2}$  as  $x \rightarrow \infty$  and the vertical asymptote  $x = 0$  as  $x \rightarrow 0^+$ .

Let us now consider the function  $f(x)$  for  $x < -1$ . It is easy to see that  $f(x) < 0$  for all  $x < -1$  and that  $f(x)$  is strictly increasing for  $x < -1$ . Moreover,  $f(x) \rightarrow \frac{1}{2}$  as  $x \rightarrow -\infty$  and  $f(x) \rightarrow \infty$  as  $x \rightarrow -1^-$ . Therefore, the function  $f(x)$  is a strictly increasing function on the interval  $(-\infty, -1)$  which approaches the horizontal asymptote  $y = \frac{1}{2}$  as  $x \rightarrow -\infty$  and the vertical asymptote  $x = -1$  as  $x \rightarrow -1^-$ .

Let us now consider the function  $f(x)$  for  $-1 < x < 0$ . It is easy to see that  $f(x) < 0$  for all  $-1 < x < 0$  and that  $f(x)$  is strictly decreasing for  $-1 < x < 0$ . Moreover,  $f(x) \rightarrow \infty$  as  $x \rightarrow -1^+$  and  $f(x) \rightarrow \frac{1}{2}$  as  $x \rightarrow 0^-$ . Therefore, the function  $f(x)$  is a strictly decreasing function on the interval  $(-1, 0)$  which approaches the vertical asymptote  $x = -1$  as  $x \rightarrow -1^+$  and the horizontal asymptote  $y = \frac{1}{2}$  as  $x \rightarrow 0^-$ .

Let us now consider the function  $f(x)$  for  $0 < x < 1$ . It is easy to see that  $f(x) > 0$  for all  $0 < x < 1$  and that  $f(x)$  is strictly increasing for  $0 < x < 1$ . Moreover,  $f(x) \rightarrow \infty$  as  $x \rightarrow 0^+$  and  $f(x) \rightarrow \frac{1}{2}$  as  $x \rightarrow 1^-$ . Therefore, the function  $f(x)$  is a strictly increasing function on the interval  $(0, 1)$  which approaches the vertical asymptote  $x = 0$  as  $x \rightarrow 0^+$  and the horizontal asymptote  $y = \frac{1}{2}$  as  $x \rightarrow 1^-$ .

Let us now consider the function  $f(x)$  for  $x > 1$ . It is easy to see that  $f(x) > 0$  for all  $x > 1$  and that  $f(x)$  is strictly decreasing for  $x > 1$ . Moreover,  $f(x) \rightarrow \frac{1}{2}$  as  $x \rightarrow \infty$  and  $f(x) \rightarrow \frac{1}{2}$  as  $x \rightarrow 1^+$ . Therefore, the function  $f(x)$  is a strictly decreasing function on the interval  $(1, \infty)$  which approaches the horizontal asymptote  $y = \frac{1}{2}$  as  $x \rightarrow \infty$  and the horizontal asymptote  $y = \frac{1}{2}$  as  $x \rightarrow 1^+$ .

tube in the upper section of the test section would be disastrous and a static would, of course, be correct for the upper surface and in error in the lower section. It was however, necessary to place the pitot tube in that portion of the tunnel to prevent its wake from impinging on the surface of the foil. The maximum error encountered, according to Poole (Ref. 13), is 2 to 3% of the dynamic head and the region of error is usually confined to a short distance from the floor at the entrance.

The possibility of a pressure gradient existing length-wise down the tunnel section exists but precautions were taken to remove this effect. The walls were tapered out. According to Ref. (10), this effect can also be caused by the presence of the body itself but is restricted however, to bodies such as fuselages and nacelles and is negligible for normal wings, by inference then, the effect must be even more negligible for such a thin section as the one tested in this experiment.

A simple calculation just to estimate the contraction effect of the foil on the jet entering the test section

$$\frac{V_1}{V_2} = \frac{A_2}{A_1} \quad (1b)$$

where  $V_1$  is the velocity at the pitot tube and  $V_2$  is the velocity, in incompressible flow, in the vicinity of the foil. This region is modeled by a section of area decreased by the cross sectional area of the foil. So,  $A_1$  is the test section area at the pitot tube and  $A_2$  is the effective flow area in the region of the foil.

The first of these is the fact that the  
 second of these is the fact that the  
 third of these is the fact that the  
 fourth of these is the fact that the  
 fifth of these is the fact that the  
 sixth of these is the fact that the  
 seventh of these is the fact that the  
 eighth of these is the fact that the  
 ninth of these is the fact that the  
 tenth of these is the fact that the

The first of these is the fact that the  
 second of these is the fact that the  
 third of these is the fact that the  
 fourth of these is the fact that the  
 fifth of these is the fact that the  
 sixth of these is the fact that the  
 seventh of these is the fact that the  
 eighth of these is the fact that the  
 ninth of these is the fact that the  
 tenth of these is the fact that the

The first of these is the fact that the  
 second of these is the fact that the  
 third of these is the fact that the  
 fourth of these is the fact that the  
 fifth of these is the fact that the  
 sixth of these is the fact that the  
 seventh of these is the fact that the  
 eighth of these is the fact that the  
 ninth of these is the fact that the  
 tenth of these is the fact that the

$$C_p = \frac{v_1^2}{v_2^2} - 1$$

$$\frac{v_2}{v_1} = \frac{72 \text{ in}^2}{1320 \text{ in}^2} = 0.0546$$

$$C_p = 0.0079 - 1$$

Thus, the correction to the pressure coefficients is two orders of magnitude less than the measured ones and need not be considered.

To summarize the preceding explanation, there exists an error in static pressure readings of sufficient magnitude that only the viscous effects on the gradients of the pressures may be discussed. The experiment was considerably more delicate than the author conceived and with greater control and calibration than was exercised is necessary to make an intelligent correction to this discrepancy.

### 8. BOUNDARY LAYER PROFILES

The data obtained for the boundary layer profiles is good and agrees with what one would expect in the presence of the measured pressure gradients.

The profiles indicate that the flow is turbulent along the surface of the foil except for the top surface of the section tested at a nominal angle of attack of  $0.0^\circ$ . Here, at station 1, the shape factor is 2.290 which corresponds to a laminar boundary layer which is fairly stable. Station 1, on the top surface is, according to figure 20, in a region of intense acceleration. The shape factor has decreased to about 1.57





as we approach station 4, which seems to indicate that transition to turbulent flow has occurred, however,  $H$  drops sharply between station 4 and 7 and by station 8, has begun to rise rapidly as flow nears the trailing edge. At station 12,  $H$  has reached the value of 2.73. This type of behavior is shown in Ref. (11) by Van Dookhoff and Telser, in their experiments with air foil sections. The trend of which I speak is the high value of  $H$  at the leading edge, decreasing and then rising in turbulent flow.

This information then removes the certainty that what we see between station 7 and 8 on the top surface is truly transition. Poole, Ref. 10, indicates that transition can be noted by taking pressure measurements a short distance from the surface and noting that a dip in the pressure envelope will indicate transition. The rake static tube provided this type of measurement and there certainly is a dip in the  $C_p$  curve at this point. However, a shape factor which is characteristic of a turbulent boundary layer has been measured ahead of this point.

The crux of this discussion of the boundary layer profiles is that the measurements appear to be in agreement with theory and the value for  $\theta$  and  $\delta$  can certainly be used (if the overall procedure is correct) to adjust the shape of the body.

It also may be observed that the relative location of the transition point on the top and bottom surfaces of the foil will make a distinct difference in the nature of the appearance of the adjusted trailing edge. Here roughness effects can be important. No attempt was made to stimulate turbulence on the model and the surface of the foil was





reasonably smooth along its forward portions so that the extensive length of the region of laminar boundary layer growth on the forward section is not particularly surprising.

Examination of this data leads us to the conclusion that at negative angles of attack, the boundary layer growth on the upper surface will be retarded, and the larger  $\delta$  which would occur at the bottom of the trailing edge would effectively increase the angle of attack. Disregarding thickness effects, this would tend to increase the lift. The reverse is true for positive angles of attack where the gradients on the upper surface may be strongly adverse. The positive angle of attack also results in strong corner flow at the leading edge which causes an intense low pressure region which could well induce turbulence all along the upper surface.

Roughness of the foil surface, if its "hydraulic" diameter is sufficiently large, may influence the behavior of the turbulent layer as well as the transition point.

#### C. FLIGHTING OF POTENTIAL FLOW CALCULATIONS WITH THE CORRECTED FLOW

As mentioned in section III, the plots of the experimental data do not agree with potential flow about the unaltered body, let alone with the form corrected for  $\delta$ . Therefore it is possible only to make qualitative remarks on the merits of the proposed method for obtaining lift alterations due to viscosity.

In figures 21 and 22, we know that the magnitude of the bottom surface data is different than the theoretical results, however, it should be noted that there is a hump between  $x/c = .4$  and  $.6$  in the





experimental pressure curve. In figure 22 we can see the same hump only in the corrected form curve. At the rear part of the foil it is extremely difficult to see which of the potential theory curves has the same slope and behavior as the trailing edge as the data. The potential flow results for the uncorrected foil section show higher value of slope at the trailing edge. This is to be expected especially when the pressure gradients are strongly adverse. The boundary layer grows rapidly on the surface in question and when the resulting  $\delta$  is added to the foil an opposing correction results. An example will illustrate the point; using the system of corrections devised in this report. Given a two-dimensional foil section at a high angle of attack but with no separation: the boundary layer measured on the top surface will be quite large and the angle of attack will be effectively decreased. The thickening of the after section of the foil and the resulting increase in flow acceleration as well as the decreased angle of attack will contribute to reduce the strong adverse gradient. Thus, potential theory about this corrected form must predict lower adverse gradients than the flow around the uncorrected body. For negative angles of attack, the lower surface will have the adverse gradients as the trailing edge is approached.  $\delta$  will consequently be greater there and the effective angle of attack will be increased and the combined effects of added thickness and angle of attack will cause a decrease in the adverse pressure gradient.

All of the plots of potential theory solutions for the corrected forms show a rapid pressure loss at  $x/c = .99$ . This has been explained



in a previous section. It is worth noting here, however, that this is the largest single shortcoming of the entire philosophy of the thesis. The flow as described in this computer program used a square tailed projectile like foil at an angle of attack, with the requirement for a stagnation point in the center of the tail. The potential flow around this form certainly will not be the analog of the actual flow. Schneider (Ref. 3), pointed out in his experiment that the displacement thickness of the boundary layer and wake joined reasonably uniformly at the trailing edge so that a better procedure would be to assume that the foil is extended a short bit by the wake and the dead air bubble which Schneider (3) observed and that it tapers to a zero thickness. This could not be attempted in this experiment without better coverage of the trailing edge region, since the point of zero thickness would be most logically chosen when the static pressure variation across the wake has fallen to some small value.





#### V. CONCLUSIONS

The large disagreement between the measured and calculated pressure distribution leads to the following conclusions:

In order to obtain meaningful data the experiment must be performed in a much better instrumented and controlled manner. The statement made earlier in the thesis to the effect that the wall corrections were negligible should not be taken out of context. The calculated correction did not suitably adjust my data, however, the magnitude of the wall corrections in sensitive boundary layer, drag, and lift effect experiments have led to increased work with flexible tunnel walls and ceilings to eliminate the constraints placed on streamline curvature by the jet boundaries. In section IV, I calculated this effect. It was 10% of the total lift at only  $0.0^\circ$ . From this, I conclude that wall effects are substantial enough to warrant running the experiment with the overhead and floor of the tunnel forced to the shape of the foil.

The method which I used to apply the " " correction to the foil is fallacious and should be replaced with one that does not predict obviously excessive streamline defects toward the trailing edge.

I noted that along the foil not in the trailing edge region, the results of the potential flow around the corrected form show similar humps and hollows as the experimental data, but the uncorrected form often misses them. Therefore, I conclude that in regions where the displacement thickness is not unrealistically truncated as it was at the trailing edge, the streamline deflection is reasonably well predicted by this theory.



The boundary layer results show behavior which would be expected under the measured conditions and is not considered as a source of the discrepancy between theory and experiment.

The design of the foil pressure sensing devices were poor as well as the angle of attack control set up. A good deal of the uncertainty about the measured pressures would have been eliminated had efficient taps been used and more of them installed. Not really knowing the angle of attack, made real numerical comparisons impossible.

In addition to thickness, Reynolds number and camber, the boundary layer distribution on the surface of the foil and indirectly the lift are dependent on foil roughness and free stream turbulence. For this reason it is felt that best results would be had if tunnel turbulence were reduced by employing screens and straighteners and different turbulence inception positions established using trip wire. Praston and Sweeting (12), show some of the results of work with and without turbulence stimulators on the wings they tested and the results are quite graphic.



...the ... of ...

...the ... of ...

...the ... of ...

...the ... of ...

...the ... of ...

...the ... of ...

...the ... of ...

...the ... of ...

...the ... of ...

...the ... of ...

...the ... of ...

...the ... of ...

...the ... of ...

...the ... of ...

...the ... of ...

...the ... of ...

...the ... of ...

...the ... of ...

...the ... of ...

...the ... of ...

...the ... of ...

...the ... of ...

...the ... of ...

...the ... of ...

...the ... of ...

...the ... of ...

## VI. RECOMMENDATIONS FOR FURTHER WORK

Before attempting to continue the investigation of viscous effects using the same apparatus, certain corrections must be made.

First, the airfoil section should have the leading and trailing edges removed and the key width doubled to avoid any wavy due to poor joints. While they are removed, pressure taps should be installed in them. Most important is a tap in the center of the vertical back side of the trailing edge. The nose should have as many taps as possible, installed. Then the center lift in the foil should be cut down and routed out so there is a  $\frac{1}{2}$  inch channel all around the wing. Taps should be installed in a flexible brass strip which will conform to the foil surface. The strip would fit into the center lift. Rather than wasting time with the steel tubes in the foil all the taps could be brought out of two channels in the foil which could be refaired.

The tunnel should be adjusted with some milled plywood to have no boundary effects on the foil behavior. For high angles of attack, this will be absolutely necessary.

To obtain a meaningful amount of data, different measuring devices must be used -- the boundary layer should be investigated using a traversing probe which could be controlled from outside the tunnel and moved both in and out of the boundary layer, and in a chord-wise direction. Conducting paint and marking lights could be used to maintain fine position control. This traversing mechanism should have accommodation for both static and total pressure tubes and also hot wire anemometers and a spherical tube with which to make detailed wake surveys.

... ..

... ..

... ..

... ..

... ..

... ..

... ..

... ..

... ..

... ..

... ..

... ..

... ..

... ..

... ..

... ..

... ..

... ..

... ..

... ..

... ..

... ..

The time constant on this system should be low. If possible, a transducer arrangement for the total pressure surveys in conjunction with an x - y plotter, should be used.

The static taps on the foil should number no less than sixty and they could be connected to a photostatic recorder bank. There is one available at N.I.T. With these modifications, data which can really be analysed would be obtained.

This experiment provides the opportunity to "kill two birds with one stone" as it were. The work is closely related with turbulent boundary layers and it provides an opportunity to obtain more data on turbulent layers. The ability to predict the behavior of these layers depends upon having data with which the skin friction or the integral of the skin friction may be found since it is an input to the "Kern" integral approach. Therefore, it would behoove us to obtain skin friction data simultaneously and correlate it with some of the boundary layer parameters.





## VII. BIBLIOGRAPHY

- (1) Pinkerton, Robert W., "Calculated and Measured Pressure Distributions Over the Midspan Section of the NACA 1112 Air Foil", NACA Report Number 561
- (2) Preston, J. W., "The Calculation of Lift Taking Account of the Boundary Layer", ARC Report No. 2725, Nov. 1949
- (3) Schneider, Kurt H., "Boundary Layer Effects on Airfoil Lift", Gas Turbine Laboratory Report No. 17, Sept. 1958
- (4) Spence, D. A. and Beanley, J. A., "The Calculation of Lift Slopes Allowing for Boundary Layer, With Applications to NACA 101 and 103 Airfoils", Reports and Memoranda No. 3137, Feb. 1948, London
- (5) Stuper, J., "Investigation of Boundary Layers on an Airplane Wing in Free Flight", NACA Technical Memorandum No. 751, (Translation)
- (6) Leopold, Rouven, "The Effect of Viscosity on the Lift Coefficient of Propeller Sections", Massachusetts Institute of Technology, Department of Naval Architecture and Marine Engineering Report No. 65-7, Sept. 1965
- (7) Moses, Hal L., "The Behavior of Turbulent Boundary Layers in Adverse Pressure Gradients", Gas Turbine Laboratory Report No. 71, Jan. 1961

1. The first part of the paper is devoted to a general discussion of the problem of the existence of solutions of the system of equations (1) and (2) under the assumption that the functions  $f$  and  $g$  are continuous and satisfy certain conditions. It is shown that under these conditions the system has at least one solution.
2. In the second part, the problem of the uniqueness of the solution is considered. It is shown that if the functions  $f$  and  $g$  satisfy certain additional conditions, then the solution is unique.
3. The third part of the paper is devoted to the study of the properties of the solution. It is shown that the solution is continuous and satisfies certain estimates.
4. In the fourth part, the problem of the stability of the solution is considered. It is shown that the solution is stable under certain conditions.
5. The fifth part of the paper is devoted to the study of the asymptotic properties of the solution. It is shown that the solution tends to zero as  $t \rightarrow \infty$ .
6. The sixth part of the paper is devoted to the study of the properties of the solution in the case of discontinuous functions  $f$  and  $g$ . It is shown that the solution exists and is unique under certain conditions.
7. The seventh part of the paper is devoted to the study of the properties of the solution in the case of non-linear functions  $f$  and  $g$ . It is shown that the solution exists and is unique under certain conditions.
8. The eighth part of the paper is devoted to the study of the properties of the solution in the case of non-local conditions. It is shown that the solution exists and is unique under certain conditions.
9. The ninth part of the paper is devoted to the study of the properties of the solution in the case of non-homogeneous boundary conditions. It is shown that the solution exists and is unique under certain conditions.
10. The tenth part of the paper is devoted to the study of the properties of the solution in the case of non-linear boundary conditions. It is shown that the solution exists and is unique under certain conditions.

- (8) Brackett, T., "Steady Two-Dimensional Pressure Distributions on Arbitrary Profiles", NACA Report No. 1081, Oct. 1944
- (9) Glauert, H., "The Interference on the Characteristics of an Airfoil in a Wind Tunnel of Rectangular Section", Report and Memorandum No. 1159
- (10) Pope, "Wind Tunnel Testing", John Wiley & Sons, Inc., Chapman & Hill, Limited, London, 1947
- (11) Van Dusenhoff, Albert E. and Peterwin, Noel, "Determination of General Relations for the Behavior of Turbulent Boundary Layers", NACA Report No. 772, 1943
- (12) Preston, J. G. and Sweating, W. E., "The Experimental Determination of the Boundary Layer and Wake Characteristics of a Simple Joukowski Aerofoil, with Particular Reference to the Trailing Edge Region", AEC Technical Report, Report and Memoranda No. 1998, 1943





APPENDIX A  
TABLES OF CASES



TABLE II

FOIL GEOMETRY FOR  $Q = 0.00$  $c = 60.07$  inches $W_C = 3.67 \times 10^6$ 

$x/c$	$y$ top	$y$ bottom	$\delta^\circ$ top	$\delta^\circ$ bottom	Corrected for $\delta^\circ$		Corrected for $\delta^\circ$ & $Q$	
					$y$ top	$y$ bottom	$x$ top ( $Q_s$ )	$y$ top $y$ bottom
1.000000	0.0665	-0.0666	0.136	0.185	0.2086	-0.2516	0.0212	0.2259 -0.2259
0.992401	0.2100	-0.0500	0.134	0.183	0.3710	-0.2130	0.0210	0.3970 -0.2070
0.969415	0.3350	0.0000	0.126	0.183	0.6110	-0.1830	0.0235	0.6215 -0.1595
0.933013	0.5700	+0.0350	0.115	0.182	0.8350	-0.1470	0.0226	0.7076 -0.1214
0.883022	0.8201	+0.0100	0.108	0.155	0.9270	-0.1150	0.0214	0.9191 -0.1236
0.821374	1.0700	-0.0200	0.103	0.130	1.1710	-0.1500	0.0199	1.1939 -0.1301
0.750000	1.3100	-0.0300	0.094	0.120	1.4040	-0.2000	0.0181	1.4221 -0.1819
0.671010	1.4700	-0.1500	0.092	0.108	1.5120	-0.2450	0.0152	1.5932 -0.2118
0.586724	1.5600	-0.2070	0.088	0.097	1.6200	-0.2770	0.0112	1.6122 -0.2128
0.500000	1.6200	-0.2200	0.084	0.085	1.6710	-0.3060	0.0121	1.6661 -0.2929
0.413176	1.6200	-0.2400	0.082	0.071	1.6720	-0.3110	0.0150	1.6520 -0.3010
0.329990	1.5100	-0.2400	0.076	0.059	1.5560	-0.2990	0.0200	1.5410 -0.2910
0.250000	1.3700	-0.2100	0.072	0.045	1.4020	-0.2450	0.0240	1.4080 -0.2790
0.178605	1.2000	-0.2400	0.070	0.036	1.2100	-0.2760	0.0270	1.2110 -0.2720
0.116976	0.9700	-0.2200	0.068	0.030	0.9720	-0.2500	0.0330	0.9810 -0.2470
0.066997	0.7300	-0.2000	0.068	0.024	0.7300	-0.2210	0.0320	0.7150 -0.2220
0.030154	0.4400	-0.1600	0.068	0.016	0.4400	-0.1750	0.0310	0.4190 -0.1750
0.007576	0.2200	-0.1200	0.068	0.014	0.2200	-0.1310	0.0300	0.2280 -0.1310
0.000000	0.0000	0.0000	0.060	0.000	0.0000	0.0000	0.0300	0.0000 0.0000

NOTE:  $y$  is measured normal to a straight line through the center of the leading edge and trailing edge.

(+ ) indicates distance above this line.

(- ) indicates distance below this line. All above dimensions in inches.





TABLE II (cont.)

FULL SPECTRA FOR  $\alpha = 2.0^\circ$ 

$$E_C = 3.67 \times 10^6$$

$\alpha_{\text{top}}$	$\alpha_{\text{bottom}}$	Corrected for $\alpha$		$x \tan \alpha$	$y_{\text{top}}$	$y_{\text{bottom}}$
		$y_{\text{top}}$	$y_{\text{bottom}}$			
0.220	0.130	0.2266	-0.1966	0.0150	0.2116	-0.2116
0.210	0.126	0.1500	-0.1760	0.0146	0.1966	-0.2266
0.202	0.121	0.5320	-0.1210	0.0136	0.1736	-0.1616
0.176	0.112	0.7060	-0.1176	0.0120	0.7020	-0.1690
0.156	0.106	0.9760	-0.1160	0.0197	0.9363	-0.1557
0.129	0.096	1.1690	-0.1160	0.0370	1.1120	-0.1550
0.120	0.092	1.1300	-0.1720	0.0337	1.3963	-0.2357
0.110	0.089	1.5760	-0.2390	0.0302	1.5396	-0.2692
0.096	0.066	1.6210	-0.2660	0.0261	1.6276	-0.2926
0.073	0.057	1.7130	-0.2770	0.0255	1.6995	-0.2995
0.070	0.066	1.6900	-0.2860	0.0185	1.6715	-0.3865
0.051	0.045	1.5960	-0.2760	0.0166	1.5792	-0.2996
0.042	0.025	1.6320	-0.2650	0.0112	1.6398	-0.2762
0.031	0.019	1.2310	-0.2590	0.0060	1.2230	-0.2690
0.023	0.015	0.9930	-0.2350	0.0052	0.9878	-0.2162
0.016	0.013	0.7690	-0.2130	0.0090	0.7650	-0.2160
0.013	0.012	0.4536	-0.1720	0.0013	0.4517	-0.2113
0.010	0.010	0.2300	-0.1300	0.0003	0.2297	-0.1300

THE UNIVERSITY OF CHICAGO

1950

THE UNIVERSITY OF CHICAGO

THE UNIVERSITY OF CHICAGO

THE UNIVERSITY OF CHICAGO

THE UNIVERSITY OF CHICAGO

THE UNIVERSITY OF CHICAGO

THE UNIVERSITY OF CHICAGO

THE UNIVERSITY OF CHICAGO

TABLE III  
BOTTOM SURFACE

ANGLE OF ATTACK =  $0.0^\circ$

$RE_c = 3.67 \times 10^6$

STATION	$x/c$	(inches)	$\delta^*$ (inches)
1	0.00757	0.162	0.01215
2	0.117	0.234	0.0315
3	0.1776	0.220	0.0330
4	0.2498	0.300	0.0461
5	0.3280	0.361	0.0588
6	0.4140	0.420	0.0711
7	0.4990	0.590	0.0834
8	0.5860	0.624	0.0961
9	0.6700	0.720	0.1086
10	0.7500	0.758	0.1207
11	0.8220	0.820	0.1390
12	0.9140	1.122	0.1742
WAKE	1.023	0.910	0.1780





TABLE III (cont)

## TOP SURFACE

ANGLE OF ATTACK =  $0.0^\circ$  $RE_\phi = 3.67 \times 10^6$ 

STATION	$x/c$	$\xi$ (inches)	$\xi^*$ (inches)
1	0.00757	0.034	0.00894
2	0.1170		
3	0.1776	0.044	0.00964
4	0.2498	0.065	0.0121
5	0.3280	0.091	0.01445
6	0.4140	0.190	0.0225
7	0.4990	0.246	0.0354
8	0.5860	0.444	0.0678
9	0.6700	0.510	0.0781
10	0.7500	0.568	0.0956
11	0.8220	0.593	0.101
12	0.9140	0.660	0.1140
WAKE	1.023	0.790	0.1400



TABLE III (cont)

## TOP SURFACE

ANGLE OF ATTACK =  $0.0^\circ$ 

$$qF_n = 5.15 \times 10^4$$

STATION	x/c	(inches)	$\eta$ (inches)
1	0.00757	0.032	0.00680
4	0.21980	0.160	0.02015
6	0.41100	0.192	0.02735
8	0.58600	0.320	0.04170
10	0.75000	0.568	0.08710
12	0.91100	0.717	0.12490
WAKE	1.02300	0.810	0.16210

## BOTTOM SURFACE

STATION	x/c	(inches)	$\eta$ (inches)
1	0.00757	0.111	0.01375
4	0.21980	0.299	0.02605
6	0.41100	0.470	0.04000
8	0.58600	0.570	0.06350
10	0.75000	0.716	0.10950
12	0.91100	0.970	0.16100
WAKE	1.02300	0.850	0.15100



TABLE 10-10  
continued

No. of hours per week	Hours worked in 1994		Hours worked in 1995	
	1994	1995	1994	1995
0	100	100	0	0
1	100	100	1	1
2	100	100	2	2
3	100	100	3	3
4	100	100	4	4
5	100	100	5	5
6	100	100	6	6
7	100	100	7	7
8	100	100	8	8
9	100	100	9	9
10	100	100	10	10
11	100	100	11	11
12	100	100	12	12
13	100	100	13	13
14	100	100	14	14
15	100	100	15	15
16	100	100	16	16
17	100	100	17	17
18	100	100	18	18
19	100	100	19	19
20	100	100	20	20
21	100	100	21	21
22	100	100	22	22
23	100	100	23	23
24	100	100	24	24
25	100	100	25	25
26	100	100	26	26
27	100	100	27	27
28	100	100	28	28
29	100	100	29	29
30	100	100	30	30
31	100	100	31	31
32	100	100	32	32
33	100	100	33	33
34	100	100	34	34
35	100	100	35	35
36	100	100	36	36
37	100	100	37	37
38	100	100	38	38
39	100	100	39	39
40	100	100	40	40
41	100	100	41	41
42	100	100	42	42
43	100	100	43	43
44	100	100	44	44
45	100	100	45	45
46	100	100	46	46
47	100	100	47	47
48	100	100	48	48
49	100	100	49	49
50	100	100	50	50
51	100	100	51	51
52	100	100	52	52
53	100	100	53	53
54	100	100	54	54
55	100	100	55	55
56	100	100	56	56
57	100	100	57	57
58	100	100	58	58
59	100	100	59	59
60	100	100	60	60
61	100	100	61	61
62	100	100	62	62
63	100	100	63	63
64	100	100	64	64
65	100	100	65	65
66	100	100	66	66
67	100	100	67	67
68	100	100	68	68
69	100	100	69	69
70	100	100	70	70
71	100	100	71	71
72	100	100	72	72
73	100	100	73	73
74	100	100	74	74
75	100	100	75	75
76	100	100	76	76
77	100	100	77	77
78	100	100	78	78
79	100	100	79	79
80	100	100	80	80
81	100	100	81	81
82	100	100	82	82
83	100	100	83	83
84	100	100	84	84
85	100	100	85	85
86	100	100	86	86
87	100	100	87	87
88	100	100	88	88
89	100	100	89	89
90	100	100	90	90
91	100	100	91	91
92	100	100	92	92
93	100	100	93	93
94	100	100	94	94
95	100	100	95	95
96	100	100	96	96
97	100	100	97	97
98	100	100	98	98
99	100	100	99	99
100	100	100	100	100

TABLE IV  
TOP SURFACE

ANGLE OF ATTACK =  $2^\circ$

$Re = 3.67 \times 10^6$

STATION	x/c	(inches)	$\eta$ (inches)
1	0.00757	0.150	0.01082
2	0.11700	0.175	0.02265
3	0.17760	0.231	0.03280
4	0.21980	0.300	0.04170
5	0.32800	0.353	0.05520
6	0.41100	0.465	0.06650
7	0.49900	0.518	0.09310
8	0.58600	0.592	0.08930
9	0.67000	0.710	0.11160
10	0.75000	0.763	0.12050
11	0.82200	0.834	0.13250
12	0.91400	0.935	0.16760
WAKE	1.02300	1.085	0.20100

# THE HISTORY OF THE

of the

of the

of the

of the

of the

of the

of the

of the

of the

of the

of the

of the

of the

of the

of the

of the

of the

of the

of the

of the

of the

of the

of the

of the

of the

of the

of the

TABLE IV (cont.)

BOTTOM SURFACE

ANGLE OF ATTACK =  $4.2^\circ$  $Re_c = 3.47 \times 10^6$ 

STATION	$x/c$	(inches)	$\eta$ (inches)
1	0.00757		
2	0.11700	0.170	0.02136
3	0.17760	0.170	0.021970
4	0.21980	0.170	0.02320
5	0.32800	0.300	0.02610
6	0.41100	0.312	0.025900
7	0.49900	0.500	0.025500
8	0.58600	0.500	0.02360
9	0.67000	0.599	0.02100
10	0.75000	0.611	0.02210
11	0.82200	0.661	0.02280
12	0.91100	0.630	0.02720
WAKE	1.02300	0.870	0.02200



# THE HISTORY OF THE

REIGN OF

CHARLES

THE FIRST

OF GREAT BRITAIN

AND

OF IRELAND

FROM THE YEAR 1625 TO 1685

TABLE V

## VELOCITY PROFILE IN THE WAKE

ANGLE OF ATTACK =  $0.0^\circ$  $RE_c = 3.67 \times 10^6$ 

$y$	$h - h_{st}$ (inches)	$v/V$
1.26	2.80	1.000
1.11	2.81	1.004
1.03	2.80	1.000
1.01	2.83	1.030
.86	2.74	0.989
.86	2.79	0.998
.82	2.75	0.991
.76	2.73	0.987
.64	2.62	0.967
.61	2.57	0.9581
.53	2.40	0.926
.51	2.44	0.933
.44	2.31	0.908
.36	2.08	0.862
.36	1.89	0.822
.32	1.93	0.8307
.26	1.57	0.749
.14	1.15	0.641
.11	1.00	0.597
.01	0.84	0.534
-.06	0.94	0.580
-.14	1.22	0.664
-.18	1.32	0.691
-.36	1.76	0.797
-.46	2.02	0.854
-.49	2.16	0.883
-.53	2.36	0.922
-.73	2.48	0.947
-.88	2.71	0.989
-.96	2.72	0.992
-.98	2.77	1.000
-.113	2.78	1.004
-.113	2.73	0.990
-.117	2.77	1.000
-.123	2.76	0.998



TABLE V (cont)

## VELOCITY PROFILE IN THE WAKE

ANGLE OF ATTACK =  $0.0^\circ$  $Re_c = 5.15 \times 10^6$ 

y	h - hat (inches)	v/v
0.90	6.00	1.0000
0.81	5.88	0.9899
0.76	5.81	0.9810
0.53	5.01	0.9590
0.46	4.65	0.8800
0.46	4.52	0.8680
0.41	4.22	0.8390
0.27	3.10	0.7190
0.24	3.17	0.7270
0.17	2.26	0.6100
-0.04	2.12	0.5950
-0.06	2.35	0.6260
-0.18	3.27	0.7270
-0.23	3.45	0.7580
-0.23	3.57	0.7710
-0.28	3.45	0.7580
-0.33	4.22	0.8300
-0.46	4.44	0.8630
-0.53	4.68	0.8830
-0.54	4.73	0.8880
-0.56	5.01	0.9130
-0.58	4.93	0.9070
-0.68	5.41	0.9500
-0.73	5.53	0.9600
-0.73	5.60	0.9660
-0.76	5.46	0.9510
-0.83	5.83	0.9860
-0.96	5.92	0.9930
-1.03	5.89	0.9900
-1.06	5.95	0.9960
-1.08	5.96	0.9970
-1.18	5.96	0.9970
-1.23	5.97	0.9980
-1.46	6.02	1.0000



Figure 1. Schematic diagram of the experimental setup.

Figure 2. Schematic diagram of the experimental setup.

The experimental setup is shown in Figure 1. The system consists of a laser source, a beam splitter, a lens, a sample, and a detector. The laser source emits a beam of light that is split into two paths by the beam splitter. One path goes through the lens and the sample, and the other path goes through the lens and the detector. The detector measures the intensity of the light that has passed through the sample.

Figure 3. Schematic diagram of the experimental setup.

The experimental setup is shown in Figure 2. The system consists of a laser source, a beam splitter, a lens, a sample, and a detector. The laser source emits a beam of light that is split into two paths by the beam splitter. One path goes through the lens and the sample, and the other path goes through the lens and the detector. The detector measures the intensity of the light that has passed through the sample.

The experimental setup is shown in Figure 3. The system consists of a laser source, a beam splitter, a lens, a sample, and a detector. The laser source emits a beam of light that is split into two paths by the beam splitter. One path goes through the lens and the sample, and the other path goes through the lens and the detector. The detector measures the intensity of the light that has passed through the sample.

TABLE V (cont)

## VELOCITY PROFILE IN THE WAKE

ANGLE OF ATTACK =  $2^\circ$  $Re = 3.47 \times 10^6$ 

$y$	$h$ - hat (inches)	$v/V$
1.41	2.79	1.0000
1.23	2.77	0.9965
1.16	2.68	0.9808
1.03	2.73	0.9889
1.02	2.73	0.9889
0.83	2.58	0.9620
0.74	2.44	0.9350
0.66	2.01	0.8490
0.58	2.02	0.8500
0.52	1.94	0.8340
0.51	1.95	0.8360
0.44	1.72	0.7850
0.33	1.47	0.7260
0.26	1.28	0.6770
0.24	1.22	0.6590
0.16	0.98	0.6190
0.08	0.83	0.5690
0.04	0.88	0.5860
0.02	0.81	0.5420
0.01	0.75	0.5141
-0.06	0.89	0.5890
-0.17	1.31	0.6850
-0.24	1.66	0.7720
-0.26	1.66	0.7720
-0.42	2.12	0.8690
-0.46	2.03	0.8710
-0.49	2.19	0.8870
-0.56	2.40	0.9280
-0.74	2.67	0.9780
-0.84	2.74	0.9910
-0.96	2.75	0.9930
-0.98	2.79	1.0000
-1.17	2.78	0.9980
-1.26	2.79	1.0000
-1.34	2.77	0.9980



TABLE VI

## SURFACE VELOCITY PROFILES

ANGLE OF ATTACK =  $0.0^\circ$  $Re_c = 3.67 \times 10^6$ TOP SURFACE

<u>STATION 1</u>		<u>STATION 3</u>		<u>STATION 4</u>		<u>STATION 5</u>	
$v/V$	$y$	$v/V$	$y$	$v/V$	$y$	$v/V$	$y$
0.990	0.03	0.995	0.05	0.983	0.05	0.964	0.05
0.703	0.015	0.999	0.10	0.998	0.10	0.9945	0.10
0.889	0.12	1.000	0.17	0.999	0.17	0.9995	0.17
0.999	0.33	0.999	0.25	0.9985	0.25	0.9995	0.25
1.000	0.37	0.999	0.41	0.999	0.41	0.9995	0.41
1.000	0.69	0.999	0.68	1.00	0.68	1.0000	0.68
1.000	0.80	0.999	0.71	1.00	0.71	1.0000	0.71
1.000	0.90	0.999	0.87	1.00	0.87	1.0000	0.87
1.000	1.00	0.999	0.91	1.00	0.91	1.0000	0.91

<u>STATION 6</u>		<u>STATION 7</u>		<u>STATION 8</u>		<u>STATION 9</u>	
$v/V$	$y$	$v/V$	$y$	$v/V$	$y$	$v/V$	$y$
0.8591	0.05	0.7457	0.05	0.5891	0.002	0.5616	0.02
0.9612	0.10	0.8837	0.10	0.8106	0.16	0.8349	0.20
0.9889	0.17	0.955	0.17	0.9072	0.26	0.9154	0.32
0.9965	0.25	0.993	0.25	0.9839	0.40	0.9803	0.45
0.9965	0.41	0.9965	0.41	0.9970	0.50	0.9945	0.53
0.9970	0.68	0.9970	0.68	0.9995	0.68	1.00	0.72
0.9965	0.71	0.9970	0.71	0.9995	0.80	1.00	0.84
0.9975	0.87	0.9965	0.87	0.9985	0.89	1.00	0.94
1.00	0.91	1.00	0.91	1.00	1.000	1.00	1.04
				0.999	1.25	1.00	1.32
				0.9985	1.58	1.00	1.61





TABLE VI (cont)

## SURFACE VELOCITY PROFILES

ANGLE OF ATTACK =  $0.0^\circ$  $Re_c = 3.67 \times 10^6$ TOP SURFACE

<u>STATION 10</u>		<u>STATION 11</u>		<u>STATION 12</u>	
$v/V$	$y$	$v/V$	$y$	$v/V$	$y$
0.5263	0.020	0.5301	0.02	0.4733	0.02
0.7635	0.180	0.7810	0.20	0.7880	0.23
0.8660	0.285	0.8712	0.30	0.9044	0.38
0.9455	0.420	0.9439	0.44	0.9434	0.52
0.9752	0.480	0.9721	0.52	0.9829	0.60
1.0000	0.690	1.0000	0.72	0.9995	0.80
1.0000	0.800	1.0000	0.73	0.9995	0.91
1.0000	0.900	1.0000	0.94	0.9990	1.02
1.0000	1.010	1.0000	1.03	1.0000	1.10
1.0000	1.310	1.0000	1.32	0.9985	1.34
1.0000	1.600	1.0000	1.62	0.9990	1.65

BOTTOM SURFACE

<u>STATION 1</u>		<u>STATION 2</u>		<u>STATION 3</u>		<u>STATION 4</u>	
$v/V$	$y$	$v/V$	$y$	$v/V$	$y$	$v/V$	$y$
0.853	0.025	0.658	0.030	0.6750	0.03	0.618	0.02
0.970	0.100	0.978	0.190	0.9150	0.13	0.869	0.15
0.996	0.110	0.996	0.320	0.9975	0.24	0.983	0.26
0.999	0.200	0.996	0.430	0.9975	0.38	0.998	0.40
0.999	0.340	0.996	0.550		0.50	0.997	0.51
0.999	0.670	0.998	0.720	1.0000	0.65	0.999	0.68
0.999	0.800	0.998	0.825	1.0000	0.78	0.999	0.80
	0.890	0.997	0.930	1.0000	0.88	0.997	0.89
1.000	1.000	1.000	1.020	1.0000	0.98	1.000	1.00



TABLE VI (cont)

## SURFACE VELOCITY PROFILES

ANGLE OF ATTACK =  $0.0^\circ$  $RE_c = 3.67 \times 10^6$ BOTTOM SURFACE

<u>STATION 5</u>		<u>STATION 6</u>		<u>STATION 7</u>		<u>STATION 8</u>	
$v/V$	$y$	$v/V$	$y$	$v/V$	$y$	$v/V$	$y$
0.597	0.02	0.598	0.02	0.597	0.03	0.715	0.120
0.838	0.16	0.745	0.16	0.749	0.14	0.781	0.200
0.955	0.27	0.913	0.27	0.864	0.25	0.877	0.310
0.998	0.41	0.987	0.40	0.950	0.39	0.960	0.450
0.999	0.51	0.998	0.51	0.992	0.50	0.978	0.525
1.000	0.68	1.000	0.67	1.003	0.65	1.001	0.720
1.000	0.81	1.000	0.80	1.003	0.78	1.001	0.850
0.999	0.96	1.000	0.89	1.001	0.89	1.000	0.940
1.000	1.00	1.000	1.00	1.003	0.98	1.002	1.050
		1.000	1.31	1.004	1.31	1.000	1.400
		1.000	1.61	1.001	1.60	1.000	1.670

<u>STATION 9</u>		<u>STATION 10</u>		<u>STATION 11</u>		<u>STATION 12</u>	
$v/V$	$y$	$v/V$	$y$	$v/V$	$y$	$v/V$	$y$
0.710	0.10	0.543	0.025	0.454	0.03	0.506	0.02
0.750	0.17	0.696	0.130	0.679	0.13	0.509	0.02
0.841	0.32	0.801	0.250	0.780	0.24	0.573	0.07
0.891	0.42	0.880	0.420	0.882	0.38	0.698	0.21
0.949	0.49	0.915	0.465	0.890	0.45	0.738	0.25
0.952	0.70	0.983	0.670	0.968	0.67	0.846	0.47
0.999	0.82	0.996	0.800	0.989	0.78	0.893	0.59
0.999	0.91	0.995	0.880	0.996	0.88	0.930	0.67
1.000	1.03	1.002	1.000	1.002	0.99	0.957	0.80
0.999	1.36	0.999	1.350	1.001	1.30	0.998	1.32
0.999	1.66	0.999	1.630	1.001	1.59	0.999	1.62





TABLE VI (cont.)

## SURFACE VELOCITY PROFILES

ANGLE OF ATTACK =  $2^\circ$  $Re_c = 3.67 \times 10^6$ TOP SURFACE

<u>STATION 1</u>		<u>STATION 2</u>		<u>STATION 3</u>		<u>STATION 4</u>	
$v/V$	$y$	$v/V$	$y$	$v/V$	$y$	$v/V$	$y$
0.9160	0.01	0.6770	0.02	0.6510	0.02	0.615	0.02
0.9915	0.11	0.7690	0.01	0.8670	0.10	0.879	0.11
0.9871	0.06	0.9690	0.12	0.9270	0.15	0.909	0.16
0.9975	0.25	0.9995	0.21	0.9960	0.21	0.968	0.23
0.9970	0.10	0.9995	0.10	0.9990	0.30	1.000	0.37
0.9960	0.57	1.0000	0.56	0.9995	0.57	0.998	0.55
0.9960	0.68	0.9995	0.67	0.9995	0.69	0.998	0.65
0.9950	0.80	0.9995	0.79	1.0000	0.78	0.997	0.79
1.0000	0.88	1.0000	0.87		0.86	1.000	0.86

<u>STATION 5</u>		<u>STATION 6</u>		<u>STATION 7</u>		<u>STATION 8</u>	
$v/V$	$y$	$v/V$	$y$	$v/V$	$y$	$v/V$	$y$
0.6810	0.05	0.6600	0.01	0.5190	0.07	0.5580	0.03
0.8120	0.15	0.7860	0.13	0.7330	0.15	0.7250	0.11
0.9020	0.19	0.8370	0.17	0.8010	0.19	0.7850	0.15
0.9580	0.27	0.8950	0.25	0.8590	0.25	0.8130	0.23
0.9965	0.10	0.9760	0.39	0.9150	0.10	0.9300	0.37
1.0000	0.58	0.9975	0.56	0.9960	0.59	0.9790	0.55
1.0000	0.68	0.9975	0.67	0.9980	0.67	0.9980	0.65
0.9995	0.82	0.9995	0.80	0.9995	0.80	0.9995	0.79
1.0000	0.88	1.0000	0.86	1.0000	0.85	1.0000	1.00

# TABLE 10-10

## UNITARY WEIGHTS

For  $\lambda = 0.01$  to  $0.10$

For  $\lambda = 0.01$  to  $0.10$

### UNITARY WEIGHTS

UNITARY WEIGHTS		UNITARY WEIGHTS		UNITARY WEIGHTS		UNITARY WEIGHTS	
$\lambda$	$V_{\lambda}$	$\lambda$	$V_{\lambda}$	$\lambda$	$V_{\lambda}$	$\lambda$	$V_{\lambda}$
0.01	0.0100	0.01	0.0100	0.01	0.0100	0.01	0.0100
0.02	0.0200	0.02	0.0200	0.02	0.0200	0.02	0.0200
0.03	0.0300	0.03	0.0300	0.03	0.0300	0.03	0.0300
0.04	0.0400	0.04	0.0400	0.04	0.0400	0.04	0.0400
0.05	0.0500	0.05	0.0500	0.05	0.0500	0.05	0.0500
0.06	0.0600	0.06	0.0600	0.06	0.0600	0.06	0.0600
0.07	0.0700	0.07	0.0700	0.07	0.0700	0.07	0.0700
0.08	0.0800	0.08	0.0800	0.08	0.0800	0.08	0.0800
0.09	0.0900	0.09	0.0900	0.09	0.0900	0.09	0.0900
0.10	0.1000	0.10	0.1000	0.10	0.1000	0.10	0.1000

UNITARY WEIGHTS		UNITARY WEIGHTS		UNITARY WEIGHTS		UNITARY WEIGHTS	
$\lambda$	$V_{\lambda}$	$\lambda$	$V_{\lambda}$	$\lambda$	$V_{\lambda}$	$\lambda$	$V_{\lambda}$
0.01	0.0100	0.01	0.0100	0.01	0.0100	0.01	0.0100
0.02	0.0200	0.02	0.0200	0.02	0.0200	0.02	0.0200
0.03	0.0300	0.03	0.0300	0.03	0.0300	0.03	0.0300
0.04	0.0400	0.04	0.0400	0.04	0.0400	0.04	0.0400
0.05	0.0500	0.05	0.0500	0.05	0.0500	0.05	0.0500
0.06	0.0600	0.06	0.0600	0.06	0.0600	0.06	0.0600
0.07	0.0700	0.07	0.0700	0.07	0.0700	0.07	0.0700
0.08	0.0800	0.08	0.0800	0.08	0.0800	0.08	0.0800
0.09	0.0900	0.09	0.0900	0.09	0.0900	0.09	0.0900
0.10	0.1000	0.10	0.1000	0.10	0.1000	0.10	0.1000

TABLE VI (cont)

## SURFACE VELOCITY PROFILES

ANGLE OF ATTACK =  $2^\circ$  $Re_c = 3.67 \times 10^6$ TOP SURFACE

<u>STATION 9</u>		<u>STATION 10</u>		<u>STATION 11</u>		<u>STATION 12</u>	
$v/V$	$y$	$v/V$	$y$	$v/V$	$y$	$v/V$	$y$
0.527	0.03	0.548	0.03	0.5570	0.03	0.623	0.13
0.752	0.18	0.682	0.10	0.7270	0.18	0.758	0.30
0.800	0.23	0.731	0.16	0.8020	0.28	0.818	0.38
0.844	0.31	0.781	0.23	0.8760	0.42	0.884	0.53
0.919	0.43	0.857	0.35	0.9220	0.53	0.926	0.62
0.966	0.62	0.926	0.52	0.9770	0.72	0.977	0.80
0.995	0.73	0.973	0.64	0.9955	0.87	0.991	0.92
0.998	0.88	0.993	0.82	0.9980	0.92	0.994	1.00
1.000	1.08	1.000	0.96	1.0000	1.03	0.999	1.10
				0.9970	1.56	0.998	1.66
					2.25		2.30

BOTTOM SURFACE

<u>STATION 2</u>		<u>STATION 3</u>		<u>STATION 4</u>		<u>STATION 5</u>	
$v/V$	$y$	$v/V$	$y$	$v/V$	$y$	$v/V$	$y$
0.653	0.02	0.471	0.02	0.4380	0.02	0.4140	0.02
0.987	0.15	0.984	0.13	0.9800	0.13	0.9330	0.16
0.995	0.29	0.984	0.28	0.9950	0.24	0.9925	0.29
0.995	0.40	0.995	0.43	0.9950	0.40	0.9950	0.40
0.996	0.50		0.51	0.9960	0.49	0.9960	0.51
0.999	0.68	1.000	0.69	0.9980	0.66	0.9985	0.69
0.998	0.84	0.9975	0.83	0.9965	0.82	0.9975	0.83
0.999	0.90	1.0000	0.88	0.9995	0.89	0.9985	0.91
1.000	1.00	1.0000	1.00	1.0000	1.00	1.0000	1.01





TABLE VI (cont.)

## SURFACE VELOCITY PROFILES

ANGLE OF ATTACK =  $2^\circ$  $Re_c = 3.67 \times 10^6$ BOTTOM SURFACE

<u>STATION 6</u>		<u>STATION 7</u>		<u>STATION 8</u>		<u>STATION 9</u>	
$v/V$	$y$	$v/V$	$y$	$v/V$	$y$	$v/V$	$y$
0.6240	0.02	0.5600	0.02	0.8006	0.08	0.6020	0.02
0.8940	0.15	0.8220	0.13	0.8200	0.14	0.7580	0.15
0.9630	0.23	0.9260	0.25	0.9120	0.27	0.8510	0.26
0.9955	0.38	0.9890	0.41	0.9710	0.40	0.9120	0.40
0.9955	0.48	0.9935	0.50	0.9910	0.53	0.9790	0.50
0.9980	0.68	0.9980	0.69	0.9980	0.70	0.9975	0.71
0.9970	0.80	0.9980	0.81	0.9970	0.85	0.9975	0.82
0.9990	0.88	0.9990	0.90	0.9985	0.93	0.9980	0.88
1.0000	1.00	1.0000	1.02	1.0000	1.02	1.0000	1.01

<u>STATION 10</u>		<u>STATION 11</u>		<u>STATION 12</u>	
$v/V$	$y$	$v/V$	$y$	$v/V$	$y$
0.6620	0.05	0.682	0.05	0.5010	0.04
0.7140	0.15	0.750	0.15	0.7220	0.13
0.8150	0.24	0.828	0.24	0.8030	0.22
0.9171	0.38	0.905	0.38	0.9140	0.36
0.9620	0.48	0.954	0.48	0.9490	0.48
0.9970	0.67	0.995	0.67	0.9920	0.64
0.9980	0.82	0.999	0.82	0.9975	0.75
0.9990	0.88	1.000	0.88	1.0000	0.86
1.0000	1.00	1.000	1.00	1.0000	0.95
		1.000	1.00		

# 1. Introduction 2. Methodology 3. Results 4. Discussion 5. Conclusion

1. Introduction  
 2. Methodology  
 3. Results  
 4. Discussion  
 5. Conclusion

1. Introduction  
 2. Methodology  
 3. Results  
 4. Discussion  
 5. Conclusion

1. Introduction		2. Methodology		3. Results		4. Discussion		5. Conclusion	
1.1	1.2	2.1	2.2	3.1	3.2	4.1	4.2	5.1	5.2
1.1.1	1.1.2	2.1.1	2.1.2	3.1.1	3.1.2	4.1.1	4.1.2	5.1.1	5.1.2
1.1.3	1.1.4	2.1.3	2.1.4	3.1.3	3.1.4	4.1.3	4.1.4	5.1.3	5.1.4
1.1.5	1.1.6	2.1.5	2.1.6	3.1.5	3.1.6	4.1.5	4.1.6	5.1.5	5.1.6
1.1.7	1.1.8	2.1.7	2.1.8	3.1.7	3.1.8	4.1.7	4.1.8	5.1.7	5.1.8
1.1.9	1.1.10	2.1.9	2.1.10	3.1.9	3.1.10	4.1.9	4.1.10	5.1.9	5.1.10
1.1.11	1.1.12	2.1.11	2.1.12	3.1.11	3.1.12	4.1.11	4.1.12	5.1.11	5.1.12
1.1.13	1.1.14	2.1.13	2.1.14	3.1.13	3.1.14	4.1.13	4.1.14	5.1.13	5.1.14
1.1.15	1.1.16	2.1.15	2.1.16	3.1.15	3.1.16	4.1.15	4.1.16	5.1.15	5.1.16
1.1.17	1.1.18	2.1.17	2.1.18	3.1.17	3.1.18	4.1.17	4.1.18	5.1.17	5.1.18
1.1.19	1.1.20	2.1.19	2.1.20	3.1.19	3.1.20	4.1.19	4.1.20	5.1.19	5.1.20
1.1.21	1.1.22	2.1.21	2.1.22	3.1.21	3.1.22	4.1.21	4.1.22	5.1.21	5.1.22
1.1.23	1.1.24	2.1.23	2.1.24	3.1.23	3.1.24	4.1.23	4.1.24	5.1.23	5.1.24
1.1.25	1.1.26	2.1.25	2.1.26	3.1.25	3.1.26	4.1.25	4.1.26	5.1.25	5.1.26
1.1.27	1.1.28	2.1.27	2.1.28	3.1.27	3.1.28	4.1.27	4.1.28	5.1.27	5.1.28
1.1.29	1.1.30	2.1.29	2.1.30	3.1.29	3.1.30	4.1.29	4.1.30	5.1.29	5.1.30
1.1.31	1.1.32	2.1.31	2.1.32	3.1.31	3.1.32	4.1.31	4.1.32	5.1.31	5.1.32
1.1.33	1.1.34	2.1.33	2.1.34	3.1.33	3.1.34	4.1.33	4.1.34	5.1.33	5.1.34
1.1.35	1.1.36	2.1.35	2.1.36	3.1.35	3.1.36	4.1.35	4.1.36	5.1.35	5.1.36
1.1.37	1.1.38	2.1.37	2.1.38	3.1.37	3.1.38	4.1.37	4.1.38	5.1.37	5.1.38
1.1.39	1.1.40	2.1.39	2.1.40	3.1.39	3.1.40	4.1.39	4.1.40	5.1.39	5.1.40
1.1.41	1.1.42	2.1.41	2.1.42	3.1.41	3.1.42	4.1.41	4.1.42	5.1.41	5.1.42
1.1.43	1.1.44	2.1.43	2.1.44	3.1.43	3.1.44	4.1.43	4.1.44	5.1.43	5.1.44
1.1.45	1.1.46	2.1.45	2.1.46	3.1.45	3.1.46	4.1.45	4.1.46	5.1.45	5.1.46
1.1.47	1.1.48	2.1.47	2.1.48	3.1.47	3.1.48	4.1.47	4.1.48	5.1.47	5.1.48
1.1.49	1.1.50	2.1.49	2.1.50	3.1.49	3.1.50	4.1.49	4.1.50	5.1.49	5.1.50
1.1.51	1.1.52	2.1.51	2.1.52	3.1.51	3.1.52	4.1.51	4.1.52	5.1.51	5.1.52
1.1.53	1.1.54	2.1.53	2.1.54	3.1.53	3.1.54	4.1.53	4.1.54	5.1.53	5.1.54
1.1.55	1.1.56	2.1.55	2.1.56	3.1.55	3.1.56	4.1.55	4.1.56	5.1.55	5.1.56
1.1.57	1.1.58	2.1.57	2.1.58	3.1.57	3.1.58	4.1.57	4.1.58	5.1.57	5.1.58
1.1.59	1.1.60	2.1.59	2.1.60	3.1.59	3.1.60	4.1.59	4.1.60	5.1.59	5.1.60
1.1.61	1.1.62	2.1.61	2.1.62	3.1.61	3.1.62	4.1.61	4.1.62	5.1.61	5.1.62
1.1.63	1.1.64	2.1.63	2.1.64	3.1.63	3.1.64	4.1.63	4.1.64	5.1.63	5.1.64
1.1.65	1.1.66	2.1.65	2.1.66	3.1.65	3.1.66	4.1.65	4.1.66	5.1.65	5.1.66
1.1.67	1.1.68	2.1.67	2.1.68	3.1.67	3.1.68	4.1.67	4.1.68	5.1.67	5.1.68
1.1.69	1.1.70	2.1.69	2.1.70	3.1.69	3.1.70	4.1.69	4.1.70	5.1.69	5.1.70
1.1.71	1.1.72	2.1.71	2.1.72	3.1.71	3.1.72	4.1.71	4.1.72	5.1.71	5.1.72
1.1.73	1.1.74	2.1.73	2.1.74	3.1.73	3.1.74	4.1.73	4.1.74	5.1.73	5.1.74
1.1.75	1.1.76	2.1.75	2.1.76	3.1.75	3.1.76	4.1.75	4.1.76	5.1.75	5.1.76
1.1.77	1.1.78	2.1.77	2.1.78	3.1.77	3.1.78	4.1.77	4.1.78	5.1.77	5.1.78
1.1.79	1.1.80	2.1.79	2.1.80	3.1.79	3.1.80	4.1.79	4.1.80	5.1.79	5.1.80
1.1.81	1.1.82	2.1.81	2.1.82	3.1.81	3.1.82	4.1.81	4.1.82	5.1.81	5.1.82
1.1.83	1.1.84	2.1.83	2.1.84	3.1.83	3.1.84	4.1.83	4.1.84	5.1.83	5.1.84
1.1.85	1.1.86	2.1.85	2.1.86	3.1.85	3.1.86	4.1.85	4.1.86	5.1.85	5.1.86
1.1.87	1.1.88	2.1.87	2.1.88	3.1.87	3.1.88	4.1.87	4.1.88	5.1.87	5.1.88
1.1.89	1.1.90	2.1.89	2.1.90	3.1.89	3.1.90	4.1.89	4.1.90	5.1.89	5.1.90
1.1.91	1.1.92	2.1.91	2.1.92	3.1.91	3.1.92	4.1.91	4.1.92	5.1.91	5.1.92
1.1.93	1.1.94	2.1.93	2.1.94	3.1.93	3.1.94	4.1.93	4.1.94	5.1.93	5.1.94
1.1.95	1.1.96	2.1.95	2.1.96	3.1.95	3.1.96	4.1.95	4.1.96	5.1.95	5.1.96
1.1.97	1.1.98	2.1.97	2.1.98	3.1.97	3.1.98	4.1.97	4.1.98	5.1.97	5.1.98
1.1.99	1.1.100	2.1.99	2.1.100	3.1.99	3.1.100	4.1.99	4.1.100	5.1.99	5.1.100

TABLE VI (cont.)

## SURFACE VELOCITY PROFILES

ANGLE OF ATTACK =  $0.0^\circ$  $Re_\rho = 5.15 \times 10^5$ TOP SURFACE

<u>STATION 1</u>		<u>STATION 4</u>		<u>STATION 6</u>		<u>STATION 8</u>	
$v/V$	$y$	$v/V$	$y$	$v/V$	$y$	$v/V$	$y$
0.9930	0.030	0.9310	0.085	0.7090	0.03	0.7310	0.060
0.7970	0.015	0.8770	0.060	0.9510	0.14	0.8170	0.130
0.9975	0.120	0.9750	0.120	0.9910	0.19	0.9180	0.160
0.9980	0.330	0.9985	0.220	0.9970	0.31	0.9880	0.295
0.9980	0.370	0.9995	0.370	0.9975	0.44	0.9975	0.425
0.9990	0.690	1.0000	0.700	0.9985	0.70	0.9990	0.670
0.9990	0.800	1.0000	0.810	0.9985	0.80	0.9990	0.800
0.9975	0.900	0.9995	0.900	0.9990	0.90	0.9990	0.900
1.0000	1.000			1.0000	1.00	1.0000	0.980

STATION 10

$v/V$	$y$
0.5820	0.02
0.7350	0.13
0.7930	0.17
0.8870	0.31
0.9560	0.44
0.9990	0.68
0.9995	0.80
0.9990	0.90
1.0000	0.99

STATION 12

$v/V$	$y$
0.5130	0.02
0.5600	0.24
0.8600	0.44
0.9210	0.45
0.9750	0.60
0.9995	0.80
1.0000	0.90
0.9985	1.02
1.0000	1.11





TABLE VI (cont.)

## SURFACE VELOCITY PROFILES

ANGLE OF ATTACK =  $2.3^\circ$ 

$$Re_\rho = 5.45 \times 10^6$$

BOTTOM SURFACE

<u>STATION 1</u>		<u>STATION 4</u>		<u>STATION 6</u>		<u>STATION 8</u>	
$v/V$	$y$	$v/V$	$y$	$v/V$	$y$	$v/V$	$y$
0.8010	0.03	0.617	0.02	0.5620	0.03	0.6050	0.08
0.9760	0.10	0.806	0.08	0.7560	0.10	0.7110	0.13
0.9980	0.11	0.906	0.15	0.8210	0.15	0.8020	0.19
0.9985	0.20	0.991	0.30	0.9170	0.29	0.8900	0.31
	0.33	0.999	0.42	0.9890	0.44	0.9580	0.44
0.9990	0.66	0.999	0.67	1.0000	0.67	0.9985	0.72
0.9990	0.80	0.999	0.78	0.9995	0.80	0.9985	0.83
0.9980	0.88	0.999	0.87	0.9995	0.88	0.9985	0.93
1.0000	0.98	1.000	0.97	1.0000	0.98	1.0000	1.02

STATION 10

$v/V$	$y$
0.5620	0.025
0.6820	0.090
0.7310	0.130
0.7420	0.260
0.9010	0.410
0.9800	0.650
0.9925	0.760
0.9960	0.870
1.0000	0.950
0.9980	1.300
0.9970	1.570

STATION 12

$v/V$	$y$
0.475	0.02
0.622	0.11
0.711	0.21
0.790	0.33
0.898	0.58
0.936	0.67
0.964	0.80
0.985	0.89
1.000	0.90
0.999	1.35

# THE UNIVERSITY OF CHICAGO

THE UNIVERSITY OF CHICAGO

THE UNIVERSITY OF CHICAGO

## THE UNIVERSITY OF CHICAGO

THE UNIVERSITY OF CHICAGO		THE UNIVERSITY OF CHICAGO		THE UNIVERSITY OF CHICAGO		THE UNIVERSITY OF CHICAGO	
NAME	ADDRESS	NAME	ADDRESS	NAME	ADDRESS	NAME	ADDRESS
1. J. D. BARNETT	1000 N. LAUREL ST.	1. J. D. BARNETT	1000 N. LAUREL ST.	1. J. D. BARNETT	1000 N. LAUREL ST.	1. J. D. BARNETT	1000 N. LAUREL ST.
2. J. D. BARNETT	1000 N. LAUREL ST.	2. J. D. BARNETT	1000 N. LAUREL ST.	2. J. D. BARNETT	1000 N. LAUREL ST.	2. J. D. BARNETT	1000 N. LAUREL ST.
3. J. D. BARNETT	1000 N. LAUREL ST.	3. J. D. BARNETT	1000 N. LAUREL ST.	3. J. D. BARNETT	1000 N. LAUREL ST.	3. J. D. BARNETT	1000 N. LAUREL ST.
4. J. D. BARNETT	1000 N. LAUREL ST.	4. J. D. BARNETT	1000 N. LAUREL ST.	4. J. D. BARNETT	1000 N. LAUREL ST.	4. J. D. BARNETT	1000 N. LAUREL ST.
5. J. D. BARNETT	1000 N. LAUREL ST.	5. J. D. BARNETT	1000 N. LAUREL ST.	5. J. D. BARNETT	1000 N. LAUREL ST.	5. J. D. BARNETT	1000 N. LAUREL ST.

## THE UNIVERSITY OF CHICAGO

NAME	ADDRESS
1. J. D. BARNETT	1000 N. LAUREL ST.
2. J. D. BARNETT	1000 N. LAUREL ST.
3. J. D. BARNETT	1000 N. LAUREL ST.
4. J. D. BARNETT	1000 N. LAUREL ST.
5. J. D. BARNETT	1000 N. LAUREL ST.

## THE UNIVERSITY OF CHICAGO

NAME	ADDRESS
1. J. D. BARNETT	1000 N. LAUREL ST.
2. J. D. BARNETT	1000 N. LAUREL ST.
3. J. D. BARNETT	1000 N. LAUREL ST.
4. J. D. BARNETT	1000 N. LAUREL ST.
5. J. D. BARNETT	1000 N. LAUREL ST.

TABLE VII  
FORMING COEFFICIENTS

BOTTOM SURFACE				ANGLE OF ATTACK = 0.0°	
STATIC READINGS FOR EACH				$CT_c = 3.67 \times 10^6$	
STATION	h stat	h stat m	hs-hm	q <sub>∞</sub>	$\frac{h_{st}-h_{st\ m}}{q_{\infty}}$
1	+2.52	+1.42	-1.10	11.74	-0.09370
2	+2.20	+1.38	-0.82	11.90	-0.06890
3	+2.10	+1.35	-0.75	11.78	-0.06370
4	+1.95	+1.31	-0.64	11.76	-0.05440
5	+1.82	+1.25	-0.57	11.80	-0.04830
6	+1.80	+1.28	-0.52	11.72	-0.04430
7	+1.55	+1.29	-0.26	11.78	-0.02208
8	+1.56	+1.25	-0.31	11.80	-0.02628
9	+1.77	+1.17	-0.10	11.75	-0.00851
10	+1.12	+1.18	+0.06	11.84	+0.00507
11	+0.86	+1.08	+0.22	11.74	+0.01871
12	-0.04	+0.86	+0.90	11.78	+0.07640

h stat and h stat<sub>m</sub> in inches of oil spg. 0.827 on inclined manometer.

q<sub>∞</sub> = dynamic head read on indirect reading manometer.

spg. 0.806 converted to same scale as inclined manometer.

+ indicates inches above datum on inclined manometer.

- indicates inches below datum on inclined manometer.



**Table 1**  
**Summary of the data used in the analysis**

Variable	Description			Units	
	Variable	Variable	Variable	Unit	Range
Demographics	Age	Age	Age	Years	18-80
	Gender	Gender	Gender	Male/Female	0-1
	Marital Status	Marital Status	Marital Status	Married/Single	0-1
	Education	Education	Education	Years	12-18
	Income	Income	Income	\$/Year	10,000-100,000
	Occupation	Occupation	Occupation	Category	1-10
	Health Status	Health Status	Health Status	Good/Bad	0-1
	Religion	Religion	Religion	Category	1-5
Attitudes	Attitude 1	Attitude 1	Attitude 1	Score	1-5
	Attitude 2	Attitude 2	Attitude 2	Score	1-5
	Attitude 3	Attitude 3	Attitude 3	Score	1-5
	Attitude 4	Attitude 4	Attitude 4	Score	1-5
	Attitude 5	Attitude 5	Attitude 5	Score	1-5
	Attitude 6	Attitude 6	Attitude 6	Score	1-5
	Attitude 7	Attitude 7	Attitude 7	Score	1-5
	Attitude 8	Attitude 8	Attitude 8	Score	1-5
Behaviors	Behavior 1	Behavior 1	Behavior 1	Score	1-5
	Behavior 2	Behavior 2	Behavior 2	Score	1-5
	Behavior 3	Behavior 3	Behavior 3	Score	1-5
	Behavior 4	Behavior 4	Behavior 4	Score	1-5
	Behavior 5	Behavior 5	Behavior 5	Score	1-5
	Behavior 6	Behavior 6	Behavior 6	Score	1-5
	Behavior 7	Behavior 7	Behavior 7	Score	1-5
	Behavior 8	Behavior 8	Behavior 8	Score	1-5

Notes: The data were collected from a survey of 1,000 respondents. The survey was conducted in 2010. The data were analyzed using SPSS 20.0. The results are presented in the following tables.

Table 1: Summary of the data used in the analysis. The table shows the variables used in the analysis, their descriptions, and their units. The variables are grouped into four categories: Demographics, Attitudes, Behaviors, and Outcomes. The units for each variable are also provided.

Table 2: Descriptive statistics for the variables. The table shows the mean, standard deviation, and range for each variable. The variables are grouped into four categories: Demographics, Attitudes, Behaviors, and Outcomes.

Table 3: Correlation matrix for the variables. The table shows the correlations between the variables. The variables are grouped into four categories: Demographics, Attitudes, Behaviors, and Outcomes.

TABLE VII (cont.)

PULSED COEFFICIENTS

TOP SURFACE

ANGLE OF ATTACK =  $0.0^\circ$ 

STATIC HEADINGS FOR BASE

 $DE_G = 3.47 \times 10^6$ 

STATION	$h_{stat}$	$h_{stat_{eq}}$	$h_{st} - h_{eq}$	$\psi_{eq}$	$\frac{h_{st} - h_{eq}}{r_{eq}}$
1	+2.31	+1.30	-1.01	11.78	-0.0656
2					
3	+3.32	+1.30	-2.02	11.78	-0.1715
4	+3.47	+1.29	-2.18	11.75	-0.1855
5	+3.60	+1.31	-2.29	11.75	-0.1950
6	+3.60	+1.23	-2.37	11.85	-0.2000
7	+3.30	+1.10	-2.20	11.76	-0.1871
8	+3.45	+1.20	-2.25	11.75	-0.1925
9	+3.62	+1.18	-2.44	11.75	-0.2076
10	+3.40	+1.09	-2.31	11.70	-0.1974
11	+3.20	+1.10	-2.10	11.70	-0.1794
12	+2.74	+1.08	-1.66	11.75	-0.1412

# Annual Review of the Department of Education

Department of Education

Annual Review

2014-2015

2014-2015

Year	2014	2015	2016	2017	2018
2014	2015	2016	2017	2018	2019
2015	2016	2017	2018	2019	2020
2016	2017	2018	2019	2020	2021
2017	2018	2019	2020	2021	2022
2018	2019	2020	2021	2022	2023
2019	2020	2021	2022	2023	2024
2020	2021	2022	2023	2024	2025
2021	2022	2023	2024	2025	2026
2022	2023	2024	2025	2026	2027
2023	2024	2025	2026	2027	2028
2024	2025	2026	2027	2028	2029
2025	2026	2027	2028	2029	2030

TABLE VII (cont)

## PRESSURE COEFFICIENTS

BOTTOM SURFACE

ANGLE OF ATTACK =  $2.0^\circ$ 

READINGS FROM RISE STATIC TUBES

 $p_0 = 3.67 \times 10^5$ 

STATION	h stat	h stat @	h <sub>0</sub> -h <sub>st</sub>	q <sub>st</sub>	$\frac{h_{st}-h_{0 \text{ stat}}}{q_{st}}$
1					
2	-0.15	+1.00	+1.15	11.86	0.1223
3	+0.10	+1.00	+0.90	11.80	0.0762
4	+0.25	+1.00	+0.75	11.85	0.0633
5	+0.37	+1.00	+0.63	11.85	0.0532
6	+0.50	+1.00	+0.50	11.85	0.0422
7	+0.19	+0.98	+0.19	11.86	0.0113
8	+0.58	+0.98	+0.40	11.86	0.0337
9	+0.15	+0.87	+0.32	11.85	0.0270
10	+0.30	+0.89	+0.59	11.85	0.0498
11	+1.25	+1.25	+0.71	11.90	0.0622
12	+1.25	+1.25	+1.25	11.95	0.1016



# 1. General Information 2. Detailed Description

Project Information			Financial Summary		
Project Name: [Project Name]			Total Budget: [Total Budget]		
Item	Quantity	Unit Price	Item	Quantity	Unit Price
Item 1	10	100	Item 2	20	200
Item 3	5	50	Item 4	15	150
Item 5	3	30	Item 6	8	80
Item 7	2	20	Item 8	4	40
Item 9	1	10	Item 10	2	20
Item 11	1	10	Item 12	1	10
Item 13	1	10	Item 14	1	10
Item 15	1	10	Item 16	1	10
Item 17	1	10	Item 18	1	10
Item 19	1	10	Item 20	1	10
Item 21	1	10	Item 22	1	10
Item 23	1	10	Item 24	1	10
Item 25	1	10	Item 26	1	10
Item 27	1	10	Item 28	1	10
Item 29	1	10	Item 30	1	10
Item 31	1	10	Item 32	1	10
Item 33	1	10	Item 34	1	10
Item 35	1	10	Item 36	1	10
Item 37	1	10	Item 38	1	10
Item 39	1	10	Item 40	1	10
Item 41	1	10	Item 42	1	10
Item 43	1	10	Item 44	1	10
Item 45	1	10	Item 46	1	10
Item 47	1	10	Item 48	1	10
Item 49	1	10	Item 50	1	10
Item 51	1	10	Item 52	1	10
Item 53	1	10	Item 54	1	10
Item 55	1	10	Item 56	1	10
Item 57	1	10	Item 58	1	10
Item 59	1	10	Item 60	1	10
Item 61	1	10	Item 62	1	10
Item 63	1	10	Item 64	1	10
Item 65	1	10	Item 66	1	10
Item 67	1	10	Item 68	1	10
Item 69	1	10	Item 70	1	10
Item 71	1	10	Item 72	1	10
Item 73	1	10	Item 74	1	10
Item 75	1	10	Item 76	1	10
Item 77	1	10	Item 78	1	10
Item 79	1	10	Item 80	1	10
Item 81	1	10	Item 82	1	10
Item 83	1	10	Item 84	1	10
Item 85	1	10	Item 86	1	10
Item 87	1	10	Item 88	1	10
Item 89	1	10	Item 90	1	10
Item 91	1	10	Item 92	1	10
Item 93	1	10	Item 94	1	10
Item 95	1	10	Item 96	1	10
Item 97	1	10	Item 98	1	10
Item 99	1	10	Item 100	1	10

TABLE VII (cont)

FLOODING CONDITIONS

TOP SURFACE

ANGLE OF ATTACK =  $2.0^\circ$ 

GRAINING FROM THE BACK SURFACE

 $\rho = 1.67 \times 10^{-3}$ 

STATION	$h$ stat	$h$ station	$h_0 - h_{\infty}$	$q_0$	$\frac{h_0 - h_{\infty} \text{ st}}{q_0}$
1	+5.38	+1.20	-4.18	11.81	-0.354
2	+4.70	+1.05	-3.65	11.95	-0.3052
3	+4.20	+0.68	-3.52	11.71	-0.2995
4	+4.19	+0.68	-3.51	11.85	-0.2960
5	+4.10	+0.70	-3.40	11.84	-0.2870
6	+3.98	+0.60	-3.38	11.80	-0.2861
7	+3.71	+0.53	-3.18	11.80	-0.2692
8	+3.58	+0.62	-2.96	11.84	-0.2500
9	+3.50	+0.65	-2.85	11.85	-0.2405
10	+3.27	+0.65	-2.62	11.76	-0.2225
11	+3.38	+0.99	-2.39	11.82	-0.2020
12	+2.73	+1.09	-1.64	11.85	-0.1385



TABLE VII (cont)

TRAFFIC COEFFICIENTS

BOTTOM SURFACE

ANGLE OF ATTACK =  $2.0^\circ$ 

PRESSURES FROM WATER GUN

$$\rho_0 = 1.03 \times 10^3$$

STATION	$h_{stat}$	$h_{stat}$	$h_{stat}$	$\phi$	$\frac{h_{stat} - h_{stat}}{h_{stat}}$
1	+2.26	-0.10	+2.66	11.85	+0.22610
2	+0.18	+0.90	+0.72	11.85	+0.06080
3	+0.51	+0.90	+0.39	11.85	+0.03290
4	+0.60	+0.90	+0.30	11.85	+0.02530
5	+0.68	+0.90	+0.22	11.85	+0.018580
6	+0.78	+0.90	+0.12	11.85	+0.010110
7	+0.87	+0.90	+0.03	11.85	+0.002531
8	-1.21	+0.90	-0.31	11.85	-0.026200
9					
10	+0.75	+0.90	+0.15	11.85	+0.012670
11	+0.79	+0.90	+0.11	11.85	+0.009280
12	+0.37	+0.90	+0.53	11.85	+0.014700
13A	-0.68	+0.37	+1.05	11.85	-0.009700
13B	-0.81	+0.33	+1.17	11.85	-0.009600



# 1990-1991 Annual Report

Total number of cases		Number of cases by age group				Number of cases by sex	
Total		0-14	15-24	25-44	45-64	Male	Female
1990	100	20	30	40	10	50	50
1991	110	22	32	42	14	55	55
1992	120	24	34	44	18	60	60
1993	130	26	36	46	22	65	65
1994	140	28	38	48	26	70	70
1995	150	30	40	50	30	75	75
1996	160	32	42	52	34	80	80
1997	170	34	44	54	38	85	85
1998	180	36	46	56	42	90	90
1999	190	38	48	58	46	95	95
2000	200	40	50	60	50	100	100

TABLE VIII

SAMPLE CALCULATION OF MONOTONIC THICKNESS VALUES

STATIONARY CALCULATION

TOP SURFACE

ANGLE OF ATTACK =  $0.0^\circ$ 

STATION 1

 $RE = 3.67 \times 10^6$ 

$Z$	$z/v$	$v/v$	$1 - v/v$	$v/v(1 - v/v)$	$SM$	$f(\theta)$
.034	1.0	.992	.008	.00796	1	.00796
.306	0.9	.989	.011	.01087	6	.06368
.272	0.8	.981	.019	.01793	2	.01726
.238	0.7	.960	.040	.05640	4	.22560
.204	0.6	.870	.130	.1131	2	.22620
.170	0.5	.783	.217	.1491	4	.47640
.136	0.4	.676	.324	.2180	2	1.3600
.0102	0.3	.610	.390	.2379	6	.95160
.0068	0.2	.499	.500	.2499	2	.69980
.0034	0.1	.250	.750	.1875	6	.75000
	0.0	0	0	0	1	0

$$\bar{\theta} = \frac{f(\theta)_{station}}{3} = \frac{(.1)(3.0512)}{3} = .129173$$

$$\theta = \bar{\theta} / \bar{z} = (.129173) / (.034) = .0038656$$

$$H = \bar{\theta} / \theta = \frac{.0120}{.0038656} = 3.100$$



APPENDIX 3  
EXAMPLES OF DATA





DISPLACEMENT THICKNESS  
VS.  
DISTANCE/CHORD  
ANGLE OF ATTACK =  $0.0^\circ$   
 $Re_c = 3.67 \times 10^6$  O-BOTTOM  
A-TOP  
NACA66 MODIFIED 10 MEANLINE  
 $Re_c = 5.45 \times 10^6$  O-TOP  
O-BOTTOM

TYPE OF BEHAVIOR OBTAINED  
BY PRESTON (REF (2))

# CHORDWISE BOUNDARY LAYER DEVELOPMENT

$$\alpha = 0.0^\circ$$

POSSIBILITY THAT  
TRANSITION OCCURS  
HERE ON THE TOP SURFACE  
AT  $Re_c = 3.67 \times 10^6$

DISTANCE/CHORD  $x/c$

TRANSITION

$\delta^*$   
(IN INCHES)

0.0

0.1

0.2

0.3

0.4

0.5

0.6

0.7

0.8

0.9

1.0

1.1

1.2

1.3

1.4

1.5

1.6

1.7

1.8

1.9

2.0

2.1

2.2

2.3

2.4

2.5

2.6

2.7

2.8

2.9

3.0

3.1

3.2

3.3

3.4

3.5

3.6

3.7

3.8

3.9

4.0

4.1

4.2

4.3

4.4

4.5

4.6

4.7

4.8

4.9

5.0

5.1

5.2

5.3

5.4

5.5

5.6

5.7

5.8

5.9

6.0

6.1

6.2

6.3

6.4

6.5

6.6

6.7

6.8

6.9

7.0

7.1

7.2

7.3

7.4

7.5

7.6

7.7

7.8

7.9

8.0

8.1

8.2

8.3

8.4

8.5

8.6

8.7

8.8

8.9

9.0

9.1

9.2

9.3

9.4

9.5

9.6

9.7

9.8

9.9

10.0

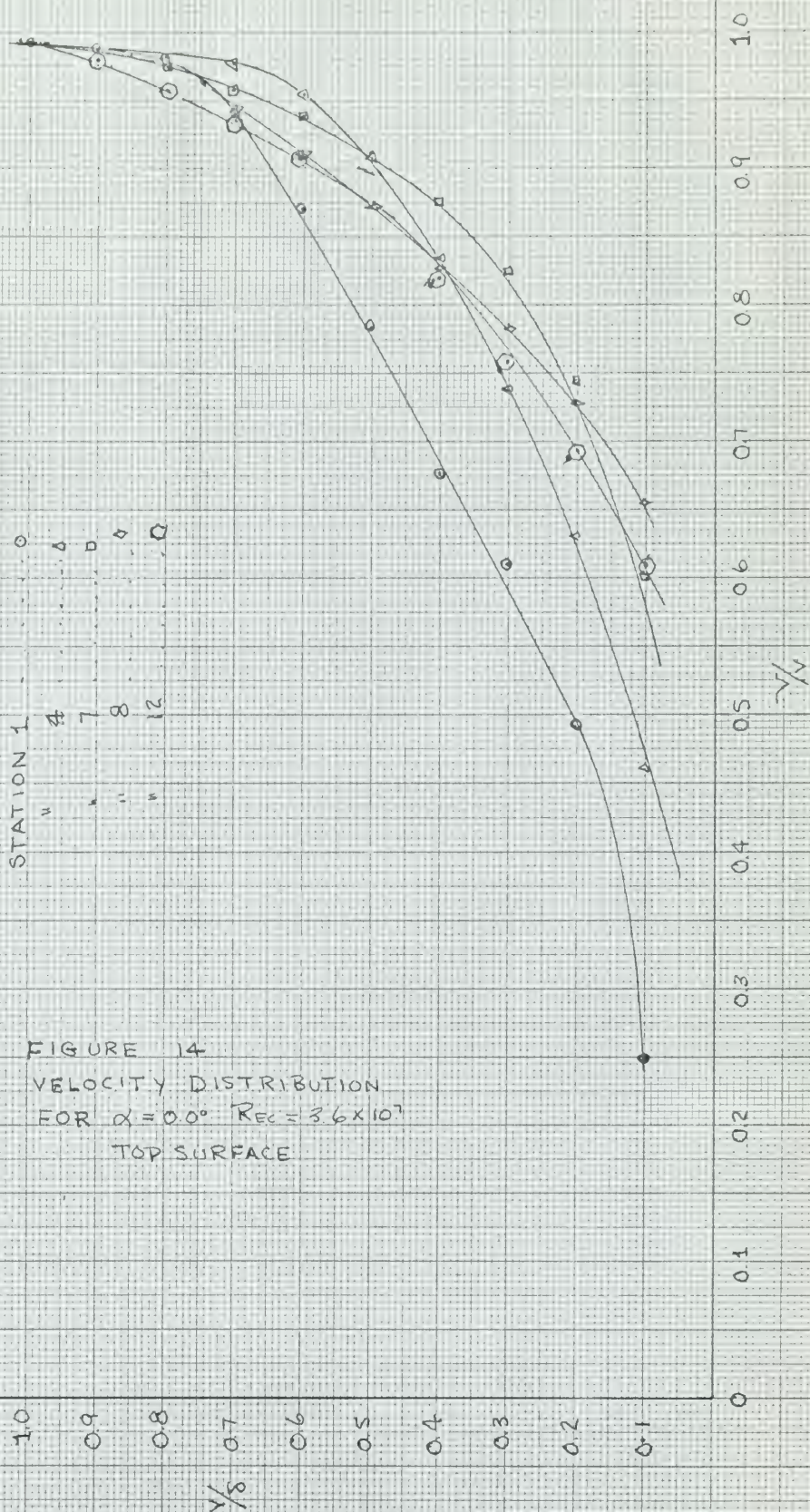




PLOT OF  $V/V$  VERSUS  $Y/\delta$   
 FOR NOMINAL  $\alpha = 0.0^\circ$   
 $Re = 3.61 \times 10^6$   
 TOP SURFACE

STATION 1  
 " 4  
 " 7  
 " 8  
 " 12

FIGURE 14  
 VELOCITY DISTRIBUTION  
 FOR  $\alpha = 0.0^\circ$   $Re = 3.6 \times 10^7$   
 TOP SURFACE







PLOT OF  $V/V_0$  VERSUS  $Y/\delta$

FOR NOMINAL  $\alpha = 0.0^\circ$

$RE = 3.67 \times 10^6$

BOTTOM SURFACE

STATION 1 ..... 0

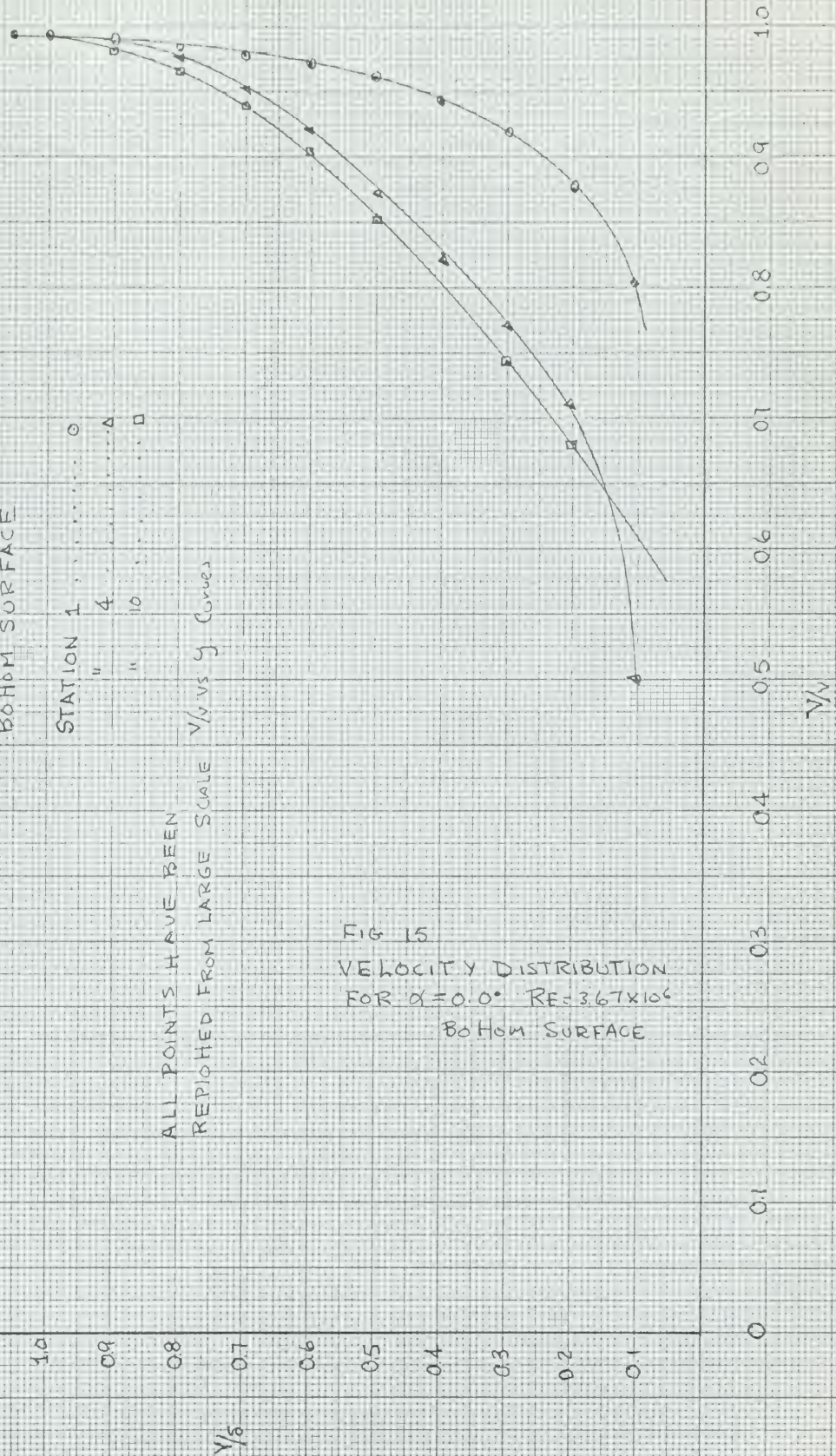
" 4 .....  $\Delta$

" 10 .....  $\square$

ALL POINTS HAVE BEEN  
REPICHED FROM LARGE SCALE

$V/V_0$  VS  $Y$  CURVES

FIG 15  
VELOCITY DISTRIBUTION  
FOR  $\alpha = 0.0^\circ$   $RE = 3.67 \times 10^6$   
BOTTOM SURFACE







PLOT OF  $V/V_\infty$  VERSUS  $Y/\delta$   
 FOR NOMINAL  $\alpha = 2.0^\circ$   
 $RE = 3.67 \times 10^6$

TOP SURFACE

STATION 1

STATION 4

STATION 12

○  
△  
□

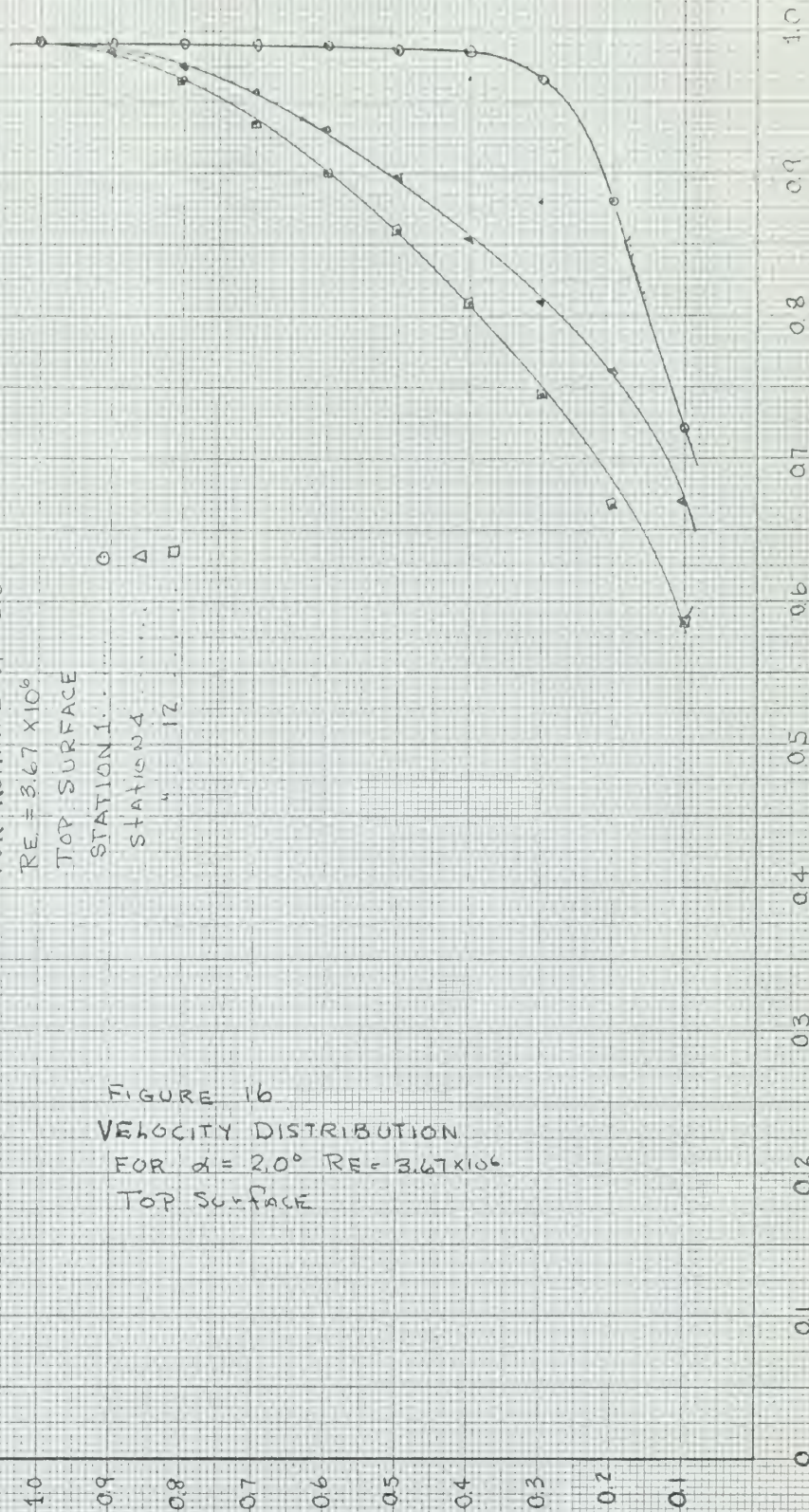


FIGURE 16  
 VELOCITY DISTRIBUTION  
 FOR  $\alpha = 2.0^\circ$   $RE = 3.67 \times 10^6$   
 TOP SURFACE





PLOT OF  $y/\delta$  VERSUS  $y/\delta$

FOR

NOMINAL ANGLE OF ATTACK =  $2.0^\circ$

$Re_c = 3.67 \times 10^6$  BOTTOM SURFACE

STATION 2

6

8

12

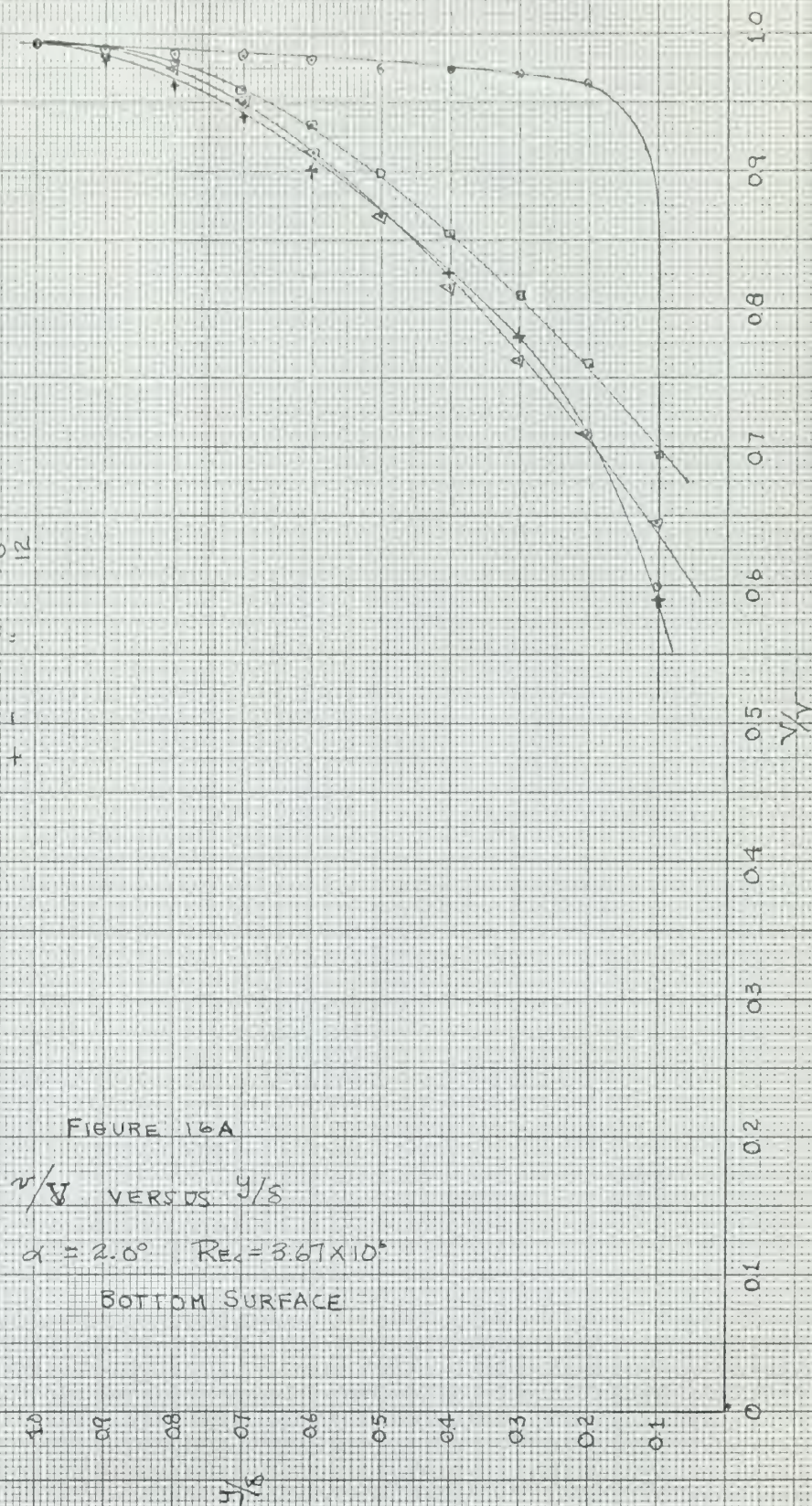


FIGURE 16A

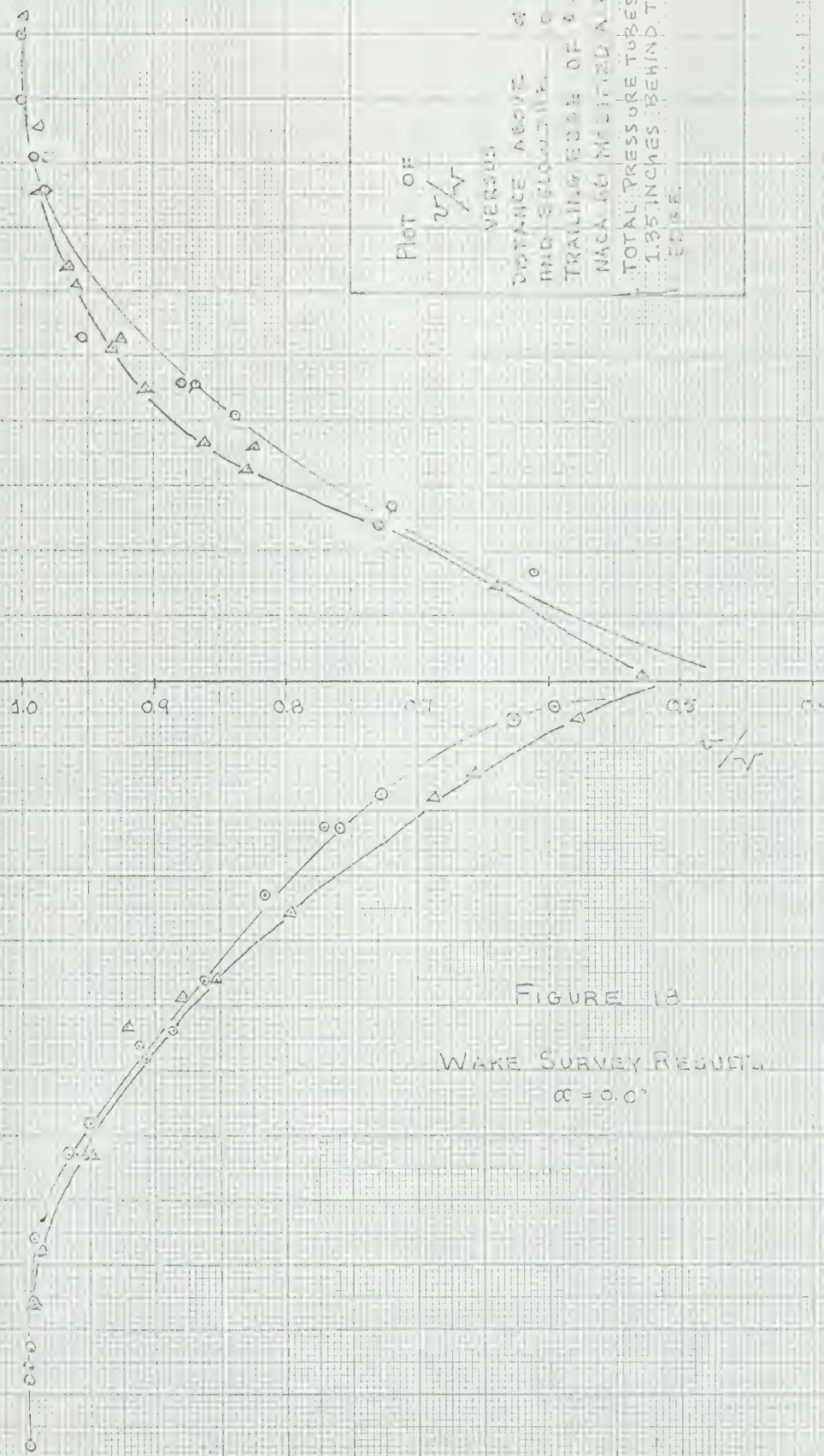
$y/\delta$  VERSUS  $y/\delta$

$\alpha = 2.0^\circ$   $Re_c = 3.67 \times 10^6$

BOTTOM SURFACE







Plot of  
 $v/v_\infty$

VERSUS  
DISTANCE ABOVE  
AND BELOW THE  
TRAILING EDGE OF A  
FOIL  
NACA NO. 14-012  
TOTAL PRESSURE TUBES ARE  
1.35 INCHES BEHIND THE  
FOIL

FIGURE 18

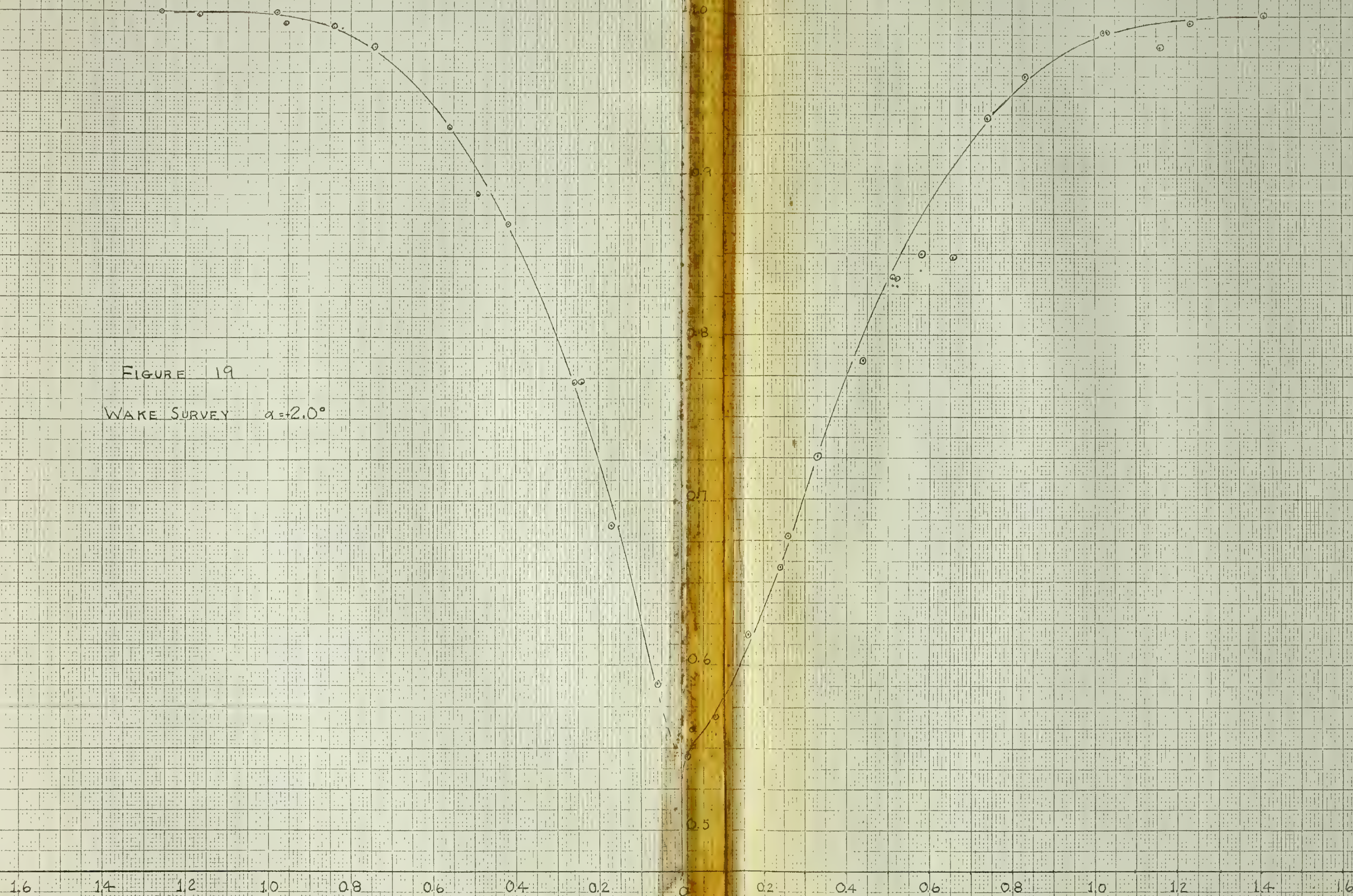
WAKE SURVEY RESULTS  
 $\alpha = 0.0^\circ$

1.0 0.9 0.8 0.7 0.6 0.5  
DISTANCE EITHER  
ABOVE OR BELOW  
SIDE OF THE CENTER OF THE TRAILING EDGE  
IN INCHES





FIGURE 19  
WAKE SURVEY  $\alpha = 2.0^\circ$







PRESSURE COEFFICIENT  
VERSUS

FRACTION OF CHORD

$RE = 2.7 \times 10^6$   $\alpha = 0.0^\circ$

MODIFIED NACA 66 FOIL

$\Delta$  - PRESSURES MEASURED USING SURFACE TAPS

$\circ$  - PRESSURES MEASURED USING STATIC TUBE ON RAKE 1.1 INCHES ABOVE SURFACE

BOTTOM SURFACE

TOP SURFACE

FIGURE 20  
EXPERIMENTAL PRESSURE  
DISTRIBUTION ALONG CHORD  
 $\alpha = 0.0^\circ$   $RE = 2.6 \times 10^6$

0.2

0.1

0

-0.1

-0.2

$\frac{P-P_\infty}{\frac{1}{2}\rho V_\infty^2}$

100

90

80

70

60

50

40

30

20

10





PRESSURE COEFFICIENT  
VERSUS

FRACTION OF CHORD LENGTH

$Re = 3.67 \times 10^6$   $\alpha = 0.0^\circ$   
MODIFIED NACA 66 AIRFOIL

TOP SURFACE ONLY

$X/L$  (FRACTION OF CHORD LENGTH)

NOTE: ALL READINGS TAKEN FROM  
SURFACE STATIC TAPS WITH  
THE BOUNDARY LAYER RAKE

IN VARIOUS POSITIONS AS FOLLOWS:

SYMBOL

RAKE STA.

3

4

5

6

9

12

FIG 21

TOP SURFACE PRESSURES  
WITH THE RAKE IN PLACE

$\frac{P - P_\infty}{\frac{1}{2} \rho V_\infty^2}$

-0.1

-0.2

0.2

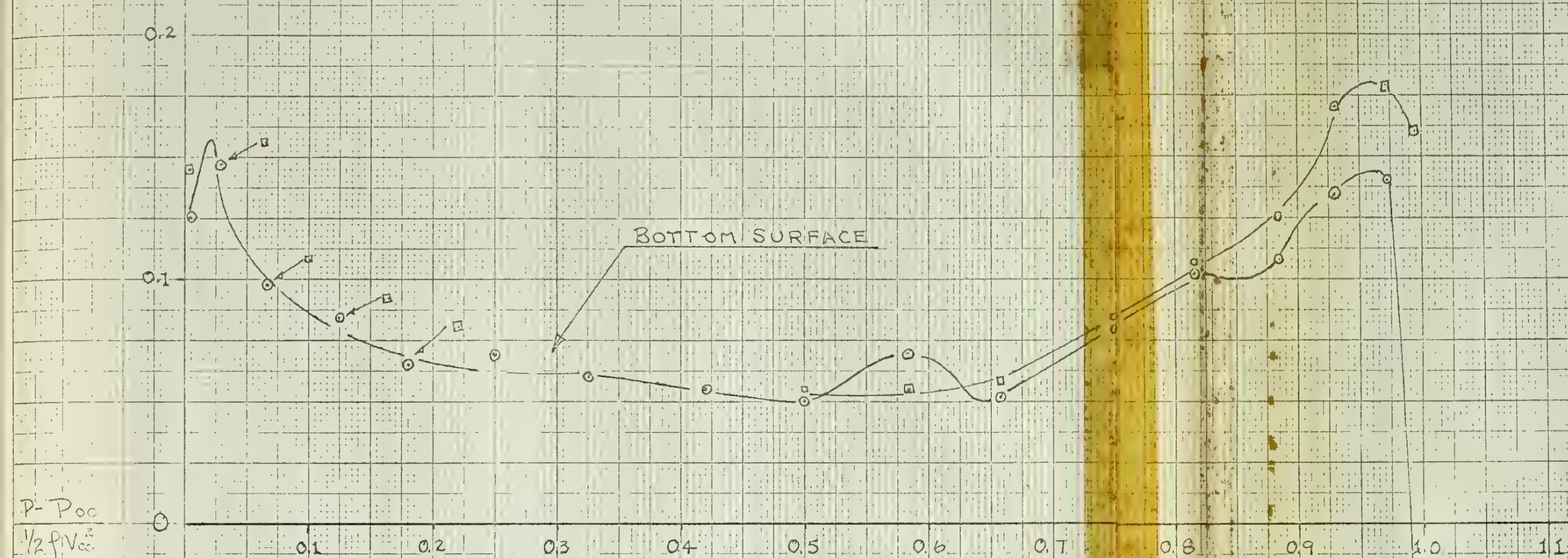
0.3







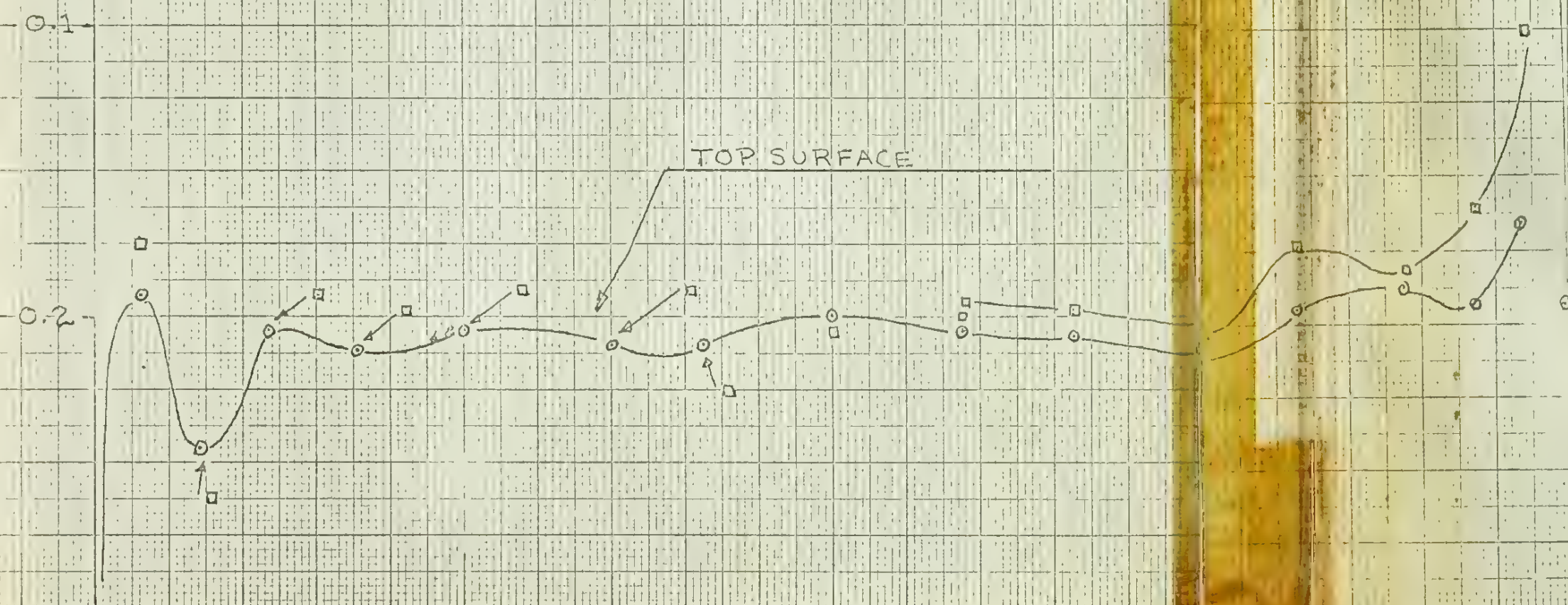
FIGURE 22 PRESSURE COEFFICIENT VS CHORD  
POTENTIAL FLOW



PRESSURE COEFFICIENT  
VERSUS  
CHORDWISE DISTANCE/CHORD  
FOR A MODIFIED NACA 66 FOIL  
NOMINAL ANGLE OF ATTACK =  $0.0^\circ$   
 $Re = 3.67 \times 10^6$

RESULTS OF POTENTIAL FLOW:

○ AROUND FOIL CORRECTED FOR  $5^\circ$  ATTACK  
□ AROUND ORIGINAL FOIL



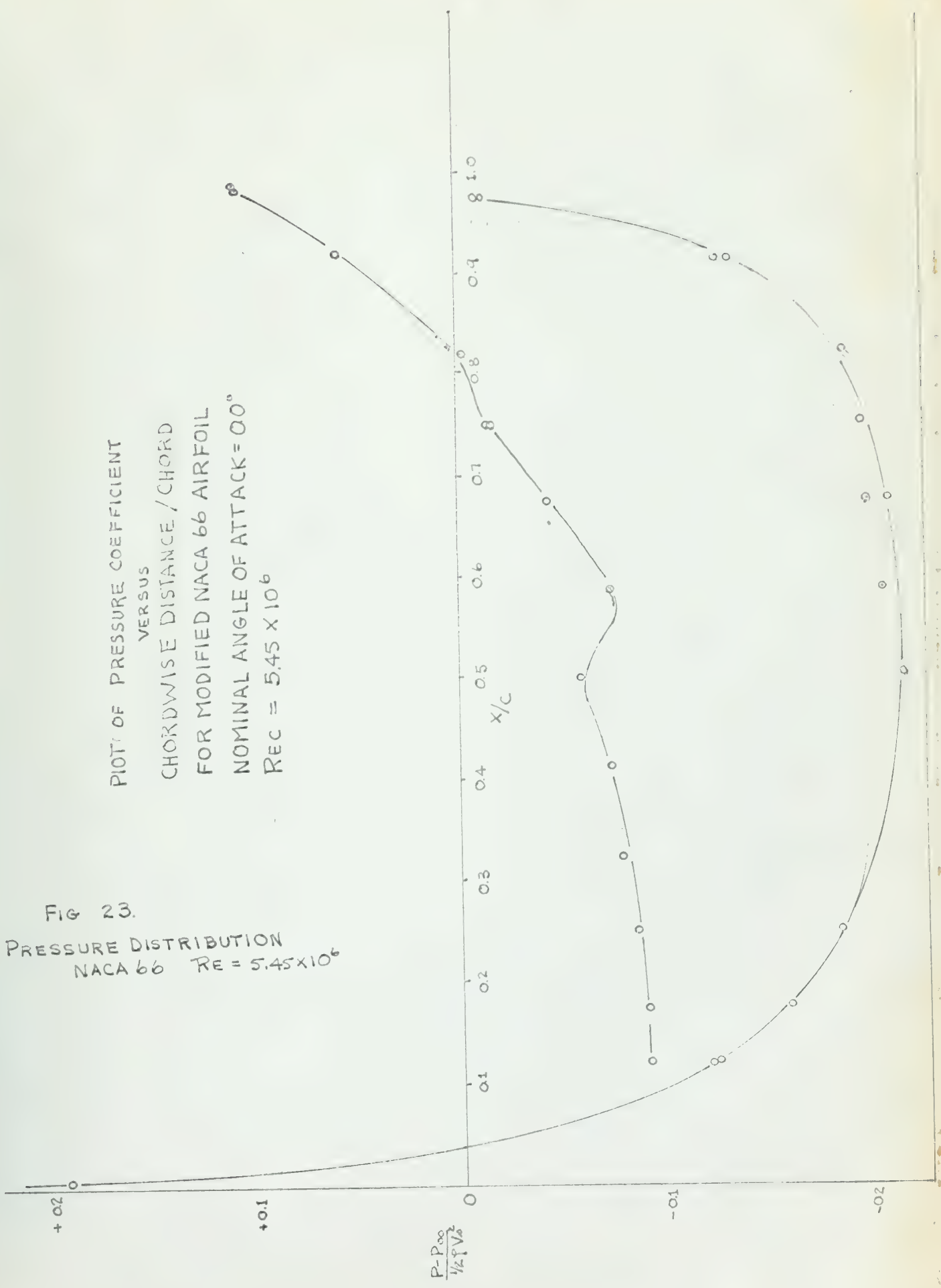






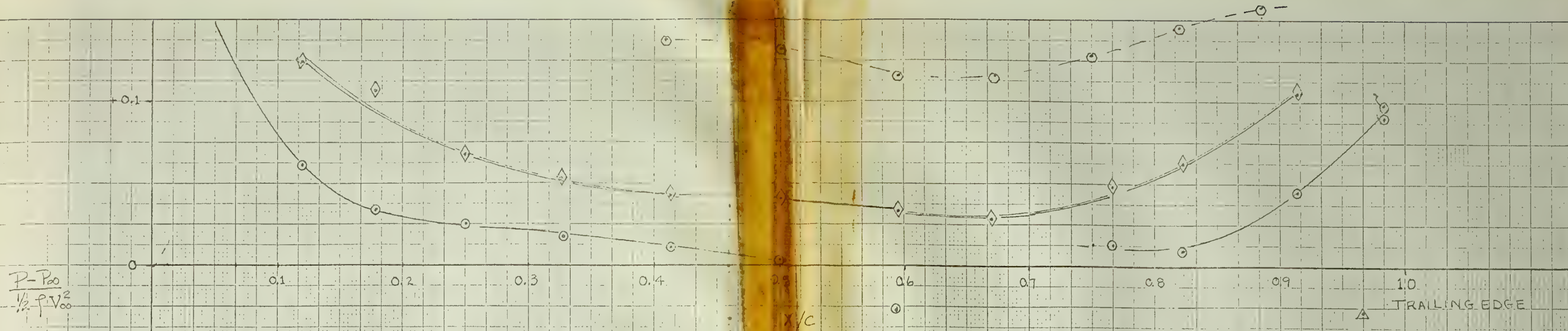
PLOT OF PRESSURE COEFFICIENT  
 VERSUS  
 CHORDWISE DISTANCE / CHORD  
 FOR MODIFIED NACA 66 AIRFOIL  
 NOMINAL ANGLE OF ATTACK =  $00^{\circ}$   
 $RE = 5.45 \times 10^6$

FIG 23.  
 PRESSURE DISTRIBUTION  
 NACA 66  $RE = 5.45 \times 10^6$

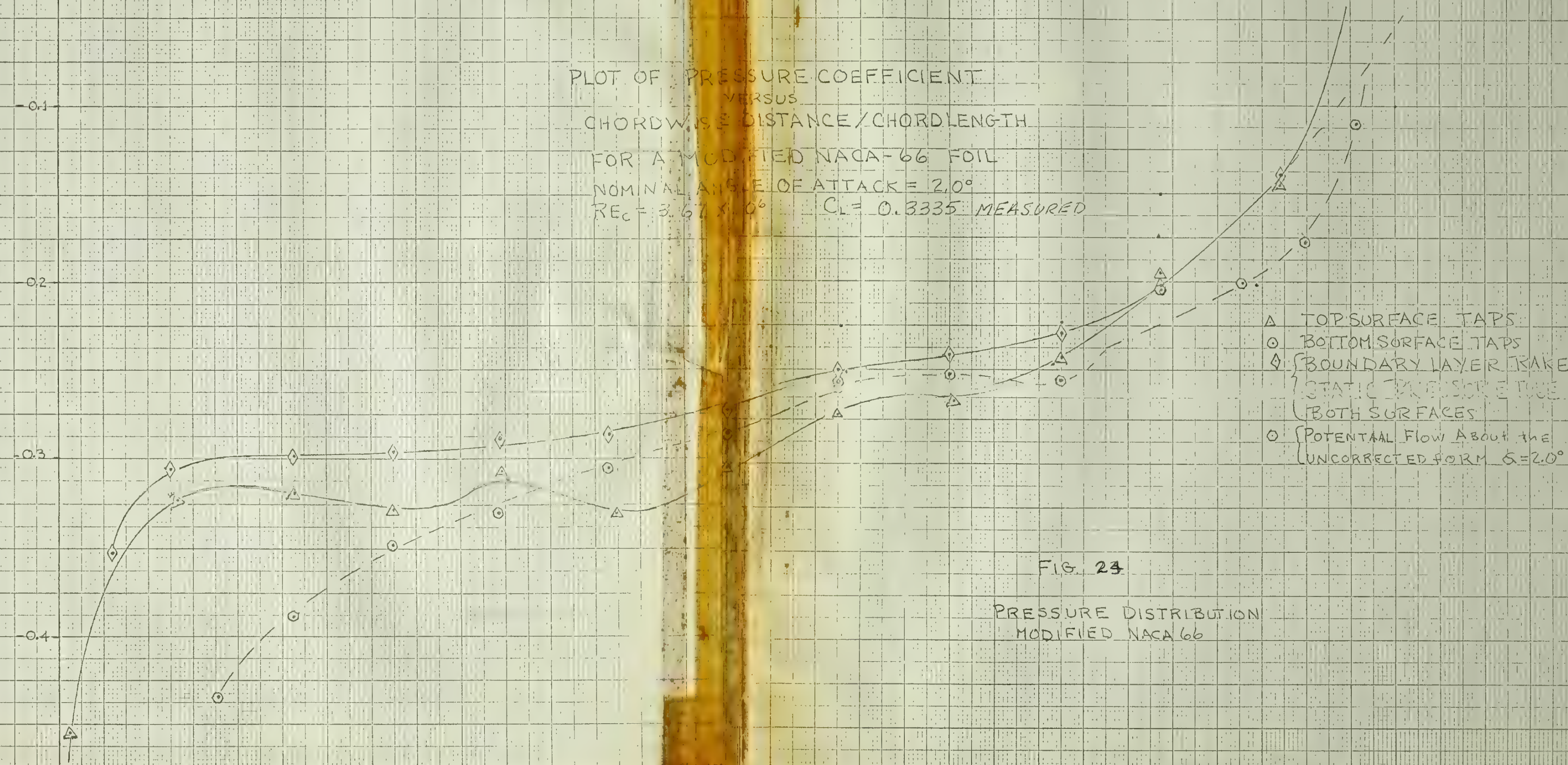








PLOT OF PRESSURE COEFFICIENT  
VERSUS  
CHORDWISE DISTANCE/CHORD LENGTH  
FOR A MODIFIED NACA-66 FOIL  
NOMINAL ANGLE OF ATTACK =  $2.0^\circ$   
 $Re_c = 3.67 \times 10^6$   $Cl = 0.3335$  MEASURED



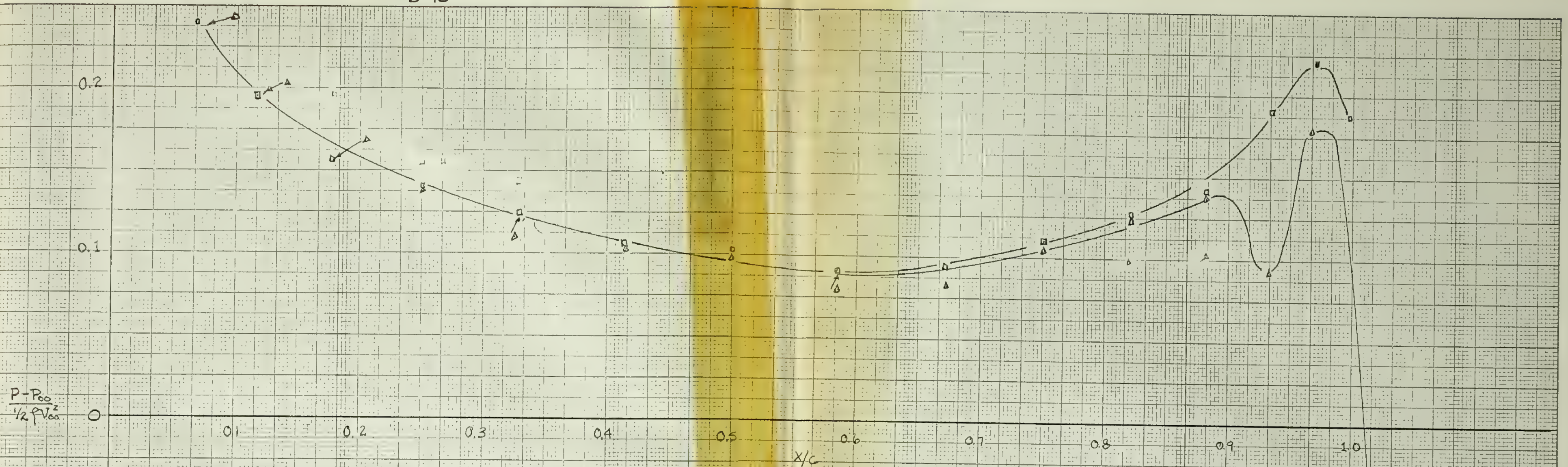
- △ TOP SURFACE TAPS
- BOTTOM SURFACE TAPS
- ◇ BOUNDARY LAYER RAKE
- STATIC PRESSURE TUBE (BOTH SURFACES)
- POTENTIAL FLOW ABOUT THE UNCORRECTED FORM  $\alpha=2.0^\circ$

FIG. 23  
PRESSURE DISTRIBUTION  
MODIFIED NACA 66









PLOT OF PRESSURE COEFFICIENT  
VERSUS  
CHORDWISE DISTANCE / CHORD LENGTH  
FOR NACA 66 MODIFIED  $\alpha = 2.0^\circ$   
 $Re = 3.67 \times 10^6$   
POTENTIAL THEORY RESULTS FOR

$\alpha = 1.9569^\circ$  FORM CORRECTED FOR  $\delta^*$  AND  $x$  LAMDS  
 $\alpha = 1.2000^\circ$  " " " " " "  
 $\alpha = 1.200^\circ$  UNCORRECTED

FIG. 25  
POTENTIAL FLOW PRESSURE  
COEFFICIENTS NOMINAL  $\alpha = 2.0^\circ$

TOP SURFACE

-0.2

-0.3





SHAPE FACTOR AND MOMENTUM THICKNESS  
VERSUS

CHORDWISE DISTANCE / CHORD

FOR  $\alpha = 0.0^\circ$   $Re_c = 5.45 \times 10^6$

TOP SURFACE ONLY

$\Delta$  - SHAPE FACTOR  $H$

$\circ$  - MOMENTUM THICKNESS



FIG 26

SHAPE FACTOR AND  
MOMENTUM THICKNESS  
VS  
CHORD





## APPENDIX C

### PROBABILITY DISTRIBUTIONS



# NON-DIMENSIONAL GEOMETRIC COEFFICIENTS

EDWARDS      ACA 66 MODIFIED IN IINVISCID FLOW  
AREA            =      .022638  
XBAR            =      .474175  
YBAR            =      .009703  
I(X,ABT LE)=      .000004  
I(Y,ABT LE)=      .006391  
I(XBAR)        =      .000001  
I(YBAR)        =      .001301









thesE254

Prediction of boundary layer effects on



3 2768 001 90353 7

DUDLEY KNOX LIBRARY